

THE PHOTOCHROMIC AND PHOTOREFRACTIVE
RESPONSE OF CZOCHRALSKI GROWN
 $\text{Bi}_{12}\text{GeO}_{20}$ DOPED WITH
CHROMIUM AND
MANGANESE

By

JEFFREY SCOTT MCCULLOUGH

Bachelor of Science

Southeastern Oklahoma State University

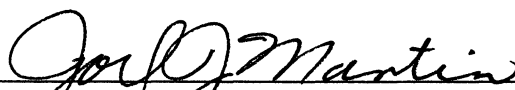
Durant, Oklahoma

1992

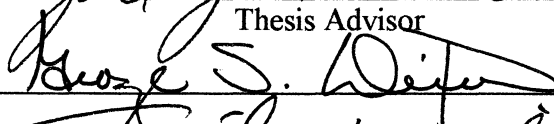
Submitted to the Faculty of the
Graduate College of the
Oklahoma State University
in partial fulfillment of
the requirements for
the Degree of
DOCTOR OF PHILOSOPHY
July, 1999

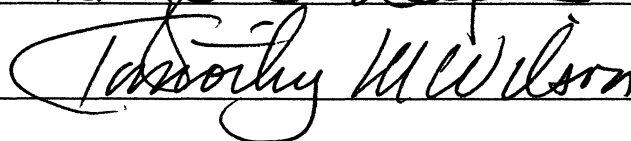
THE PHOTOCHROMIC AND PHOTOREFRACTIVE
RESPONSE OF CZOCHRALSKI GROWN
 $\text{Bi}_{12}\text{GeO}_{20}$ DOPED WITH
CHROMIUM AND
MANGANESE

Thesis Approved:



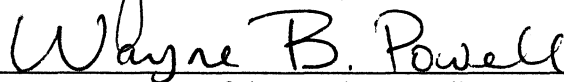
Thesis Advisor











Dean of the Graduate College

ACKNOWLEDGEMENTS

I would like to first thank my advisor, Dr. Joel Martin, for giving me the opportunity to learn and work in his laboratory, and for his supervision, guidance, and patience. I would also like to thank the members of my graduate committee, Drs. George Dixon, Tim Wilson, David Peakheart, and Elizabeth Holt, for donating their time to serve on my committee. A special thanks goes to Dr. Dixon for his help with the modeling of the photorefractive effect. I would also like to thank Dr. Peakheart for his help and encouragement whenever I needed it.

I would like to thank for Mr. Charles Hunt for teaching me the science (art?) of growing crystals and the finer points of polishing samples.

I would like to thank Mr. Meckie Harris at Rome Laboratories, Hanscom Air Force Base, MA for providing a BGO:Mn sample used in this study.

I would like to thank the OSU Department of Physics, including faculty, staff, and students, for encouragement, help, and support, and the OSU Physics/Chemistry Machine Shop for their assistance with several experiments.

Finally, I would like to thank my wife, Desiree', and our parents, Bill and Helen McCullough, and George and JoAnn Butler, for their love, support, encouragement, and understanding while working towards this degree.

TABLE OF CONTENTS

Chapter	Page
1. Bi ₁₂ GeO ₂₀	1
1.1 Introduction	1
1.2 Crystal Structure	4
1.3 Material Properties	4
1.4 Dissertation Project	8
2. CRYSTAL GROWTH AND SAMPLE PREPARATION	10
3. ABSORPTION SPECTRA AND THE PHOTOCHROMIC EFFECT	13
3.1 Introduction	13
3.2 Experimental Procedure	14
3.3 Results And Discussion	16
3.3.1 Chromium	16
3.3.2 Manganese	29
3.4 Summary And Conclusions	43
4. PHOTOREFRACTIVE MEASUREMENTS	44
4.1 Introduction	44
4.2 Experimental Procedure	49
4.3 Results And Discussion	53
4.3.1 Chromium	56
4.3.2 Manganese	61
4.4 Summary And Conclusions	66
5. PHOTOREFRACTIVE SIMULATION MODEL	68
5.1 Introduction	68
5.2 The Theory	69
5.3 Simulations	75
5.4 Summary And Conclusions	78
6. CONCLUSIONS	80
6.1 Summary	80
6.2 Future Work	81

BIBLIOGRAPHY	82
APPENDICES	93
A. Program For Writing A Grating And Monitoring The Grating At Different Temperatures	94
B. Program For Writing A Grating And Monitoring The Grating As The Sample Is Heated.....	103
C. Program For Writing A Grating And Monitoring The Grating Over Long Time Periods	109

LIST OF TABLES

Table	Page
1.1 Material Properties of the Sillenites Compiled From Reference 14.....	7
2.1 BGO crystals used in this study.....	12

LIST OF FIGURES

Figure	Page
3.1 The absorption spectra of BGO and BGO:Cr at 300 K and 10 K	17
3.2 The absorption spectra of BGO and BGO:Cr at 10 K on an expanded scale.....	18
3.3 The photochromic effect in BGO:0.1%Cr. The sample was exposed to 442 nm light for 1 hr at 300 K	20
3.4 The photochromic spectra of BGO:Cr. The samples were exposed to 442 nm light for 1 hr at 300 K	21
3.5 The photochromic spectra of BGO:0.1%Cr at 300 K and 10 K. The sample was illuminated with 442 nm light for 1 hr at 300 K	22
3.6 Excitation spectra for the BGO:Cr samples.....	23
3.7 The low temperature photochromic anneal of BGO:0.1%Cr. The sample was exposed to 413 nm light for 1 hr at 10 K.....	25
3.8 The high temperature photochromic anneal of BGO:0.1%Cr. The sample was exposed to 442 nm light for 1 hr at 300 K. The inset shows the decay of the photoinduced absorption at 700 nm	26
3.9 The absorption spectra of BGO:Mn at 300 K and 10 K. The insets show the absorption spectra of BGO and BGO:0.5%Mn on an expanded scale at 300 K and 10 K	30
3.10 The photochromic effect in BGO:0.5%Mn. The sample was exposed to 442 nm light for 1 hr at 300 K. The inset shows the photochromic effect on an expanded scale.....	32
3.11 The photochromic spectra of BGO:Mn. The samples were exposed to 442 nm light for 1 hr at 300 K	33
3.12 The photochromic spectra of BGO:0.5%Mn at 300 K and 10 K. The sample was illuminated with 442 nm light for 1 hr at 300 K	34

3.13	Excitation spectra for the BGO:Mn samples	36
3.14	The low temperature photochromic anneal of BGO:0.5%Mn. The sample was exposed to 413 nm light for 1 hr at 10 K.....	37
3.15	The low temperature photochromic anneal of BGO:0.5%Mn on an energy scale. The sample was exposed to 413 nm light for 1 hr at 10 K.....	38
3.16	The high temperature photochromic anneal of BGO:0.5%Mn. The sample was exposed to 413 nm light for 1 hr at 300 K. The inset shows the decay of the photoinduced absorption at 496 nm.....	40
4.1	The photorefractive effect. Two coherent light beams intersect in an electro-optic crystal and form an interference pattern. Charges are excited from the bright regions and are transported to the dark regions by drift and diffusion. The charge density matches the light intensity and sets up an electric field which creates a refractive index grating by the linear electro-optic effect.....	47
4.2	Interference pattern formed by the intersection of two light waves and the corresponding wavevector diagram.....	48
4.3	Bragg diffraction of light from a periodic medium and the corresponding wavevector diagram	50
4.4	Experimental arrangement for photorefractive measurements. M stands for mirror, S for shutter, ND for neutral density filter, BS for beam splitter, PMT for photomultiplier tube, BE for beam expander, DMM for Digital Multimeter, Scope for Oscilloscope, I to V AMP for Current to Voltage Amplifier, and PC for Personal Computer.....	51
4.5	Typical photorefractive response of BGO and its normalized dark decays	54
4.6	Typical photorefractive response of BGO:0.1%Cr and its normalized dark decays	57
4.7	The temperature dependence of a grating written in BGO:0.1%Cr at room temperature	59
4.8	Gratings were written in BGO:0.1%Cr at room temperature and monitored for 24 hours.....	60
4.9	Typical photorefractive response of BGO:0.5%Mn and its normalized dark decays	62

4.10	The temperature dependence of a grating written in BGO:0.5%Mn at room temperature	64
4.11	Gratings were written in BGO:0.5%Mn at room temperature and monitored for 24 hours	65
5.1	Model used for simulations of the photorefractive effect in BGO. CB is the conduction band, VB is the valence band, N is the concentration of electrons in the conduction band, N_D is the concentration of donors, and N_T is the concentration of traps	70
5.2	Simulation of the write power dependence on grating formation and the dark decay for undoped BGO at room temperature	76
5.3	Simulation of the temperature dependence on grating formation and the dark decay for undoped BGO	77
5.4	Simulation of the grating formation and the temperature dependence of the dark decay in BGO:Cr and BGO:Mn	79

CHAPTER 1

Bi₁₂GeO₂₀

1.1 Introduction

Bi₁₂GeO₂₀, bismuth germanium oxide, BGO, and the closely related compounds Bi₁₂SiO₂₀, bismuth silicon oxide, BSO, and Bi₁₂TiO₂₀, bismuth titanium oxide, BTO, are photorefractive materials of current interest for optical signal processing applications including optical data storage, optical phase conjugation, optical correlation, and many other applications.¹⁻¹³ Recently, Arizmendi, Cabrera, and Aguillo-Lopez have reviewed the crystal structure, crystal growth, defects, material properties, and photorefractive behavior of this group of materials.¹⁴ The photorefractive effect is a reversible light induced change in a crystal's refractive index and was discovered in 1966 by researchers at Bell Laboratories as unwanted optical damage in LiNbO₃, lithium niobate, and LiTaO₃, lithium tantalate, crystals.¹⁵ Exposing the crystals to visible or ultraviolet laser light introduced inhomogeneities in the refractive index. The initial response was that this effect was detrimental to the field of nonlinear optics, but it was soon realized that this effect could be utilized in holographic storage. Other photorefractive materials include BaTiO₃, barium titanate, Sr_xBa_{1-x}Nb₂O₆, strontium barium niobate, SBN, Ba₂NaNb₅O₁₅,

sodium barium niobate, NBN, KNbO_3 , potassium niobate, semiconductors such as GaAs, gallium arsenide, CdTe, cadmium telluride, and InP, indium phosphide, and organic polymers.¹⁻¹³

The photorefractive effect occurs in materials that both are electro-optic and photoconductive. Electro-optic materials change their index of refraction when a DC electric field is applied.^{5,6,8-11,16} In noncentrosymmetric (lacking inversion symmetry) materials, the change in the refractive index is linearly proportional to the electric field. This is known as the linear electro-optic or Pockels effect. In centrosymmetric materials, the change in refractive index is quadratically proportional to the electric field. This is known as the quadratic electro-optic or Kerr electro-optic effect. The Pockels effect dominates in most photorefractive materials.^{5,6,8-11} Photoconductive materials increase their conductivity when illuminated with light of the proper wavelength by exciting charge into the conduction or valence band. Consequently, photorefractive materials contain donors and/or acceptors and this plays an important role in the photorefractive effect.

The photorefractive effect is induced by illuminating the sample with nonuniform light, such as an interference pattern formed by crossed laser beams. Charges in the bright region will be photoexcited into the conduction and/or valence band where they will drift and diffuse to the dark regions where they can be trapped. The redistribution of trapped charge is also non-uniform and creates a matching electric field pattern in the crystal. In noncentrosymmetric crystals such as BGO, the electric field causes a corresponding change in the index of refraction through the linear electro-optic or Pockels effect.^{5,6,8-11,16} The index change will be periodic like the interference pattern and will behave like a diffraction grating.

If information was encoded in one or both of the laser beams, the information would then be stored in the photorefractive material as a hologram. The information could be read by illuminating the sample with one of the write beams or a different laser at the Bragg angle. The information is stored throughout the medium as the Fourier transform of the bit pattern and not the bit pattern itself, so imperfections in the medium or damage to the material would not cause the information to be lost.¹ However, the information would be noisy. The hologram can be destroyed by illumination with one of the write beams or by illumination with another laser energetic enough to excite the charge out of the traps. Heating the sample will also erase the grating.

Defects play a very important role since the photorefractive effect requires the generation of carriers and the subsequent trapping of those carriers. At room temperature, shallow traps will contribute to gratings with a short lifetime, and deep traps will contribute to long lasting gratings. For optical storage, it is desirable to have deep traps for long lasting holograms. However, for an optical switch, a very fast decay is desirable so shallow traps are desirable. The mobility determines the speed of the response. High photosensitivities are desirable so relatively low light intensities can be used to generate carriers.

Temperature, dielectric constant, absorption coefficient, electro-optic coefficient, depth and concentration of donors and acceptors, mobility, and properties of the incident light including intensity, wavelength, and time of exposure, determine the photorefractive response. With the electro-optic coefficient given and no external electric field applied, the strength of the grating at steady state depends upon the internal electric field which in turn depends on the dielectric constant and the concentration of traps.

The sillenites, BGO, BSO, and BTO, are faster and require a lower light intensity than several other photorefractive materials. However, they have a smaller electro-optic coefficient resulting in smaller index changes.^{11,14}

1.2 Crystal Structure

BGO, BSO, and BTO have the body centered cubic (bcc) structure known as sillenite¹⁴, initially associated by Sillen to the γ -phase of Bi_2O_3 .¹⁷ The lattice constant of BGO is 10.145 Å.¹⁸ The crystals belong to the space group I23, corresponding to a two fold symmetry along the cube axis, and a three fold symmetry along the body diagonal. The complicated structure has 66 atoms in the cubic cell. However the germanium, silicon, or titanium atom occupies a simple site. It is tetrahedrally bonded to four oxygen atoms. The tetrahedral site is at the center and the eight corners of the unit cell. The bismuth atoms are bonded to seven oxygen atoms in what may be thought of as a distorted octahedron. Each Bi-O distance and O-Bi-O angle is different. The atomic positions of each atom can be found in the paper by Abrahams, Jamieson, and Bernstein.¹⁹

1.3 Material Properties

BGO and BSO crystals are usually grown by the Czochralski (Cz) method from a stoichiometric ratio, a melt growth technique, and are amber in color. BTO melts incongruently and it is grown from non-stoichiometric melts using the top seeded solution growth (TSSG) or flux method. Excess Bi_2O_3 in the melt acts as a flux. BTO has the same amber color as BGO and BSO. The amber color is due to a deep electron donor

with an absorption shoulder extending from about 2.5 eV to the band edge. Undoped Cz BGO and BSO are n-type, meaning electrons dominate the photocurrent when light is incident.²⁰ BSO grown by a hydrothermal method, a solution growth technique, is colorless.^{21,22} Hydrothermal BTO has the normal amber coloration;²² this will be explained later. Interestingly, Cz BSO crystals pulled from melts of hydrothermal material show the characteristic amber color. This suggests that the absorption shoulder is from an intrinsic growth defect and not an impurity.²¹

Hou, Lauer, and Aldrich first suggested that the absorption shoulder is due to a germanium (or silicon or titanium) vacancy since it was known that excess bismuth is present in the crystal.²⁰ Oberschmid proposed a different model.²³ He suggested a Bi_M center where M stands for Ge, Si, or Ti. The Bi_M center consists of a bismuth atom sitting on a M site. M vacancies were discounted for thermodynamic reasons. The work of Craig and Stephenson supports this possibility.²⁴ They found that the compound $\text{Bi}_{25}\text{FeO}_{40}$, which perhaps is better expressed as $\text{Bi}_{24}\text{BiFeO}_{40}$, has the same structure as BGO with Fe on one Ge site and Bi on the other Ge site in the bcc unit cell. More recently, Reyher et al.²⁵ and Briat et al.²⁶ have used optically detected magnetic resonance to confirm the existence of the anti-site bismuth defect. They found that it consists of a highly covalent tetrahedrally coordinated Bi^{3+} with a hole trapped on one of the adjacent oxygen atoms. Since the bonding only uses three of bismuth's electrons, the anti-site bismuth behaves as a donor. The presence of the hole suggests that the center can also act as an acceptor. The absorption shoulder consists of absorption from the hole, which acts as a small polaron,²⁷ and electronic transitions from the anti-site bismuth to the conduction band.

Doping the sillenites with aluminum or gallium removes the absorption shoulder.^{20,22,23,28-32} Aluminum and gallium most likely replace germanium (or silicon or titanium) since most impurities will occupy the tetrahedral site.¹⁴ Aluminum and gallium will act as acceptors taking one of the electrons from the deep donor, and since bismuth prefers a 3+ or 5+ valence state, the other electron fills the hole. Since the hole is absent and there are no electrons to be photoexcited, the absorption shoulder is absent. Aluminum and gallium doped BGO crystals are p-type photoconductive.^{20,28} Doping the sillenites with phosphorous also removes the absorption shoulder.^{28,33} Phosphorous will replace germanium (or silicon or titanium) and act as a donor. The extra electron from phosphorous will fill the hole on the anti-site bismuth removing the absorption shoulder. Phosphorous doped BGO is n-type photoconductive.²⁸

The band gap of BGO is approximately 3.25 eV at room temperature. The band gap of BSO is also approximately 3.25 eV at room temperature and increases to approximately 3.4 eV at 80 K. The band gap of BTO is approximately 3.1 eV at room temperature. The sillenites are optically active with both left and right handed rotations seen. The sillenites are also piezoelectric. A summary of several material properties for the sillenites is given in Table 1.1.

Iron is often an unwanted trace impurity in the sillenites. Wardzynski, Baran, and Szymczak³⁴ and von Bardeleben³⁵ have reported their results of an EPR study on BGO and BSO doped with iron. They concluded that iron replaces germanium and silicon and is in a 3+ (d^5) valence state. Jani and Halliburton reported the same EPR signal in undoped BGO and BSO and attributed the signal to iron.³⁶ Martin, Foldvari, and Hunt found that the low temperature photochromic spectra of BGO and BGO:Fe are very

Table 1.1 Material Properties of the Sillenites Compiled From Reference 14.

	BGO	BSO	BTO
Dielectric Constant	38.7	56	47
Refractive Index			
488 nm	2.650	2.650	
514 nm	2.615	2.615	
633 nm	2.530	2.530	2.58
Rotary Power			
488 nm	45 ° mm ⁻¹	44 ° mm ⁻¹	14 ° mm ⁻¹
514 nm	38 ° mm ⁻¹	38 ° mm ⁻¹	11 ° mm ⁻¹
633 nm	22 ° mm ⁻¹	22 ° mm ⁻¹	6 ° mm ⁻¹
Optical Bandgap at RT	3.25 eV	3.25 eV	3.1 eV
Electro-optic Coefficient, r	3.8 × 10 ⁻¹² m/V	4.1 × 10 ⁻¹² m/V	5.2 × 10 ⁻¹² m/V
Lattice Constant	10.145 Å	10.102 Å	10.175 Å
Piezoelectric Constant	3.39 × 10 ¹¹ C/N	4.5 × 10 ¹¹ C/N	4.82 × 10 ¹¹ C/N
Melting Point Temperature	1173 K	1198 K	1153 K
Dark Resistivity	5.3 × 10 ¹⁵ Ωcm	7.5 × 10 ¹⁵ Ωcm	

similar, which suggests that there is some iron in the undoped sample.²⁸ Baquedano, Lopez, and Cabrera reported a similar EPR signal in undoped BSO and attributed it to an intrinsic hole.³⁷ Wardzynski et al. had to subtract the EPR signal due to iron when studying the ESR signal of BGO:Cr and BSO:Cr.³⁸ Again, iron was an unwanted impurity.

Sillenite crystals have many defects and their material properties vary between crystals grown at different locations, and even crystals grown at the same location. The defects are most likely point defects such as impurities and anti-site defects. A number of point defect studies including thermally stimulated conductivity, thermoluminescence, photoluminescence, EPR, and the photochromic response, and material properties measurements such as absorption spectra, electro-optic coefficient measurements, and mobility measurements have been carried out.^{20-23,25,26,28-64}

1.4 Dissertation Project

This project involves the investigation of doping BGO with chromium and manganese and observing how these dopants affect the photochromic and photorefractive response of BGO. Chromium and manganese are transition metals and should introduce deep trapping states into the material. Chapter 2 discusses the crystal growth and sample preparation for the samples used in this study.

The absorption spectra and the photochromic response of BGO:Cr and BGO:Mn are found in Chapter 3. Absorption spectra were taken at 300 K and 10 K. The wavelength of light which cause the photochromic effect and the temperatures at which the photo-induced absorption anneal are reported.

Chapter 4 discusses the photorefractive effect in BGO:Cr and BGO:Mn. Gratings were written at various temperatures starting at 300 K and ending at 500 K. The thermal stability of gratings were determined by writing a grating at room temperature and monitoring the grating as the sample was slowly heated to 500 K. Finally, gratings were written at room temperature and monitored for 24 hours while being held at this temperature.

A simple model for the kinetics of grating formation and decay in photorefractive materials is presented in Chapter 5. The model presented is the standard semiconductor band transport model and is solved numerically using a finite difference technique in a spreadsheet such as Excel or Quattro Pro.

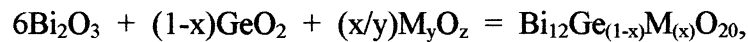
Chapter 6 summarizes the work performed in this study and provides a few possible directions for future work related to this study.

CHAPTER 2

CRYSTAL GROWTH AND SAMPLE PREPARATION

Ballman first grew single crystals of BGO and BSO in 1966 using Bi_2O_3 and GeO_2 or SiO_2 in a 6:1 ratio using the Czochralski method.⁶⁵ Brice, Hight, Hill, and Whiffin found that this ratio can be varied slightly,⁶⁶ but this will affect the number of defects and consequently, the photorefractive behavior. BTO cannot be grown using the Czochralski method because Bi_2O_3 and TiO_2 melt incongruently.⁶⁷ BTO can be grown using the top seed solution growth (TSSG) or flux method.^{22,68} This is similar to the Czochralski method except that Bi_2O_3 and TiO_2 are not mixed together in a stoichiometric ratio. Excess bismuth is added to the melt and acts as a flux. Excess bismuth is also present when growing BTO hydrothermally since it is grown with Cz material.²² This causes hydrothermal BTO crystals to show the same amber color seen in Cz crystals. Hydrothermal BSO is grown from a stoichiometric ratio and is colorless.^{21,22} Phase diagrams for the sillenites can be found in several of the above references⁶⁶⁻⁶⁸ or in the review paper.¹⁴ Several additional papers on various aspects of the growth of the sillenites have been published.⁶⁹⁻⁷⁵

The crystals used in this study were grown by the Czochralski method at the Crystal Growth Laboratory located at Oklahoma State University (OSU) and Rome Laboratories, Hanscom Air Force Base, Massachusetts. High purity starting materials (greater than 5-9s purity) were placed in a platinum crucible according to the following formula:



where x is the doping amount and M_yO_z was either Cr_2O_3 or MnO_2 . The mass of the starting materials was usually 120 grams. At OSU, the crucible was then placed in a flowing oxygen atmosphere at 800 °C for 48 hours. Next, the crucible and starting material was transferred to the growth chamber. For samples grown at OSU, the crucible was inductively heated using a Lepel 20 kW 450 Hz Rf generator. Resistance heating was used at Rome Laboratories. A BGO seed crystal oriented in the (100) direction was attached to the pull rod. The growth process was computer controlled. Once the starting materials were melted, the seed was dipped into the material. The seed was rotated at approximately 30 rpm. If poly-crystalline growth was present, the melt was raised to a slightly higher temperature to melt the poly-crystalline material off the seed. The seed was then dipped into the melt again. Once mono-crystalline growth was present, the pull rod was slowly raised at 1 - 1.5 mm/hr. The melt was also slowly cooled. The cool rate was changed throughout the growth process in order to change the shape of the crystal. The crystal was allowed to grow for 2 - 3 days. Once the crystal reached sufficient size, the crystal was pulled out of the melt and allowed to cool over a 48 - 72 hour period. This allowed the crystal to cool slowly and avoid cracks due to thermal stress.

At OSU, the crystal was taken out of the growth chamber and the crystal was cut into samples using a diamond saw. The samples were then polished to an optical finish. For the sample from Rome Laboratories, the crystal was sent to a commercial company for cutting and polishing. The samples used in this study were either (100) or (111). Samples were typically 1 - 1.5 mm thick. Crystal samples from OSU are identified by the date in which the growth process is started while samples from Rome Labs are labeled by their growth run. Table 2.1 shows the samples used in this study.

Table 2.1 BGO Crystals Used in this Study

Crystal ID	Dopant	Growth Location
970622	Undoped	OSU
030591	0.5% Cr	OSU
960729	0.1% Cr	OSU
971208	1% Cr	OSU
BGO44	0.5% Mn	ROME LAB
970818	1% Mn	OSU

CHAPTER 3

ABSORPTION SPECTRA AND THE PHOTOCHROMIC EFFECT

3.1 Introduction

The defects which are responsible for the photorefractive effect in the sillenites are most likely point defects. However, the various grating experiments do not directly identify these defects. Other techniques must be used in conjunction with photorefractive measurements. Looking at absorption and photochromic spectra is useful because the photochromic effect relies in part upon the same donors and acceptors that are required for the photorefractive effect.

The absorption spectrum of a material can yield very important information about that material. Vibrational and electronic states of a material can be studied by observing how the material absorbs the infrared, IR, visible, VIS, and ultraviolet, UV, portions of the electromagnetic, EM, spectrum. Exposing samples with light may yield additional information. Light can excite electronic levels in the crystal which reveal themselves in an absorption spectrum. Light can also excite charges from impurities or other defects in the

material to the conduction or valence band where they are able to move around until they are trapped at another impurity or defect resulting in a change in the absorption spectrum. In either case, this is known as the photochromic effect. Photochromic spectra, the difference between absorption spectra after and before illumination, are very useful. Photochromic spectra enhance the absorption changes caused by illumination and eliminate the absorption associated with things that do not change. In some materials, the photochromic effect may be present only at low temperature while in others the effect may occur at room temperature. Heating the sample eliminates the photoinduced absorption and returns the sample to its original state.

3.2 Experimental Procedure

Absorption spectra were taken with a Varian Cary05E UV-VIS-IR Spectrophotometer. During this study, the Cary05E was upgraded and is now essentially a Cary 500. Spectra were taken with the samples mounted on sample holders provided by Varian with double sided tape in air, on the cold finger of a CTI closed-cycle cryogenic refrigerator, and on a hot stage. All scans were taken either at 300 K or at 10 K. For scans taken in air, the samples were perpendicular to the beam; for scans taken on the cold finger or the hot stage, the samples were either perpendicular or at a 45° angle to the beam. The 45° angle allowed the sample to be exposed to light without removing it from the sample compartment. The monochromatic source used for excitation consisted of an Oriel 200 W Xe lamp and a Spex minimate monochromator with 2.5 mm slits. The samples were illuminated from one side only. The samples were exposed for an hour at

each wavelength. Although the intensity was not the same for each wavelength, an hour of exposure at each wavelength should have saturated the sample. After each experiment, the samples were annealed at 450 °C for several hours to rid all effects of the previous exposure.

Low temperature and high temperature isochronal anneals were also carried out to determine the thermal stability of the defects causing the photochromic absorption. For the low temperature photochromic response, an absorption spectrum was taken at 10 - 15 K. The sample was exposed to light and another absorption spectrum was taken. The sample was then heated to the desired temperature and allowed to cool back down to 10 - 15 K where a new spectrum was recorded. This process was repeated in approximately 50 K increments up to 300 K. A similar procedure was used for the high temperature photochromic response. An absorption spectrum was taken at 300 K. The sample was exposed to light, and another absorption spectrum was taken. The sample was then heated to the desired temperature, allowed to cool to 300 K, and another absorption scan was taken. The process was continued up to 500 K.

Data were taken from 2500 to 350 nm every 1 nm with a signal averaging time of 0.5 seconds. The data from the spectrophotometer were either transmission or absorbance which are related by

$$T = 10^{-A}, \quad (2.1)$$

where T is the transmission and A is the absorbance. The absorption coefficient, α , is related to T by

$$\alpha = \frac{-\ln(T)}{t}, \quad (2.2)$$

where t is the thickness of the sample in cm. If the sample was at a 45° angle to the beam, it was necessary to multiply the thickness by $\sqrt{2}$ to account for the increased thickness. All absorption spectra plotted on the same graph were normalized to the same value at 2500 nm so direct comparisons could be made. One final note, to determine the energy of a photon of a particular wavelength, divide 1240 by the wavelength in nm. For example, a photon with an energy of 2 eV has a wavelength of 620 nm.

3.3 Results And Discussion

3.3.1 Chromium

Figure 3.1 shows the room temperature and low temperature absorption spectra of undoped BGO and samples doped with 0.1%, 0.5%, and 1% Cr. The addition of chromium causes an increase in the absorption coefficient starting around 1100 nm in the IR and continues on to the band gap. The small bump around 1375 nm is due to the windows on the cold head of the cryogenic refrigerator. Undoped BGO has a amber color due to the absorption shoulder from about 500 nm to the band edge. Doping with chromium caused the crystals to turn a reddish brown color due to strong absorption throughout visible spectrum except in the red. This is observed in the absorption spectra by noticing the lower absorption coefficient around 650 nm. As more chromium is added to BGO, the absorption due to chromium gets larger. Also notice at 10 K, the absorption due to chromium sharpens up, and the band edge gets larger. Figure 3.2 shows the low temperature absorption spectra in Figure 3.1 on an expanded scale.

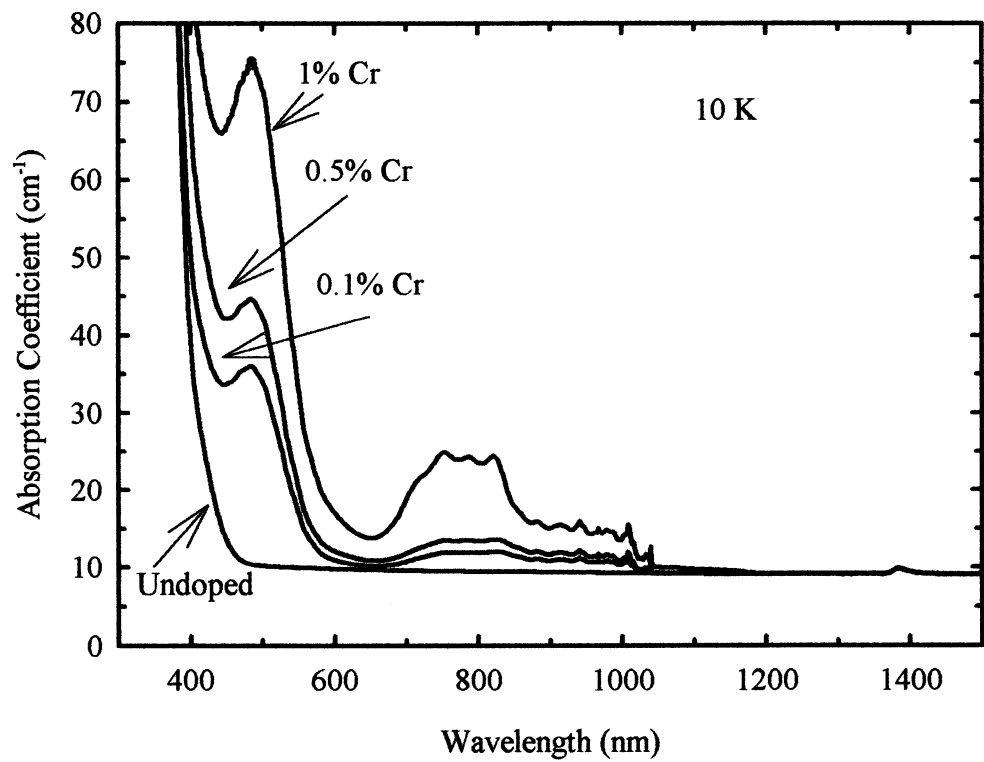
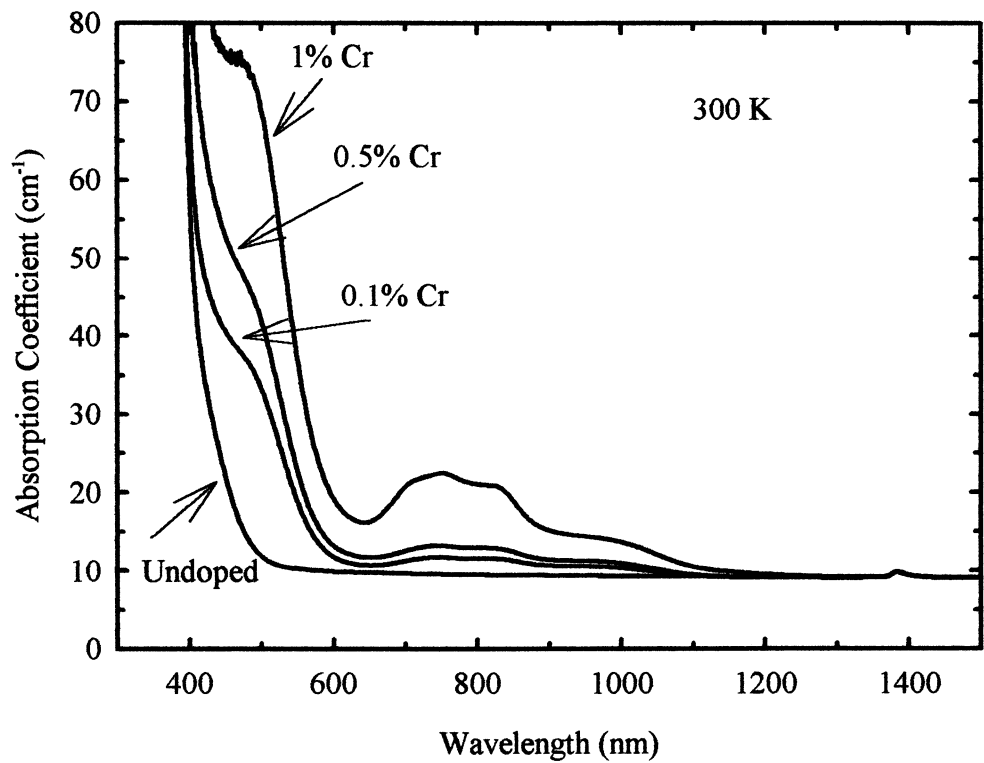


Figure 3.1 The absorption spectra of BGO and BGO:Cr at 300 K and 10 K.

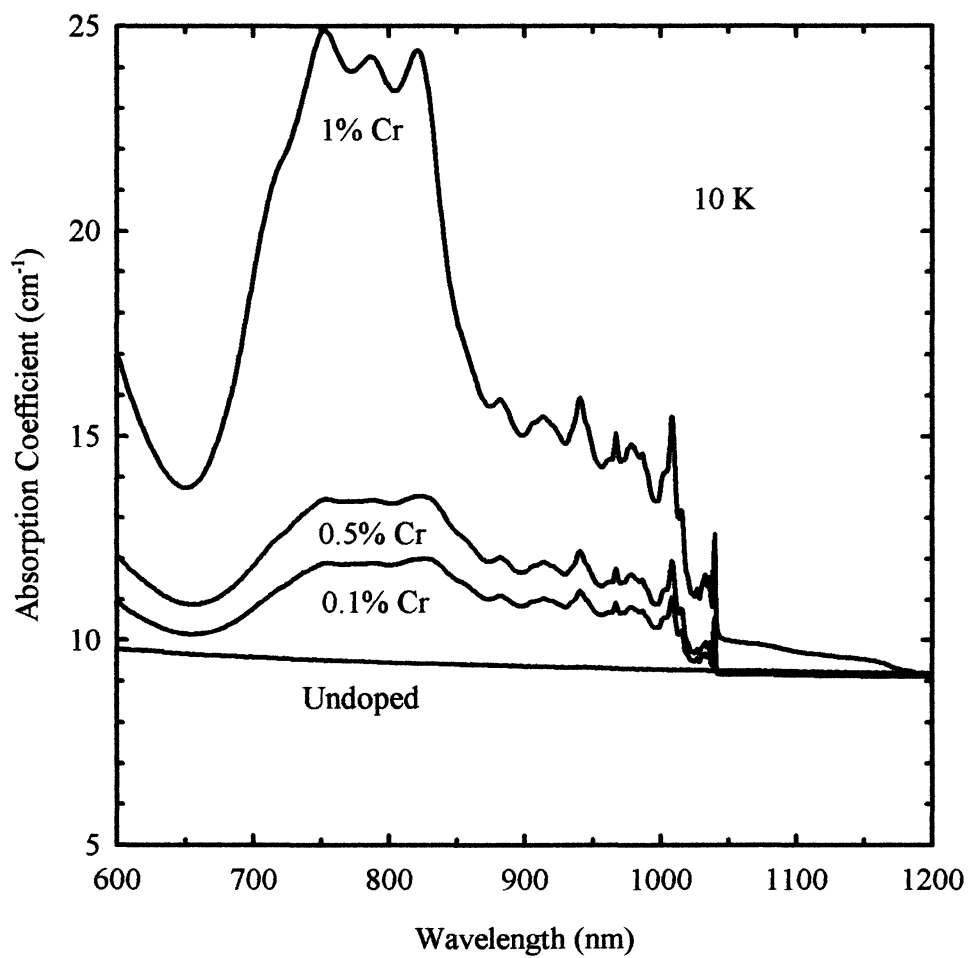


Figure 3.2 The absorption spectra of BGO and BGO:Cr at 10 K on an expanded scale.

Figure 3.3 shows the absorption spectra of the 0.1% Cr sample before and after exposure to 442 nm light for 1 hr at room temperature. The exposure causes the absorption coefficient to increase beginning in the IR and continuing throughout the visible. This occurs in the other two samples as well. In undoped, Fe, Ga, Al, and P doped BSO or BGO, the photochromic effect occurs only at low temperature, not room temperature.³⁰⁻³³ Subtracting the “before” spectra from the “exposed spectra” gives the photochromic spectra. This is shown in Figure 3.4 for all three samples. The photochromic spectra for the 0.1% and 0.5% Cr are very similar in size and shape. The photochromic spectrum for 1% Cr sample is smaller than the other two BGO:Cr samples but has the same overall shape. The 1% Cr spectrum was truncated at around 500 nm due to a large amount of noise in the spectrum although there is a peak present similar to the peak seen in the 0.1% and 0.5% Cr samples.

Figure 3.5 compares the room temperature and low temperature photochromic spectra for the 0.1% Cr sample. The sample was illuminated with 442 nm light for 1 hr at room temperature. The slight differences between the 300 K photochromic spectra of shown in Figure 3.4 and Figure 3.5 are most likely due to different sample mounts. As expected, the low temperature spectra resolve and sharpen up the peaks seen at room temperature. The data were truncated around 450 nm due to noise present in the spectra. The 425 nm peak seen in Figure 3.4 was still present. The 0.5% Cr and 1% Cr samples give similar spectra.

Excitation with other wavelengths besides 442 nm will induce the photochromic effect in BGO:Cr. Figure 3.6 shows the photoinduced absorption change at 700 nm versus excitation energy. This shows that photoinduced absorption begins near 1.8 eV,

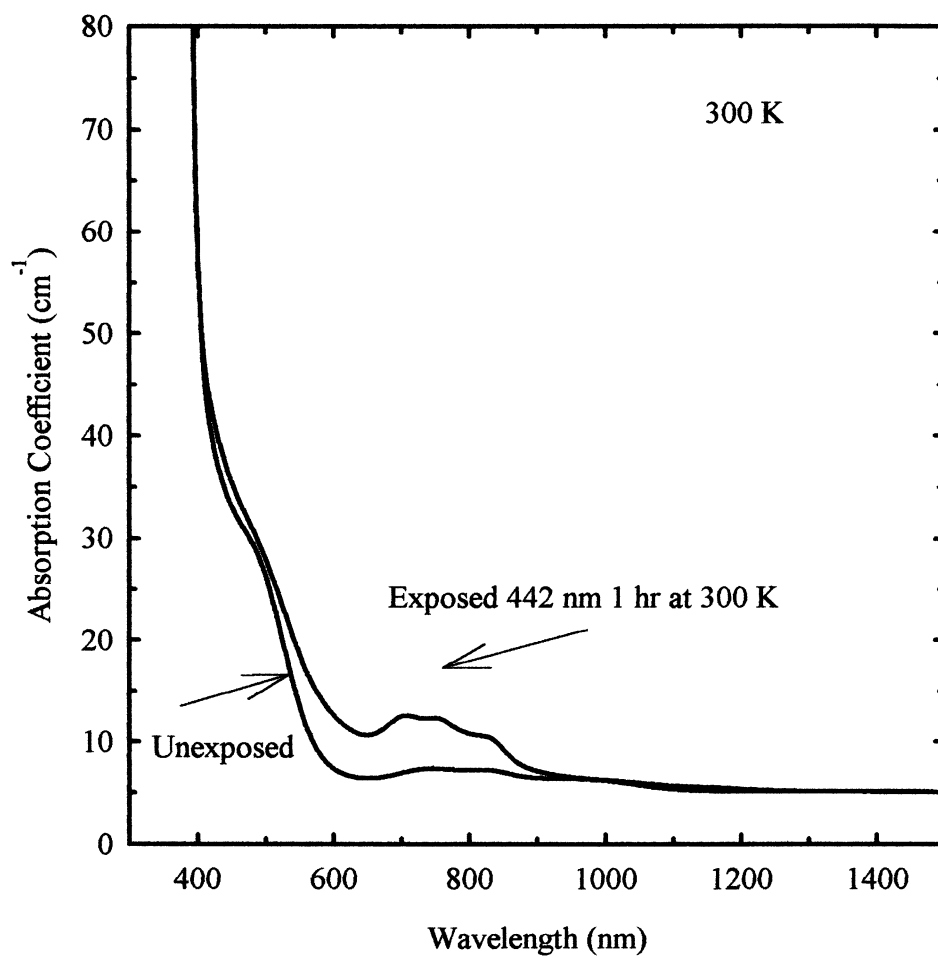


Figure 3.3 The photochromic effect in BGO:0.1%Cr. The sample was exposed to 442 nm light for 1 hr at 300 K.

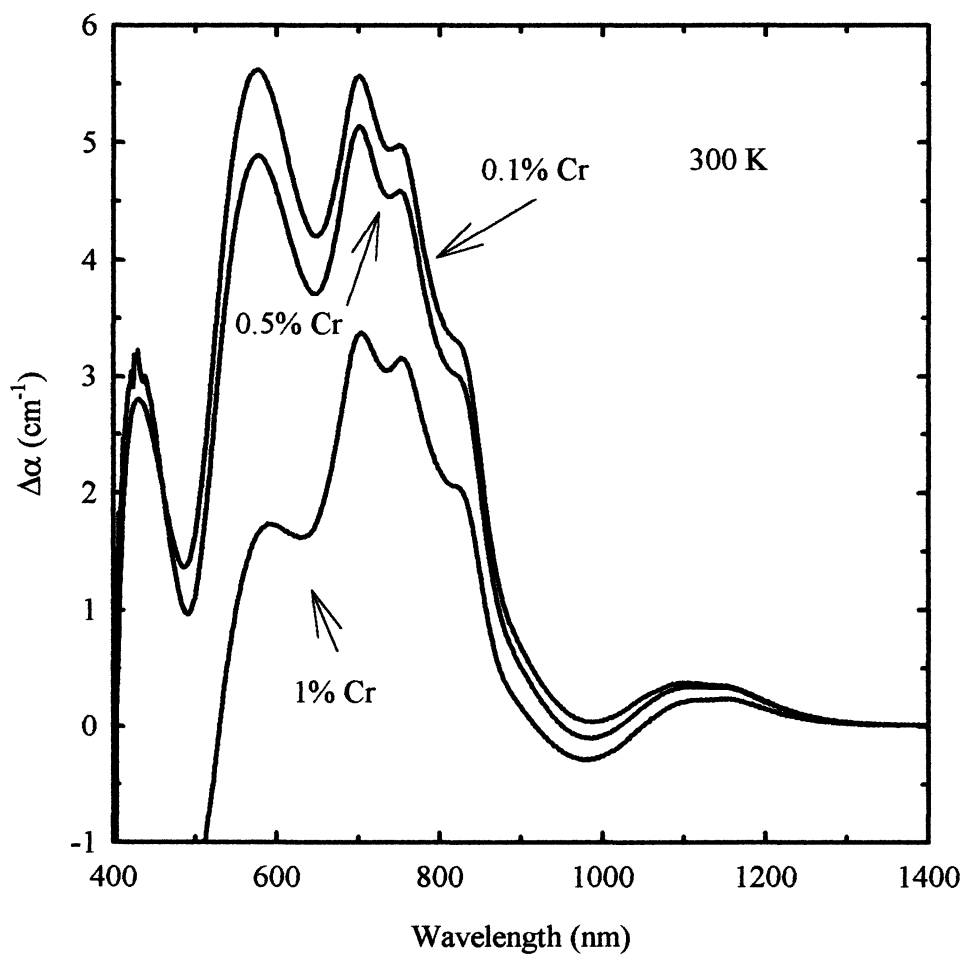


Figure 3.4 The photochromic spectra of BGO:Cr. The samples were exposed to 442 nm light for 1 hr at 300 K.

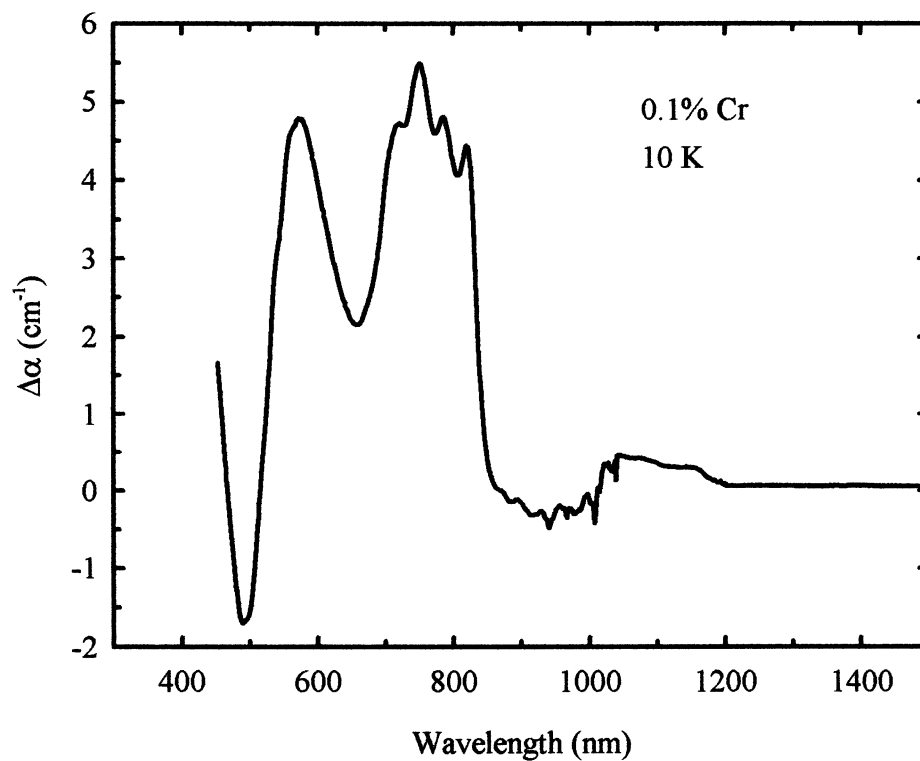
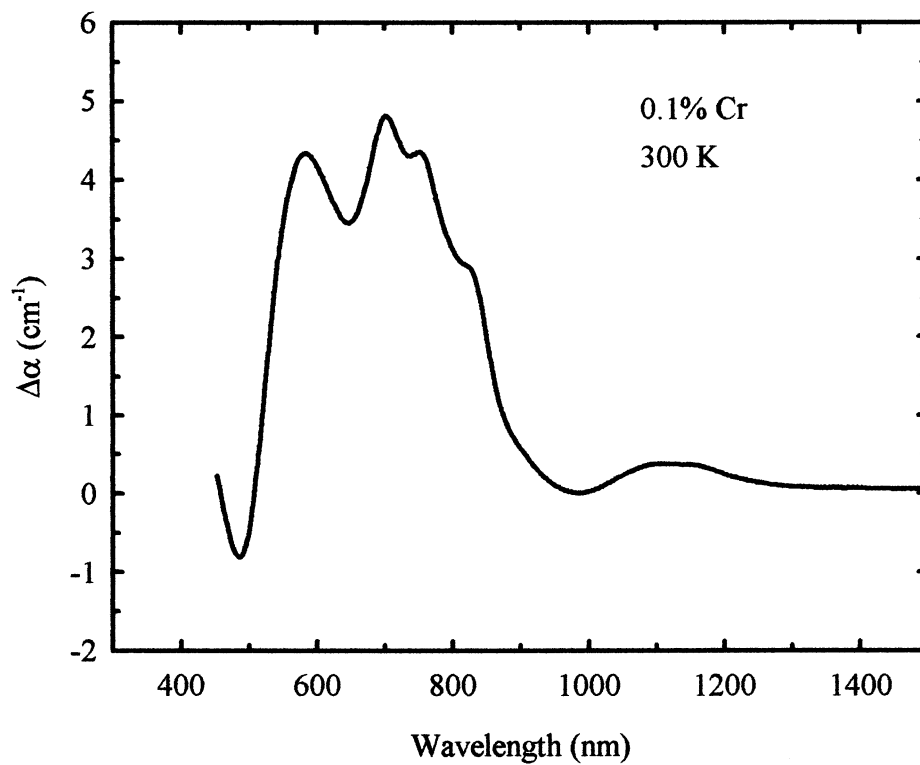


Figure 3.5 The photochromic spectra of BGO:0.1% Cr at 300 K and 10 K. The sample was illuminated with 442 nm light for 1 hr at 300 K.

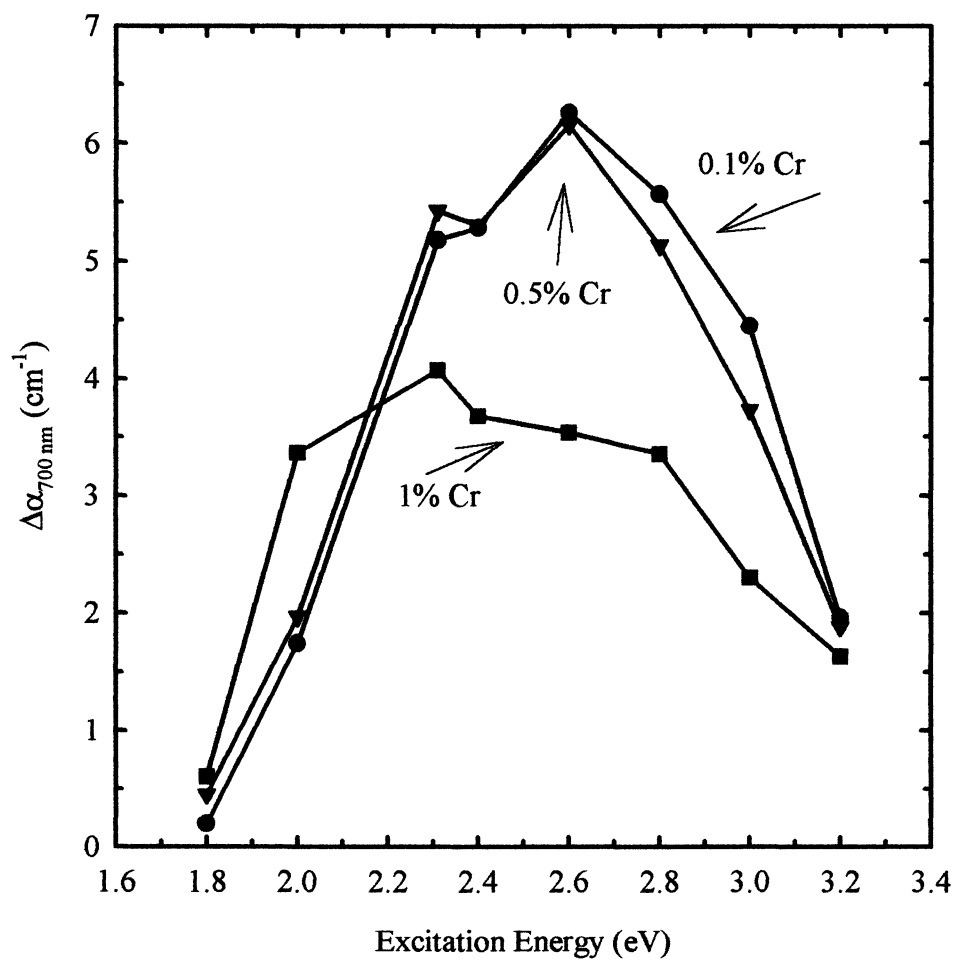


Figure 3.6 Excitation spectra for the BGO:Cr samples.

689 nm, for all three samples and falls off near 3.2 eV, 388 nm, for all three samples. Part of the fall off is due to the incident light not fully penetrating the sample.

Isochronal anneals were also carried out to determine the thermal stability of the defects causing the photoinduced absorption. Figure 3.7 shows the low temperature isochronal anneal. The sample was exposed to 413 nm light at 10 K. Comparing Figure 3.7 with Figure 3.5 shows that the photochromic spectrum produced by exposing the sample at low temperature is nearly identical to the photochromic spectrum obtained by exposing at room temperature and then cooling to 10 K. The low temperature isochronal anneal showed almost no decay as the sample was heated to room temperature which is why only the 10 K and 293 K spectra are shown in Figure 3.7. Figure 3.8 shows the high temperature isochronal anneal. The sample was exposed to 442 nm light at 300 K. The high temperature isochronal anneal shows that there is not much additional decay until the sample is around 425 K. The photoinduced absorption decays rapidly above this temperature. The different peaks in the photochromic spectra also appear to decay at the same rate. This suggests the photochromic effect is due to the same defect. The inset shows the decay at 700 nm.

Several research groups have published papers discussing the sillenites doped with chromium.^{28,38,76-95} Unfortunately, in some cases there was no discussion about the valence state or the location of chromium, and in the other cases there is disagreement over the valence state of chromium before and after exposure to light and the location of chromium. In BGO, chromium can either replace bismuth in the distorted octahedral site or germanium in the tetrahedral site. Chromium could also be in an interstitial site.

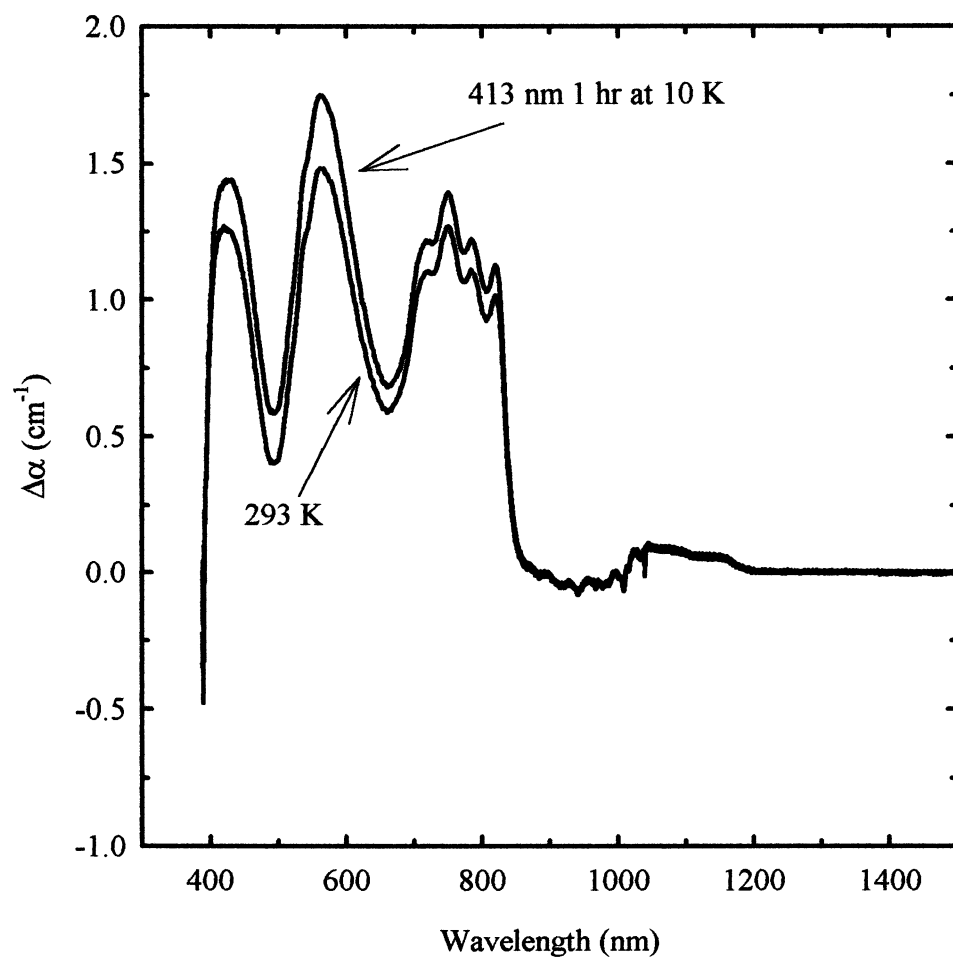


Figure 3.7 The low temperature photochromic anneal of BGO:0.1%Cr. The sample was exposed to 413 nm light for 1 hr at 10 K.

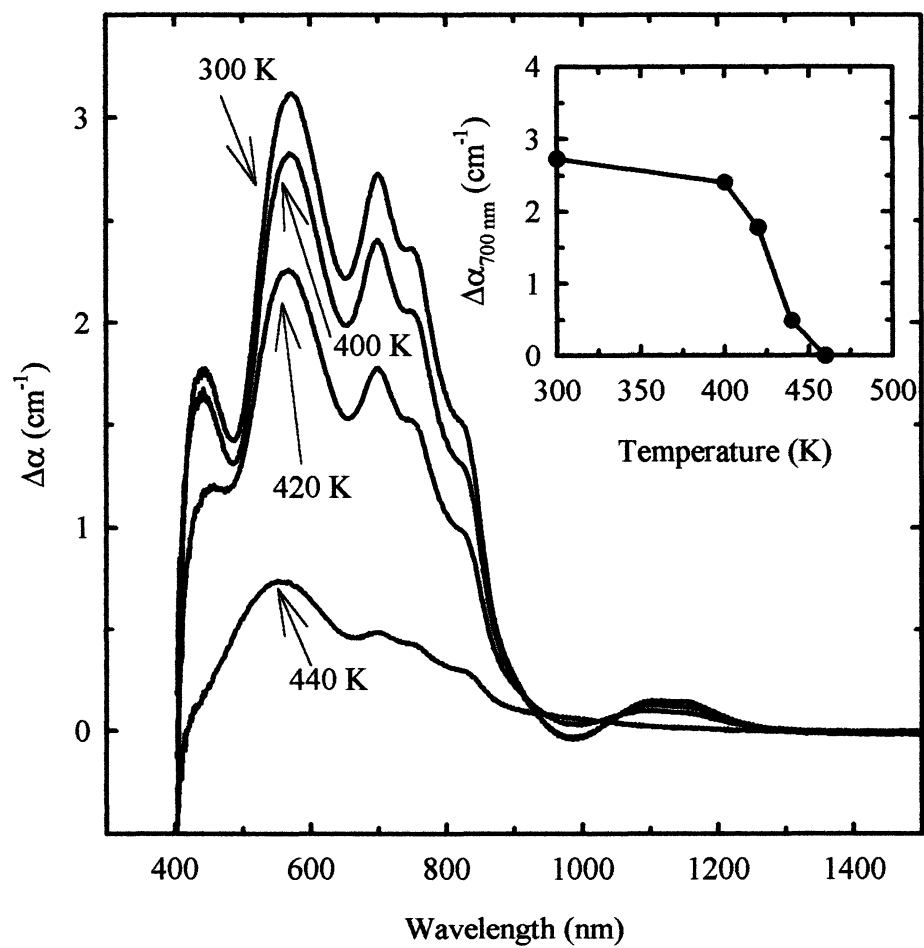


Figure 3.8 The high temperature photochromic anneal of BGO:0.1%Cr. The sample was exposed to 442 nm for 1 hr at 300 K. The inset shows the decay of the photo-induced absorption at 700 nm.

EPR measurements show that most impurities occupy the germanium site.¹⁴ The electronic configuration of atomic chromium is $4s^13d^5$ since a half-filled d shell is preferred. When chromium is added to the melt, chromium's 4s electron can join three 3d electrons to form $4(sp^3)^4$ hybrid orbitals to bond with the adjacent oxygen atoms. Wilson's unpublished results show that this happens when chromium replaces silicon in the SiO_4 group in quartz.⁹⁶ This is a highly-covalent tetrahedrally-coordinated site. Two electrons are left in the d-shell giving the appearance of a $Cr^{4+} (d^2)$ in a tetrahedral site.

Wardzynski et al. reported the EPR and absorption spectra of BGO:Cr.³⁸ Their absorption spectra agree with the results here. Using EPR, they confirmed that chromium occupies a tetrahedral site. They reported that BGO:Cr has an EPR spectrum that is indicative of either a $d^5 (Cr^{1+})$ configuration or a $d^2 (Cr^{4+})$ configuration. The d^5 configuration was ruled out since all transitions would be spin forbidden resulting in no optical absorption. Therefore, they concluded Cr^{4+} is present in BGO:Cr.

In the scintillator material, $Bi_4Ge_3O_{12}$, prepared from a different ratio of Bi_2O_3 and GeO_2 , chromium has been introduced as an impurity.^{79,97,98} $Bi_4Ge_3O_{12}$, like BGO, has germanium tetrahedrally bonded to four oxygen atoms. Reported in the above papers, chromium replaces germanium and is in a $4+, d^2$, valence state.

Further evidence for the existence of $Cr^{4+} (d^2)$ in the tetrahedral site lies in the recent interest of near infrared lasers by doping chromium in inorganic crystals.⁹⁹⁻¹¹³ The laser action is from a $Cr^{4+} (d^2)$ ion. Chromium enters a tetrahedral structure with four oxygen atoms just like is present in the sillenites. Other d^2 transition metal ions in tetrahedral sites besides chromium such as vanadium and manganese are of interest for

lasers also.¹¹²⁻¹²³ The absorption spectra of d^2 ions in tetrahedral sites are very similar to what is seen when chromium is introduced into the sillenites.^{101,103,105,107-112,117,120,124-129}

Wardzynski et al.³⁸ observed that shining light on the sample increased the EPR signal as well as the absorption coefficient, as was observed here. This implies more Cr^{4+} is produced. The light is exciting charge into the conduction band or valence band where it can be trapped somewhere else. So there should be either a mixture of Cr^{4+} and Cr^{3+} or a mixture of Cr^{4+} and Cr^{5+} before exposure to light since most likely illumination changes the charge state by one. Wardzynski et al. reported that the most likely transition is Cr^{5+} to Cr^{4+} .³⁸ This is probably the correct interpretation. The anti-site bismuth can be an acceptor or donor. During the growth process, one of the chromium d electrons fills the hole on the anti-site bismuth producing Bi^{3+} . It is also possible that this d electron goes to some other defect. In either case, a Cr^{5+} is left behind. Excitation with light promotes an electron from either the Bi^{3+} or the other defect to Cr^{5+} producing more Cr^{4+} . This causes an increase in the Cr^{4+} absorption and the EPR signal to increase. This increase is stable at room temperature. Heating the sample to ~ 425 K allows an electron to go back to either the anti-site bismuth or to the other defect, reducing the absorption coefficient and the EPR signal.

As shown in Figure 3.4, the photochromic spectrum for the 0.5% Cr sample is slightly smaller than the photochromic spectrum for the 0.1% Cr sample. The photochromic spectrum for the 1% Cr sample is noticeably smaller. A possible explanation for this is that as more chromium is added, there is more Cr^{4+} and less Cr^{5+} present. This result is reasonable if one assumes that the amount of anti-site bismuth remains constant throughout all three samples. The 1% sample has much more Cr^{4+}

because there was only so many holes on the anti-site bismuth to fill with electrons given up the Cr^{5+} . One should also point out the absorption spectra for the samples with more chromium show more absorption so less light is fully penetrating the sample allowing less photoexcitation. The smaller photochromic spectra for the samples with more chromium is most likely due to both of these reasons.

Wardzynski and Szymczak also reported in a subsequent paper that chromium occupies an interstitial site as well and is responsible for the sharp absorption peaks in the 1100 to 850 nm region at low temperature.⁷⁷ Of course, interstitials are a possibility, as is chromium replacing bismuth in the distorted octahedral. Interstitials seem unlikely though since the unit cell is packed tightly. Also, it was observed here that part of the absorption in the 1100 to 850 nm region increased along with the other absorption due to chromium as the sample was illuminated. The photoinduced absorption also seemed to decay at the same rate, indicating only one location. However, it is possible that this low temperature absorption is a combination of absorption from chromium in the tetrahedral site and absorption from a chromium interstitial. It appears that chromium in the tetrahedral site is responsible for most of the absorption and the photochromic effect present in BGO:Cr.

3.3.2 Manganese

Figure 3.9 shows the absorption spectra of BGO doped with 0.5% and 1% Mn at 10 K and 300 K. As before, the small bump near 1375 nm is due to the windows on the cold finger. The addition of manganese causes very weak absorption in the region beginning around 1000 nm and ending near 600 nm. This weak absorption is not seen in BGO. The insets in Figure 3.9 show the absorption spectra of BGO and BGO:0.5%Mn

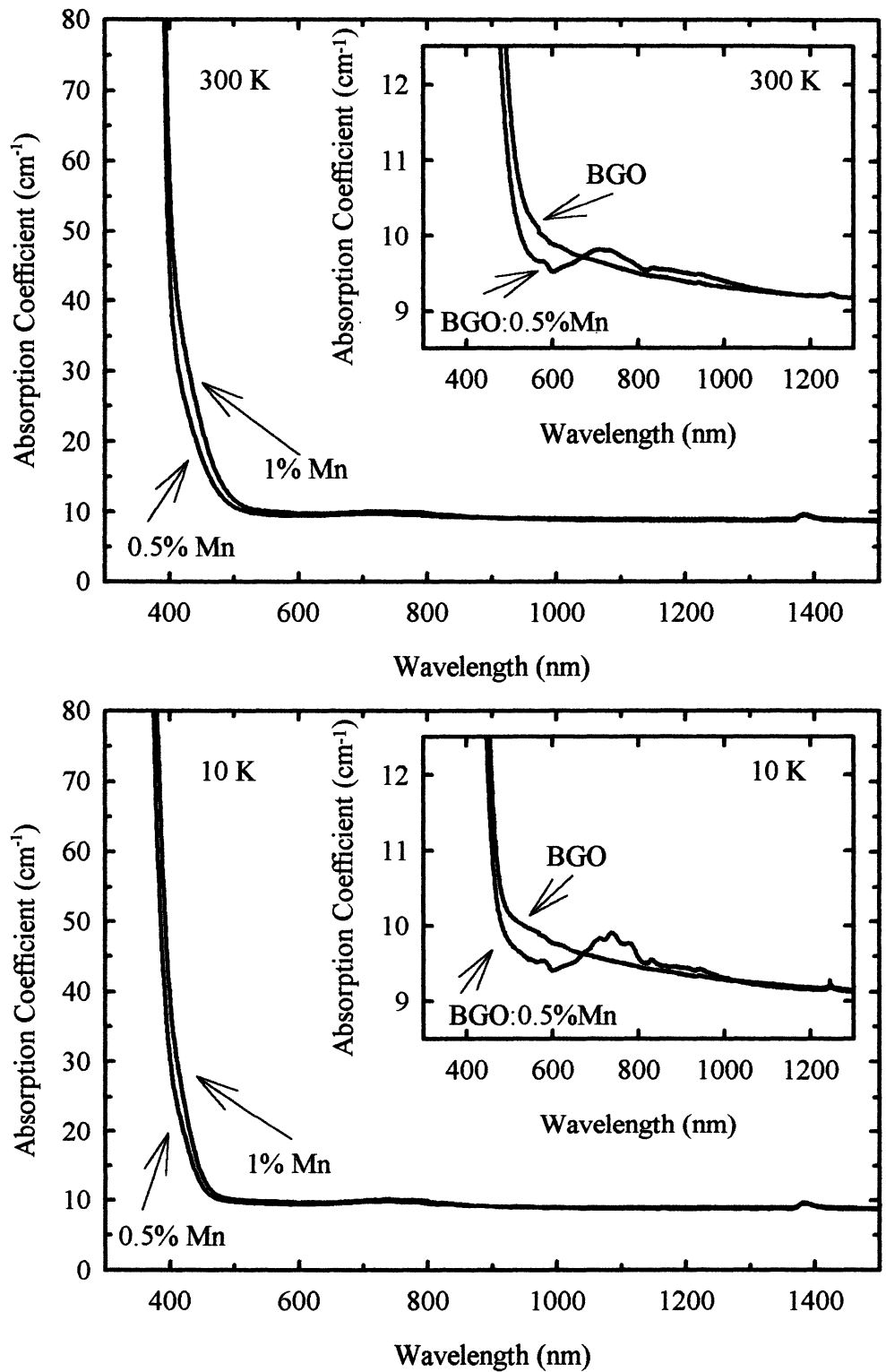


Figure 3.9 The absorption spectra of BGO:Mn at 300 K and 10 K. The insets show the absorption spectra of BGO and BGO:0.5%Mn on an expanded scale at 300 K and 10 K.

on an expanded scale. Both BGO and BGO:Mn have a weak broad peak near 1250 nm. The broad peak near 1250 nm sharpens up in the BGO:Mn sample at 10 K. Also, at low temperature, the band edge is shifted to lower wavelengths which corresponds to higher energy.

Figure 3.10 shows the absorption spectra of the 0.5% Mn sample before and after exposure to 442 nm light for 1 hr at 300 K. The inset in Figure 3.10 shows the absorption spectra of the 0.5% Mn sample before and after exposure to 442 nm light for 1 hr at 300 K on an expanded scale. The absorption coefficient increases throughout the visible. The weak absorption in the 1000 to 600 nm region due to manganese also goes away. BGO:1%Mn has a similar response. Subtracting the “before” spectra from the “exposed spectra” gives the photochromic spectra. This is shown in Figure 3.11. The samples were exposed to 442 nm light for 1 hr at 300 K. The photochromic spectra for 0.5% and 1% Mn are very similar in shape with the 1% Mn spectra larger. The photochromic spectra at 300 K appear to be a broad positive band with its peak near 500 nm and a small negative bands in the IR. Figure 3.12 compares the photochromic spectra at 300 K and 10 K for the 0.5% Mn sample. The spectra for the 1% Mn sample are similar. The slight differences between the 300 K photochromic spectra shown in Figure 3.11 and Figure 3.12 are most likely due to different sample mounts. As expected, the low temperature resolves the room temperature peak. This shows that the room temperature band consists of several bands throughout the visible which reveal themselves at low temperature. Interestingly, the low temperature photochromic spectra of BGO:Mn are similar to the low temperature photochromic spectra of undoped BGO and BGO:Fe,³⁰ except for the region around 1000 to 700 nm. In this region, the change in absorption

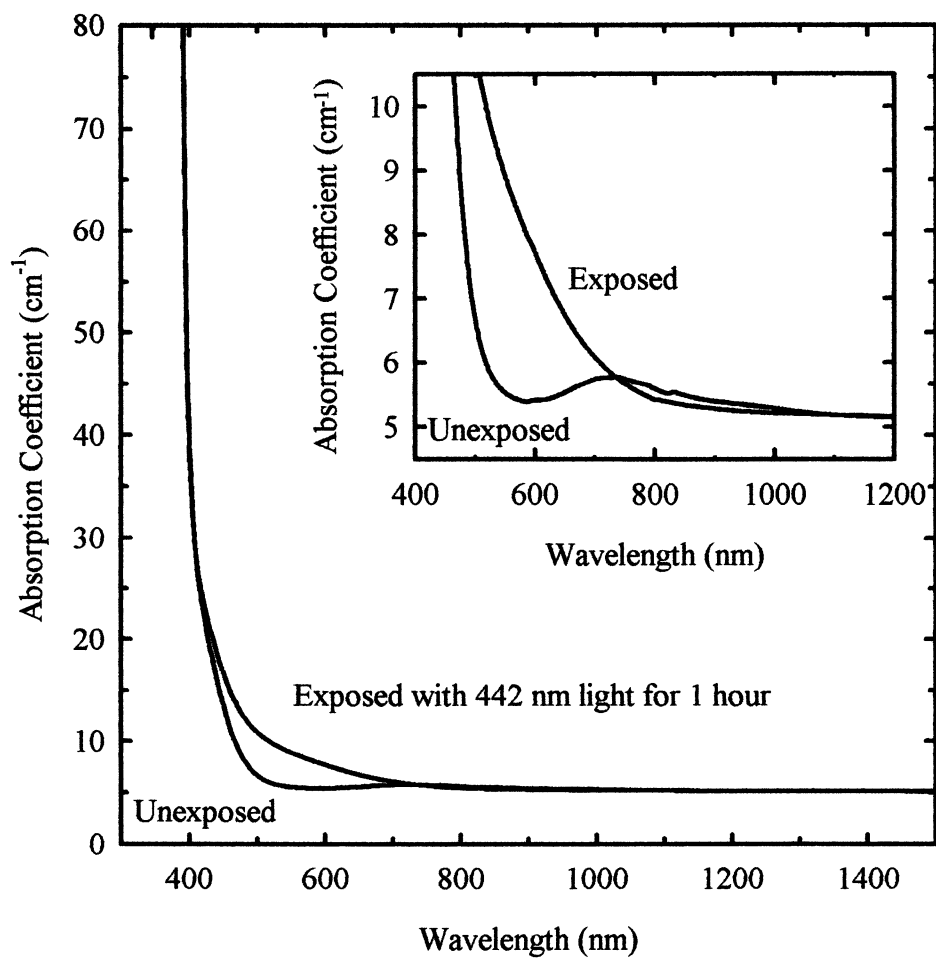


Figure 3.10 The photochromic effect in BGO:0.5%Mn. The sample was exposed to 442 nm light for 1 hr at 300 K. The inset shows the photochromic effect on an expanded scale.

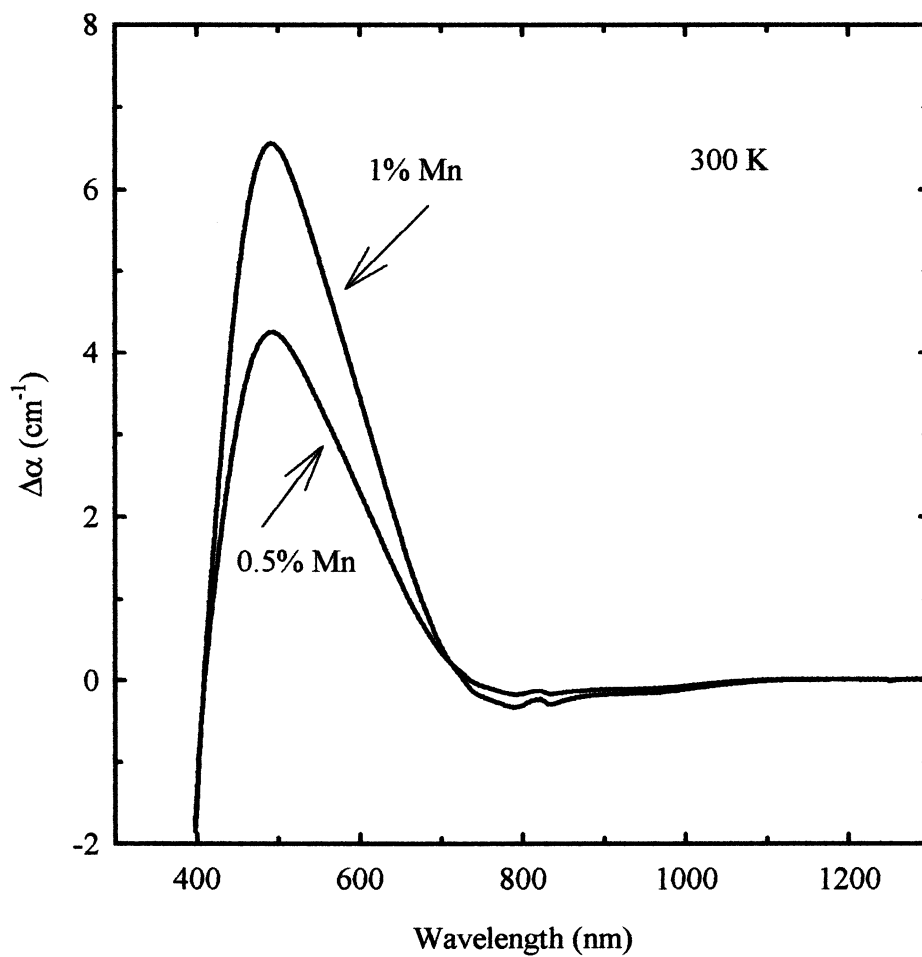


Figure 3.11 The photochromic spectra of BGO:Mn. The samples were exposed to 442 nm light for 1 hr at 300 K.

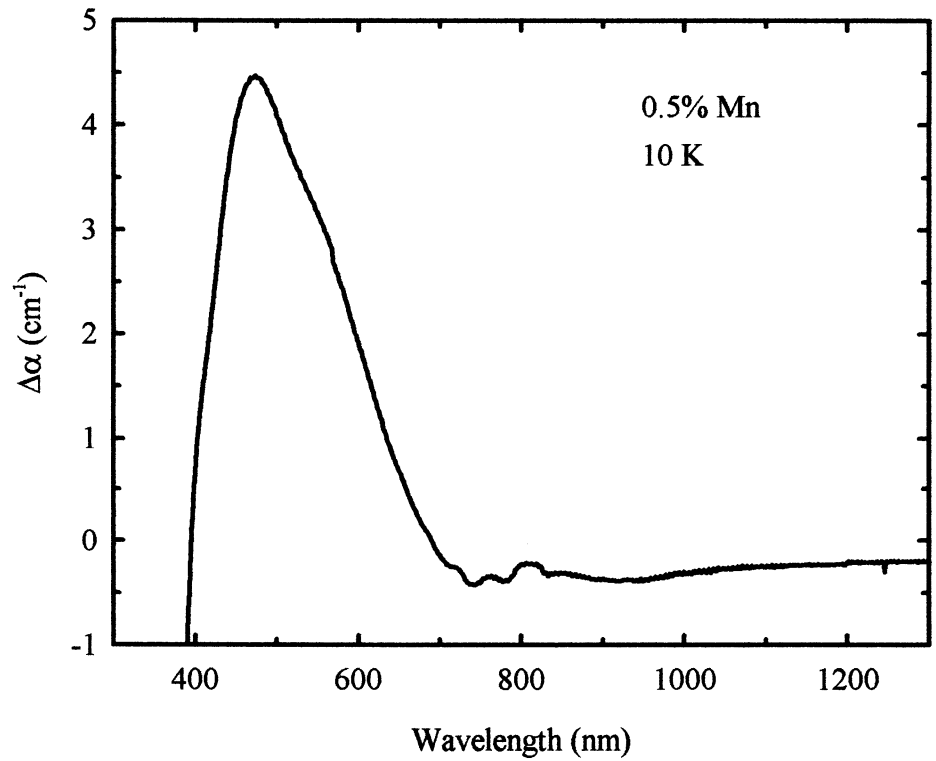
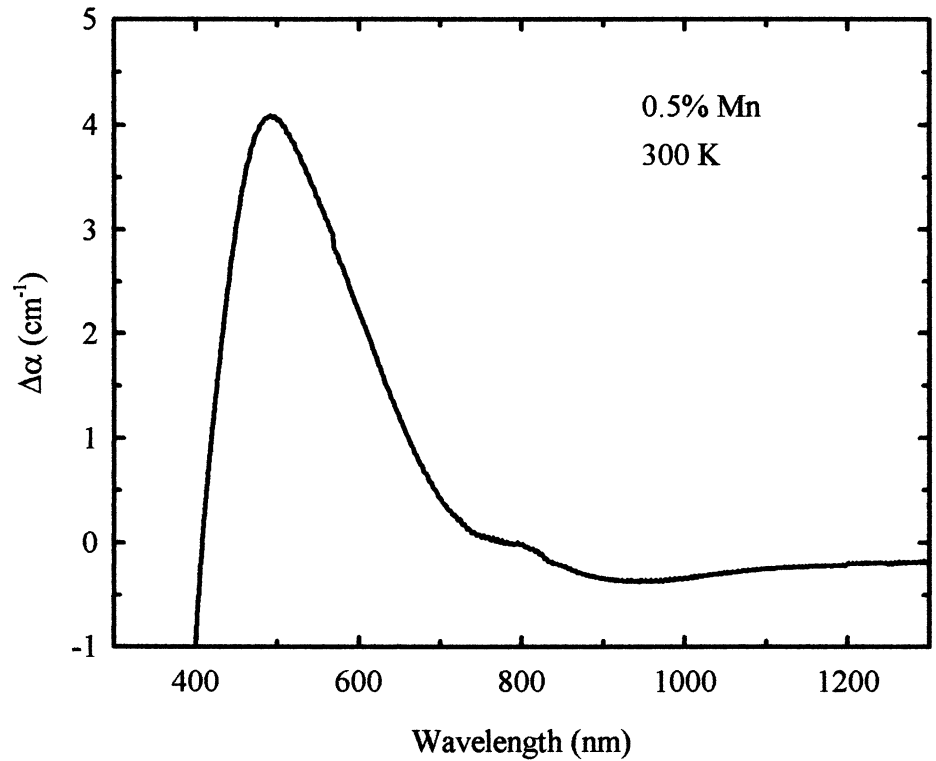


Figure 3.12 The photochromic spectra of BGO:0.5% Mn at 300 K and 10 K. The sample was illuminated with 442 nm light for 1 hr at 300 K.

coefficient is negative for BGO:Mn, but the change in absorption coefficient is positive for BGO and BGO:Fe. The sharp peak at 1250 nm seen in BGO:Mn also goes away with exposure to light. This is seen in the 10 K photochromic spectrum in Figure 3.12.

Excitation at other wavelengths besides 442 nm will induce the photochromic effect in BGO:Mn. Figure 3.13 shows the photoinduced absorption change at 496 nm versus excitation energy. This indicates that photoinduced absorption begins at 2 eV, 620 nm, and falls off near 3.2 eV, 388 nm. Part of the fall off is due to the incident light not fully penetrating the sample.

Isochronal anneals were also carried out to determine the thermal stability of the defects causing the photochromic absorption. Figure 3.14 shows the low temperature isochronal anneal. As pointed out earlier, Figure 3.12, the low temperature photochromic spectrum looked similar to that of undoped and iron doped BGO. In fact, Figure 3.14 looks even more like the photochromic spectra for BGO and BGO:Fe. This can be seen more clearly by graphing the photochromic spectrum versus energy as in Figure 3.15 and comparing to the spectra present in the paper by Martin et al.³⁰ Figure 3.14 shows there is a positive change in absorption coefficient in the region 700 nm to 1000 nm, unlike Figure 3.12. Exposing the sample at 300 K and cooling the sample to 10 K gives a slightly different photochromic spectrum than the one found if the sample is exposed at 10 K. However, as the sample is heated, the change in absorption coefficient in the 700 nm to 1000 nm region goes from positive to negative. The photochromic spectrum now appears like the one seen in Figure 3.12. Also, part of the photoinduced absorption centered near 500 nm goes away as the sample is heated to 300 K. This could indicate

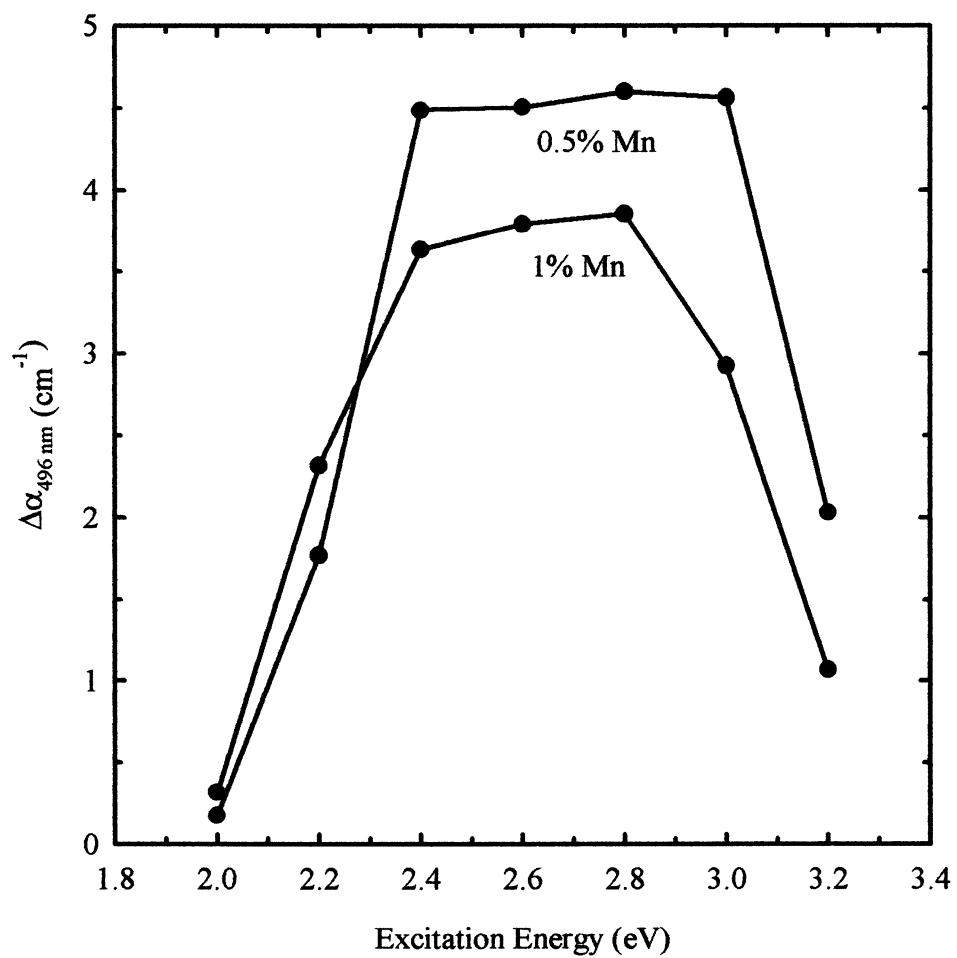


Figure 3.13 Excitation spectra for the BGO:Mn samples.

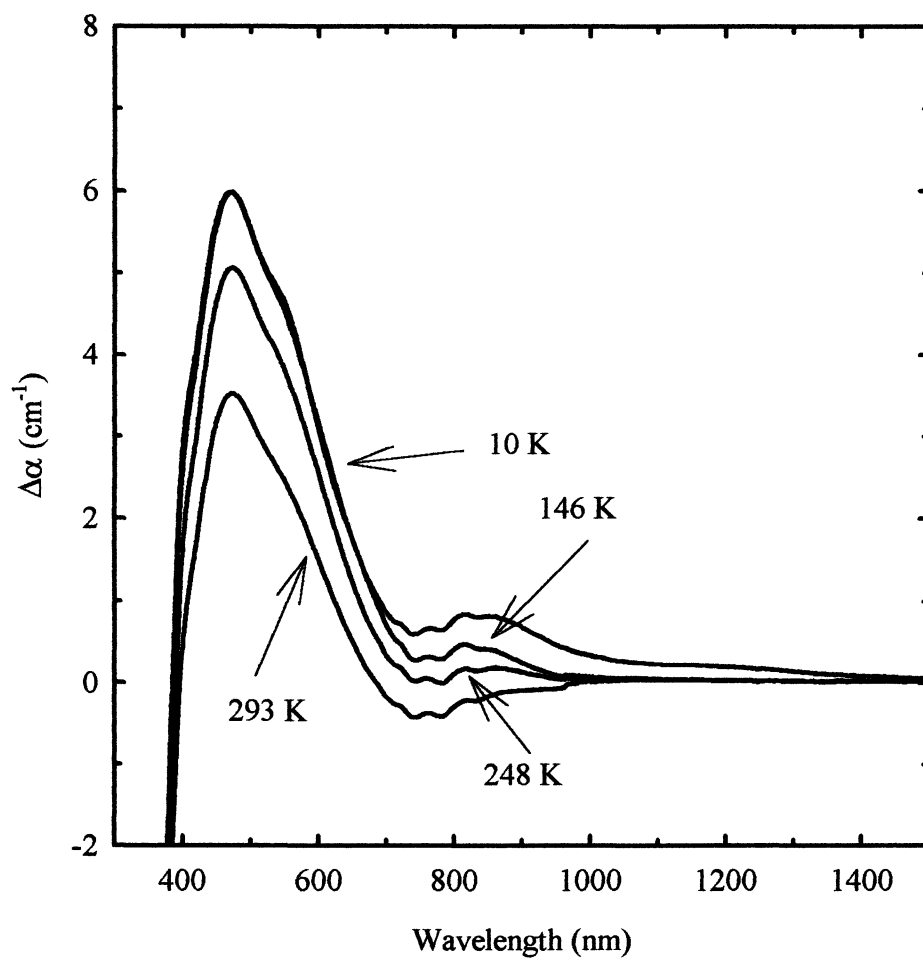


Figure 3.14 The low temperature photochromic anneal of BGO:0.5%Mn. The sample was exposed to 413 nm light for 1 hr at 10 K.

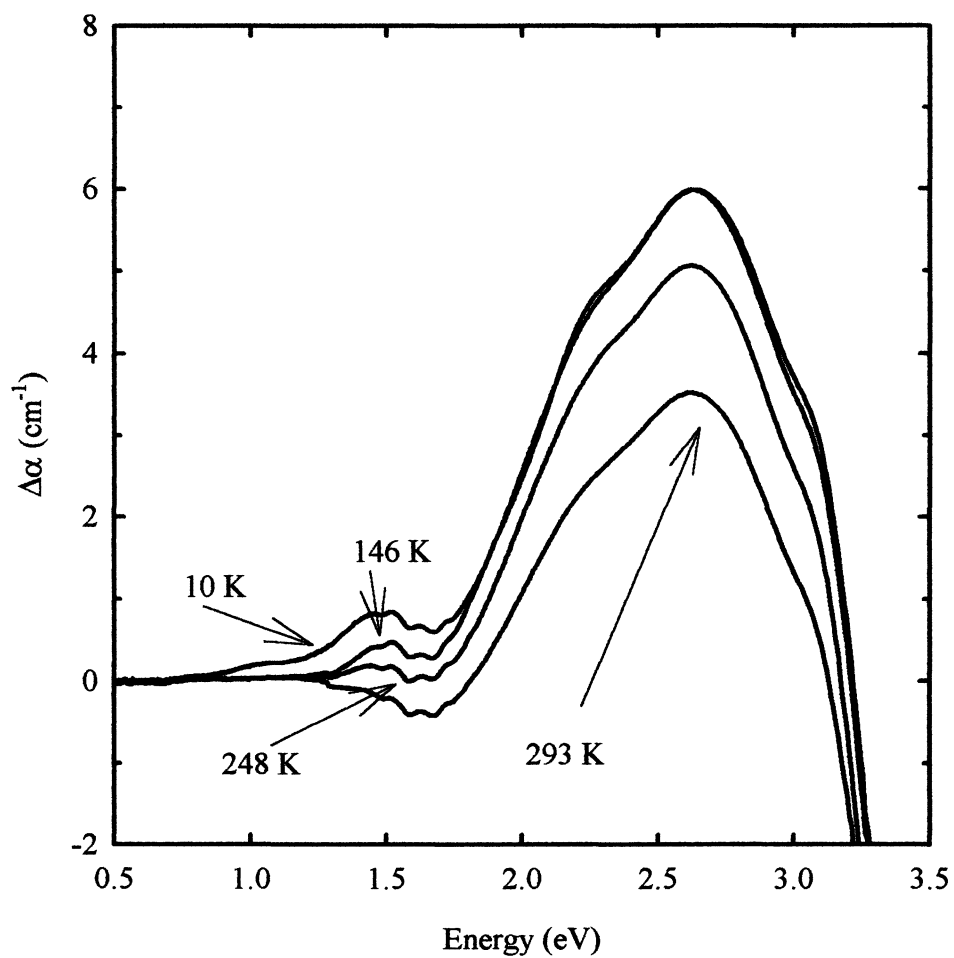


Figure 3.15 The low temperature photochromic anneal of BGO:0.5%Mn on an energy scale. The sample was exposed to 413 nm light for 1 hr at 10 K.

that there is some iron present in BGO:Mn. In undoped and iron doped BGO, all of the photochromic bands go away at room temperature.

The high temperature isochronal anneal shows that there is not much additional decay until the sample reaches ~ 425 K. The photoinduced absorption decays rapidly above this temperature. The inset in Figure 3.16 shows the decay of the photoinduced absorption at 496 nm. This high temperature decay is similar to BGO:Cr.

Several research groups have published papers discussing the sillenites doped with manganese.^{76,85-95,130-132} Unfortunately, in some cases there was no discussion about the valence state or the location of manganese, and in the other cases there is disagreement over the valence state of manganese before and after exposure to light and the location of manganese. In BGO, manganese can either replace bismuth in the distorted octahedral site or germanium in the tetrahedral site. Manganese could also be in an interstitial site.

EPR measurements show that most impurities occupy the germanium site.¹⁴ The electronic configuration of atomic manganese is $4s^23d^5$. Assuming manganese will behave similarly to chromium, it seems likely the two 4s electrons can join two of the 3d electrons and form $4(sp^3)^4$ hybrid orbitals and bond to the adjacent oxygen atoms. As before in BGO:Cr, this is a highly-covalent tetrahedrally-coordinated site. Three electrons are left in the d-shell and manganese would appear as $Mn^{4+} (d^3)$. The anti-site bismuth defect is present in all melt grown sillenite material and could accept an electron from manganese. This would suggest that BGO:Mn would have a mixture of $Mn^{4+} (d^3)$ and $Mn^{5+} (d^2)$. The existence of the d^2 would further suggest that the absorption spectra of BGO:Cr and BGO:Mn would be similar. However, the BGO:Mn samples are much lighter in color than BGO:Cr samples since manganese does not introduce strong absorption in the visible.

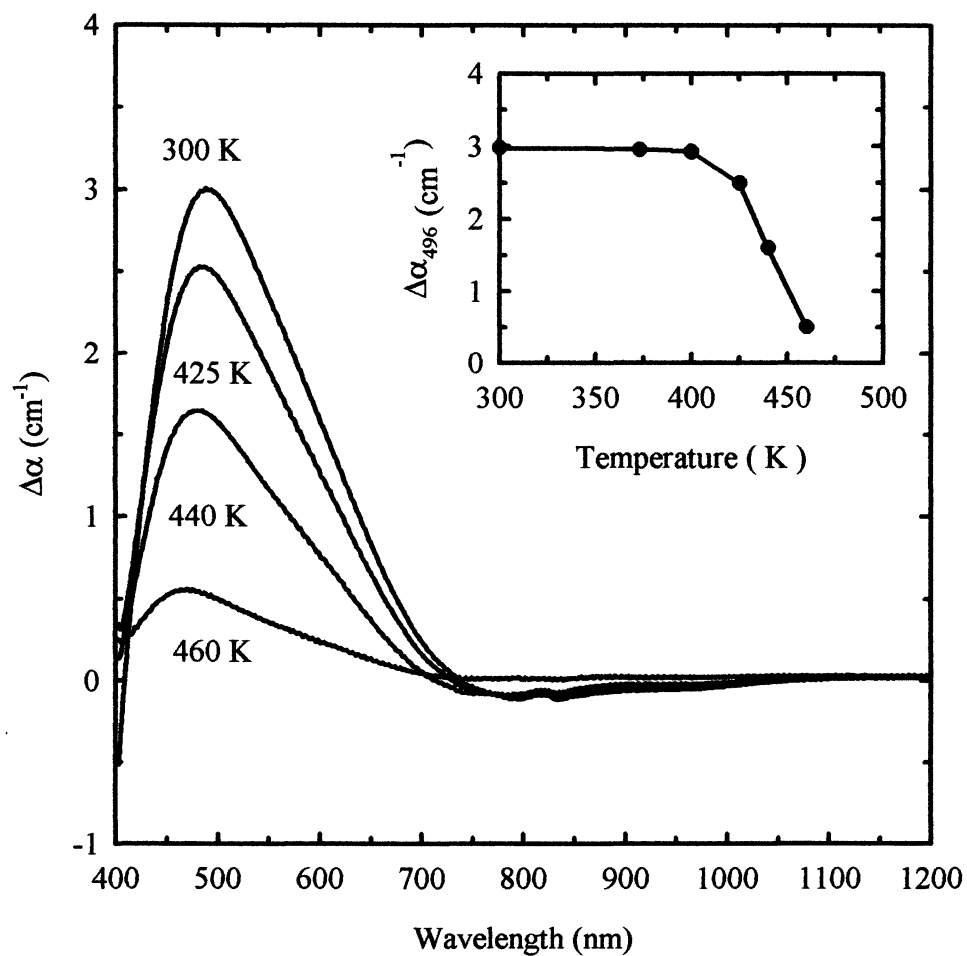


Figure 3.16 The high temperature photochromic anneal of BGO:0.5%Mn. The sample was exposed to 413 nm light for 1 hr at 300 K. The inset shows the decay of the photoinduced absorption at 496 nm.

The 0.5% Mn sample is slightly lighter in color than undoped BGO while the 1% Mn sample is about the same color as undoped BGO. Clearly, manganese is behaving differently than one would reasonably expect at first glance.

Wardzynski et al. have studied the EPR and absorption spectra of BGO:Mn.¹³⁰ Their absorption spectra agree with what was seen here. The EPR spectra indicated that manganese was in a tetrahedral site. It also indicated that manganese is in either a d^2 (Mn^{5+}) or a d^5 (Mn^{2+}) configuration. The d^2 configuration should have a similar spectra to the spectra seen for Cr^{4+} . Therefore, the d^2 configuration was ruled out. The d^5 configuration would have no absorption since all transitions are forbidden, so it was concluded that Mn^{2+} is present in BGO:Mn.

In the scintillator material, $Bi_4Ge_3O_{12}$, prepared from a different ratio of Bi_2O_3 and GeO_2 , manganese has been introduced as an impurity.¹³³ $Bi_4Ge_3O_{12}$, like BGO, has germanium tetrahedrally bonded to four oxygen atoms. Reported in the above paper, manganese replaces germanium and is in a $2+$, d^5 , valence state.

Wardzynski et al.¹³⁰ observed that exposing the sample to light increased the EPR signal and introduced no new spectra except for an increased absorption shoulder near the band edge as was seen here. In fact, the exposure took away the weak absorption, just as was seen here. This implies more Mn^{2+} is produced. The light excites charge into the conduction band or valence band where it can be trapped somewhere else. So there should be either a mixture of Mn^{2+} and Mn^{3+} or a mixture of Mn^{2+} and Mn^{1+} before exposure to light since most likely illumination changes the charge state by one. Wardzynski et al. reported that the most likely transition is Mn^{2+} to Mn^{3+} .¹³⁰ This is probably the correct interpretation. During the growth process, some of the manganese

enters the germanium site and takes an electron from the anti-site bismuth or some other unknown defect. Manganese has seven electrons to begin with. With the addition of the electron from the anti-site bismuth or other defect, three electrons bond with the four oxygen atoms and the other five electrons are in the d shell. This is Mn^{2+} . This indicates that there is a hole on one of the manganese-oxygen bonds.

A hole in the tetrahedral site is not unprecedented. It is known that the anti-site bismuth has a hole on one of the oxygen bonds.^{25,26} Also, iron enters the germanium site and is in a $3+$, d^5 , valence state.^{24,34-36} This implies that there is a hole present in this tetrahedral structure also since the electronic configuration of atomic iron is $4s^23d^6$. Exposure to light at low temperature in BGO:Fe causes a charge transfer involving an electron from the anti site bismuth to the Fe^{3+} converting it to Fe^{2+} . The electron enters the d level. Iron is now in a $2+$, d^6 , valence state since the EPR spectra representing a d^5 has disappeared. This is stable only at low temperatures because iron prefers the d^5 state.

Mn^{3+} is also present in the germanium site. Shining light on BGO:Mn at room temperature excites electrons from the anti-site bismuth to the Mn^{3+} , d^4 , increasing the amount of Mn^{2+} , d^5 . This is stable at room temperature because of the half-filled d-shell. Once the sample is heated to ~ 425 K, some of these electrons return to the anti-site bismuth. It is possible that manganese atoms replace bismuth in the distorted octahedral site or that manganese interstitials exist, but manganese replacing germanium is more likely. Annealed BGO:Mn samples have a mixture of Mn^{3+} and Mn^{2+} present. The broad 500 nm peak observed at room temperature in BGO:Mn is present at low temperature in BGO and BGO:Fe.

3.4 Summary And Conclusions

Chromium and manganese are transition metals that predominantly occupy the germanium site in BGO. Chromium introduces strong absorption beginning in the IR and continues on throughout the visible. The strong absorption is caused by Cr^{4+} ; however, Cr^{5+} is present also. Exposing BGO:Cr to visible light caused additional absorption as the result of the formation of more Cr^{4+} . The additional Cr^{4+} is stable to ~ 425 K. Manganese does not introduce any strong absorption. The absorption spectra of BGO:Mn are similar to undoped BGO. There is some weak absorption due to manganese. Exposure to light removes this weak absorption and introduces increased absorption throughout the visible. Before exposure, there is a mixture of Mn^{2+} and Mn^{3+} . After exposure, Mn^{2+} is present. The additional Mn^{2+} is stable to ~ 425 K.

CHAPTER 4

THE PHOTOREFRACTIVE EFFECT

4.1 Introduction

Most of the possible applications of the sillenites depend on the photorefractive effect. In this chapter, the photorefractive response of BGO doped with chromium and manganese is reported. The emphasis is on the temperature dependence of writing a grating and its dark-decay and the stability of gratings written at room temperature. A brief introduction to the photorefractive effect was given in Chapter 1, but it is instructive to go through the photorefractive effect with more detail.

When writing a grating, nonuniform light, such as an interference pattern produced by two crossed laser beams, is incident on a photorefractive crystal. The interference pattern can be described by

$$I = I_o(1 + m \cos(Kx)), \quad (4.1)$$

where I_o is the maximum intensity, m is the modulation index, and K is the magnitude of the grating wavevector. The modulation index, m , is defined as

$$m = \frac{2\sqrt{I_1 I_2}}{I_1 + I_2}, \quad (4.2)$$

and allows the possibility of the two write beams to have unequal intensities. K is related to the grating spacing, Λ , by

$$K = \frac{2\pi}{\Lambda}. \quad (4.3)$$

The intensity pattern varies only in the x-direction. Charges will be photoexcited in the bright region into the conduction band and/or valence band and can drift and diffuse to the dark regions where they can be trapped. Drift is caused by either an applied electric field or the electric field created by the redistribution of charge. The charge density, ρ , will be proportional to I , so the charge density can be written as

$$\rho \sim \cos(Kx). \quad (4.4)$$

The charge density will create a space charge field E . Solving Poisson's equation,

$$\nabla \cdot \epsilon \mathbf{E} = 4\pi\rho, \quad (4.5)$$

where ϵ is the permittivity of the material, in one dimension gives

$$E \sim \sin(Kx). \quad (4.6)$$

Thus, the space charge field is 90° out of phase with the interference pattern and depends only on the charge density. Varying the light intensity will only affect the speed at which the electric field forms, not its maximum value because the electric field depends only on the charge density. The electric field modulates the index of refraction through the linear electro-optic effect. The modulation is

$$\Delta n = -\frac{1}{2} n_0^3 r E, \quad (4.7)$$

where n_o is the linear index of refraction, r is the electro-optic coefficient, and E is the space charge field. The photorefractive effect is demonstrated in Figure 4.1 by nonuniform illumination, photoionization of charge in the bright region, redistribution of charge by drift and diffusion to the dark region, formation of space charge field, and finally modulation of the index of refraction by the linear electro-optic effect.

In Figure 4.2, two laser beams with wavelength λ_w intersect in a crystal. Both beams make an angle θ_w with the normal. Let one have wavevector \mathbf{k}_1 and the other \mathbf{k}_2 . Both wavevectors have the same magnitude

$$k = |\mathbf{k}_1| = |\mathbf{k}_2| = \frac{2\pi}{\lambda_w}. \quad (4.8)$$

Constructive interference occurs when

$$\mathbf{k}_1 - \mathbf{k}_2 = \mathbf{K}, \quad (4.9)$$

where \mathbf{K} is the wavevector of the interference pattern that connects \mathbf{k}_1 and \mathbf{k}_2 . From the geometry in Figure 4.2,

$$K = |\mathbf{K}| = 2k \sin \theta_w. \quad (4.10)$$

Analogously with the magnitude of \mathbf{k}_1 and \mathbf{k}_2 ,

$$K = \frac{2\pi}{\Lambda}, \quad (4.11)$$

where Λ is the period of the grating. Inserting Equations 4.8 and 4.11 into Equation 4.10 and simplifying yields,

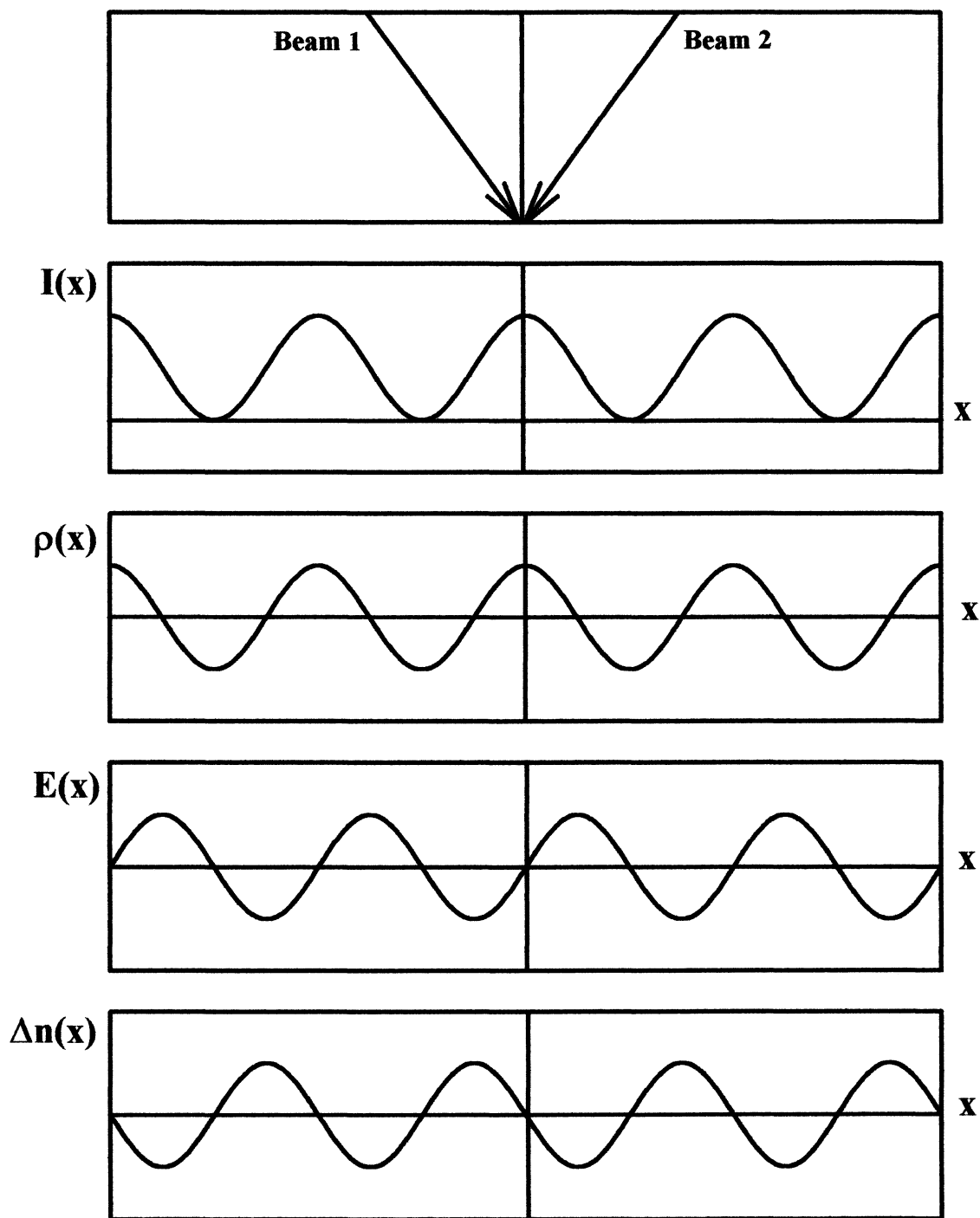


Figure 4.1 The photorefractive effect. Two coherent light beams intersect in an electro-optic crystal and form an interference pattern. Charges are excited from the bright regions and are transported to the dark regions by drift and diffusion. The charge density matches the light intensity and sets up an electric field which creates a refractive index grating by the linear electro-optic effect.

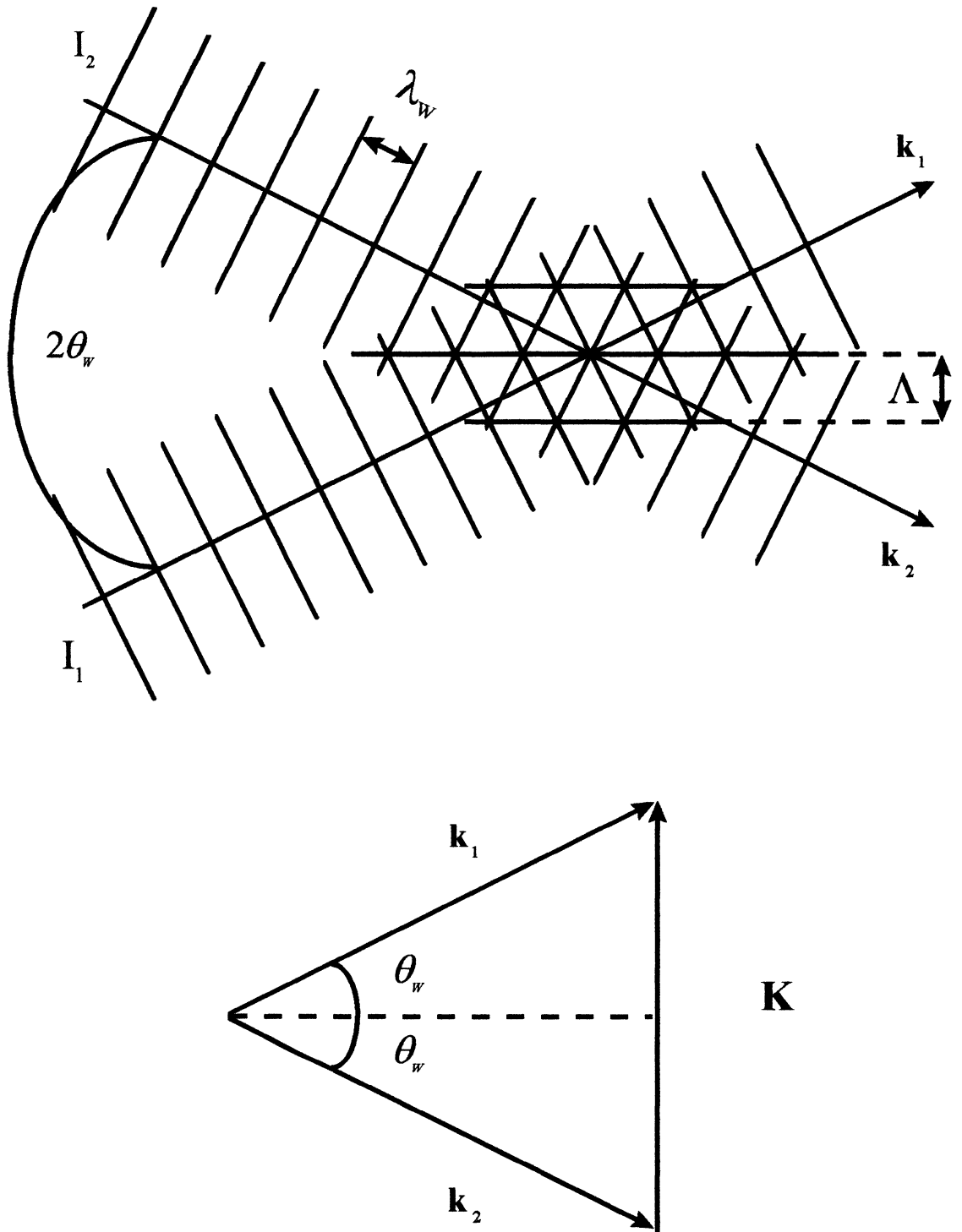


Figure 4.2 Interference pattern formed by the intersection of two light waves and the corresponding wavevector diagram.

$$\Lambda = \frac{\lambda_w}{2 \sin \theta_w}. \quad (4.12)$$

The grating spacing depends on the wavelength of the laser beams and the angle at which they cross.

The index grating consists of planes perpendicular to the sample surface. To “read” the grating, the read beam needs to be incident on the sample at the Bragg angle.

For first order diffraction,

$$\lambda_R = 2\Lambda \sin \theta_R. \quad (4.13)$$

This is shown in Figure 4.3.

4.2 Experimental Procedure

Photorefractive measurements were taken using the arrangement shown in Figure 4.4. A Liconix HeCd CW laser operating at 442 nm was used to write the gratings. The output of the HeCd laser was first sent through a beam expander and then split into two approximately equal laser beams. The two laser beams were then reflected off mirrors to cross in the sample. The path length for each beam was the same to ensure coherence and an interference pattern in the sample. An angle of approximately 6.3° from the normal was used to write approximately $2 \mu\text{m}$ gratings. A HeNe laser operating at 633 nm incident at the Bragg angle was used to read the gratings. A neutral density filter was placed in the path of HeNe laser to reduce the power to 0.5 mW. JML optical shutters were placed in the path of HeCd laser and in the path of the HeNe laser. The shutter in the path of HeCd laser allows one to write a grating for a certain length of time. The shutter in the path of the HeNe laser allows the HeNe either to continuously monitor

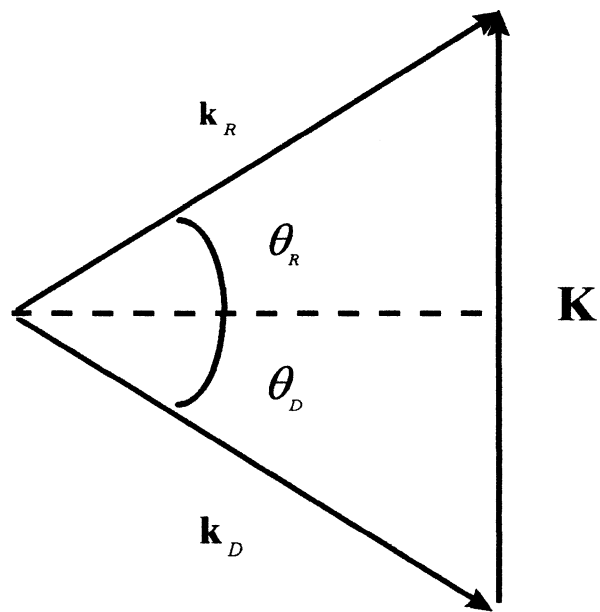
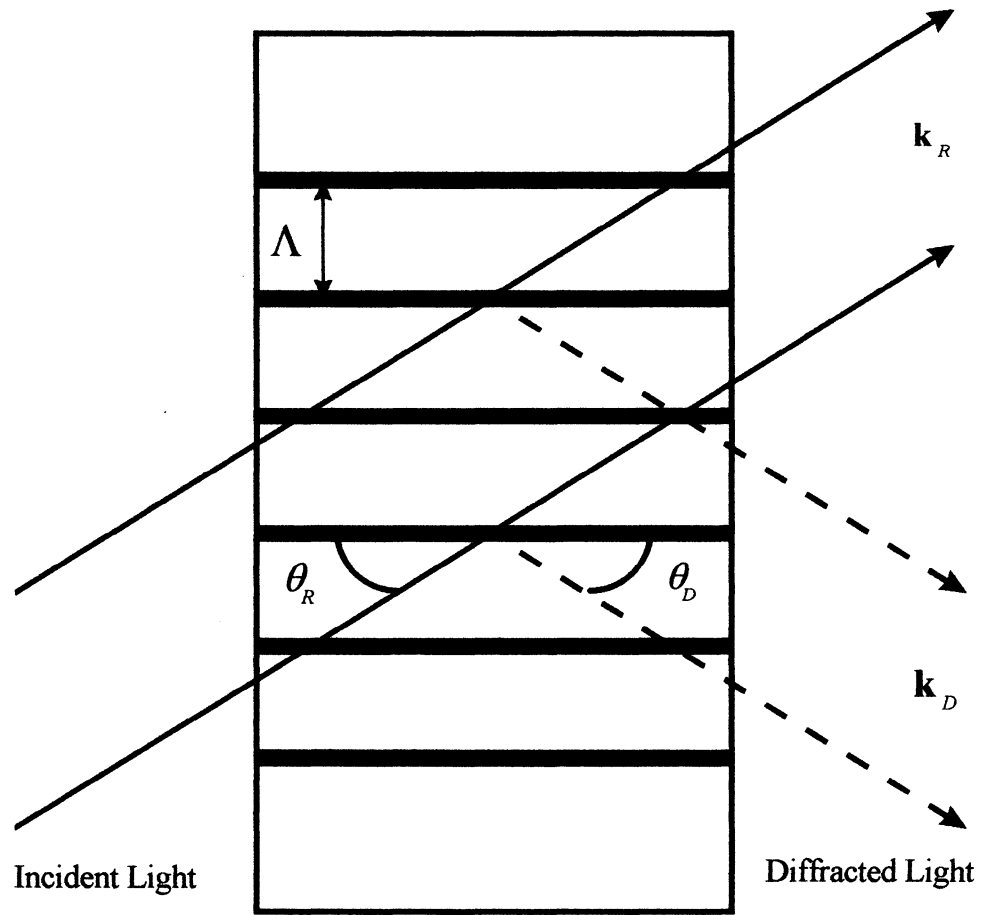


Figure 4.3 Bragg Diffraction of light from a periodic medium and the corresponding wavevector diagram.

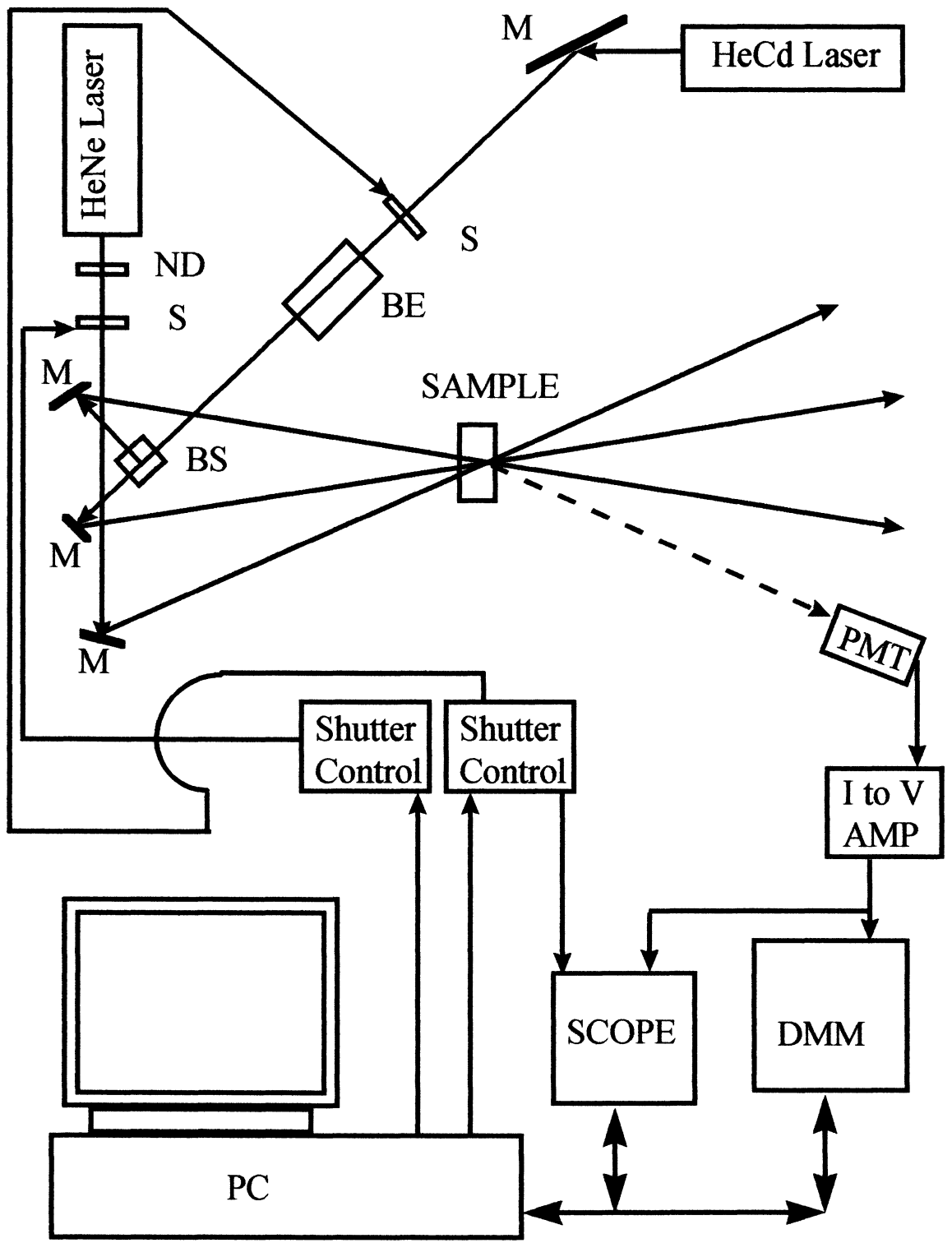


Figure 4.4 Experimental Arrangement for photorefractive measurements. M stands for Mirror, S for Shutter, ND for Neutral Density filter, BS for Beam Splitter, PMT for Photo-multiplier Tube, BE for Beam Expander, DMM for Digital Multimeter, SCOPE for Oscilloscope, I to V AMP for Current to Voltage Amplifier, and PC for Personal Computer.

the grating, simply by leaving the shutter open, or to discretely monitor the grating only at certain temperatures or times.

The diffracted signal was detected by a photomultiplier tube (PMT). A 633 nm filter was placed in front of the PMT so stray light would not be detected. The current signal from the PMT was amplified and converted to a voltage using a Keithley 427 Current Amplifier. The resulting voltage signal was measured by both a HP 54600A Digital Storage Oscilloscope and a Keithley 199 Digital Multimeter (DMM). The oscilloscope was used for “fast” measurements while the DMM was used for “slow” measurements. The oscilloscope was triggered by the write shutter. The oscilloscope and DMM were connected to a personal computer (PC) by GPIB cables through an IEEE-488 interface. The two shutters were triggered using the PC’s two serial ports. However, the time the shutters are open are programmed by hand using the shutter driver/controller. Programs were written in Transera HTBasic to control the equipment and take the data. These programs are listed in the appendices.

Photorefractive measurements were taken at room temperature and higher temperatures up to 500 K. This was accomplished by mounting the samples on a hot stage. The hot stage was the same piece of equipment that was used to collect the high temperature photochromic data reported in Chapter 3. For data collection at a certain temperature, the sample was heated manually by applying a voltage across a cartridge heater and monitoring the temperature by a Chromel-Alumel (Type K) thermocouple and HP 3478A DMM. At the desired temperature, the voltage applied was turned off and the photorefractive measurement was made. The actual temperature was within ± 5 K of the recorded temperature. The HeNe beam was on continuously in this type of experiment.

The Bragg angle was not changed for the measurements taken at temperatures greater than 300 K.

The temperature dependence of a grating was also measured by writing a grating at 300 K and monitoring the grating as the temperature was slowly raised to 500 K. The grating was monitored every 1 K. The heating was computer controlled using a cartridge heater, an HP 6289A DC Power Supply, an HP 59501b Isolated DAC/Power Supply Programmer, a Chromel-Alumel (Type K) thermocouple, and an HP 3478A DMM interfaced to the PC through the IEEE-488 interface. The shutter in front of the HeNe laser beam was closed except when taking a measurement. This was done to minimize the possibility of the HeNe beam erasing the grating. As before, the Bragg angle was not changed as the sample was heated.

Another experiment consisted of writing a grating a room temperature and monitoring the grating over a 24 hour period. The data could be taken at different time intervals. For example, in one experiment, data was taken every 30 minutes. In another, data was taken every hour. This allowed one to see if optical erasure played a role in the decay. Obviously, for this experiment, the shutter in the path of the HeNe beam was closed except when taking a measurement.

4.3 Results And Discussion

The typical photorefractive response of undoped BGO is shown in Figure 4.5. The write power was 60 mW before reaching the beam splitter, the grating was written for 500 ms, and the HeNe laser was on continuously. At 300 K, the photorefractive write response consists of a fast initial spike which quickly decays to a steady state value. A

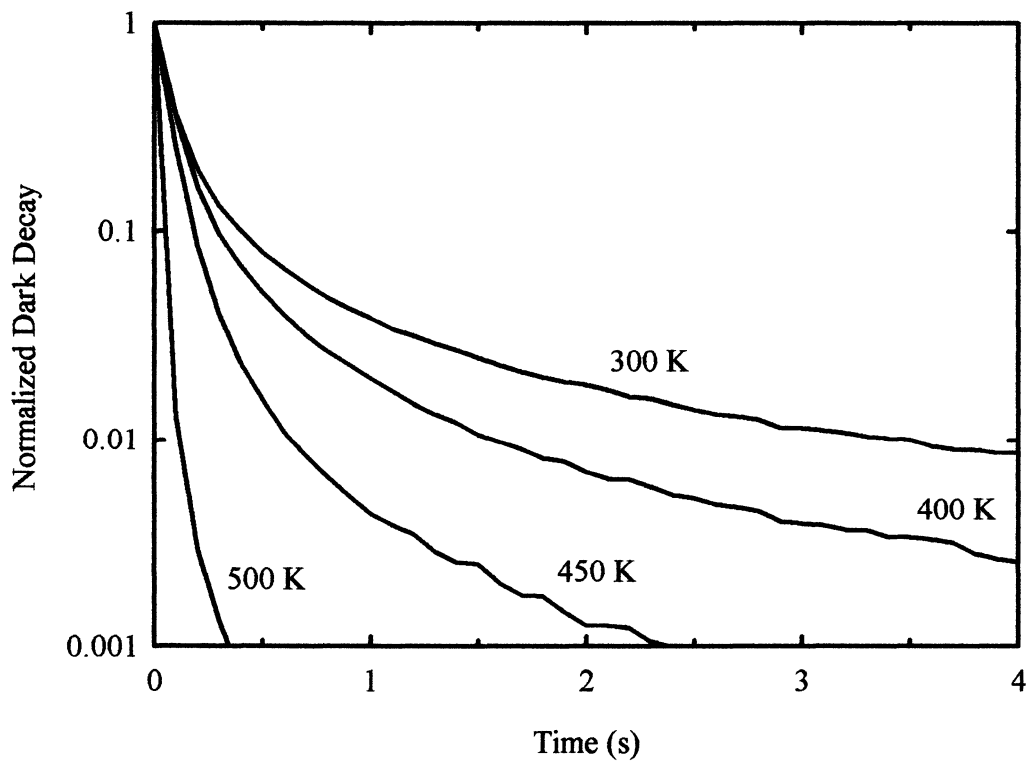
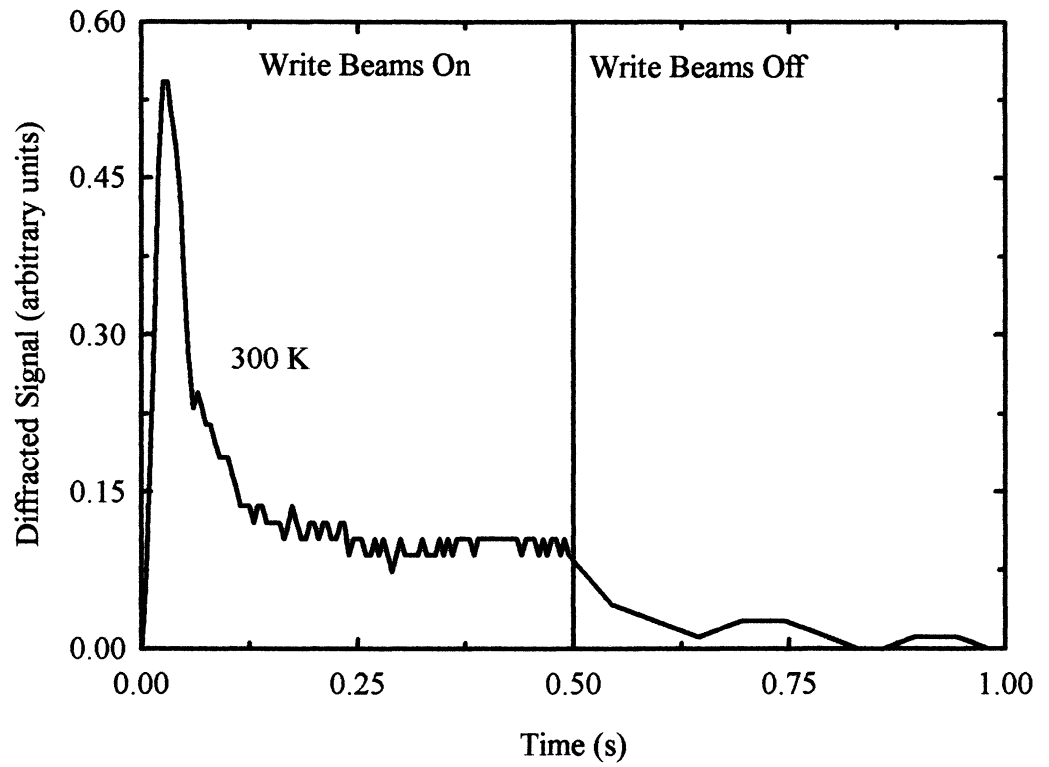


Figure 4.5 Typical photorefractive response of BGO and its normalized dark decays.

similar write response is seen in gratings written at higher temperatures up to 500 K.

Once the write beams are turned off, the diffracted signal decays rapidly. As the sample is heated up to 500 K, this dark-decay becomes even faster.

Several groups have reported on the photorefractive effect in the sillenites.¹³⁴⁻¹⁶⁴ Unfortunately, only a few of these papers present the kinetics of the write process and dark-decay at different temperatures.^{161,164} Bloom et al.¹⁶⁴ and Martin¹⁶⁵ found that by writing gratings in undoped BGO as the temperature is lowered to 10 K, the leading edge spike goes away, and the steady state diffracted signal is much larger. It also takes longer to reach steady state at low temperature. They also observed that the dark-decay is much slower at low temperatures. Additionally, they wrote gratings at low temperature and monitored the grating as the sample was slowly warmed to 300 K. Some experiments kept the HeNe on continuously while others shuttered the read beam open and closed. Optical erasure definitely played a role in the decay. They observed a major anneal stage around 150 K. Martin¹⁶⁵ also performed power dependence measurements. Martin observed that when writing with lower write powers, the leading edge spike disappears, and the signal slowly builds up to the same steady state value.

The initial spike seen at room temperature in undoped BGO is most likely due to rapid generation of charge. This is followed by decay to a steady-state grating due to recombination and trapping. Lowering the write power reduces the charge generation, but the steady-state grating strength remains the same since the grating strength depends on the charge density. The dark-decays shown in Figure 4.5 are not straight lines, and thus, the decays are not a simple exponential. Unfortunately, the dark-decays in undoped BGO are much more complicated.^{148,151,153,154}

The photoconductivity in undoped BGO has been reported an n-type meaning the dominant carriers are electrons.^{20,41,61} Bloom and et al.^{63,64} measured the electron mobility of undoped BGO. They found that the electron mobility of undoped BGO is three orders of magnitude smaller at 210 K than at 300 K. They were unable to take electron mobility measurements at lower temperatures. The fact that the electron mobility decreases with temperature explains the slower photorefractive write response seen at low temperatures. The larger grating strength seen at low temperatures is explained by realizing the traps are thermally activated. At low temperatures, the traps are stable. The stable traps at low temperature also explain the persistent gratings seen at low temperature. However, the traps are so shallow, electrons are able to escape at room temperature, resulting in gratings that decay very rapidly at room temperature.

4.3.1 Chromium

The typical photorefractive response of BGO:0.1%Cr is shown in Figure 4.6. The gratings were written for 500 ms, and the read beam was on continuously. At 300 K, the diffracted signal slowly builds up. This is much slower than that seen in undoped BGO. As the sample was heated to 500 K, the diffracted signal continues to slowly build up. In some sets of experiments, the grating was strongest at 300 K; in other sets of experiments, the grating was strongest at a higher temperature. This is probably due to the history of the sample. In other words, the initial conditions were not exactly the same. Attempts were made to reach a maximum diffracted signal by writing for longer periods of time, but the diffracted signal became unstable, fluctuating with no obvious periodicity. Consequently, this was not pursued. At 300 K, once the write beams are turned off, the

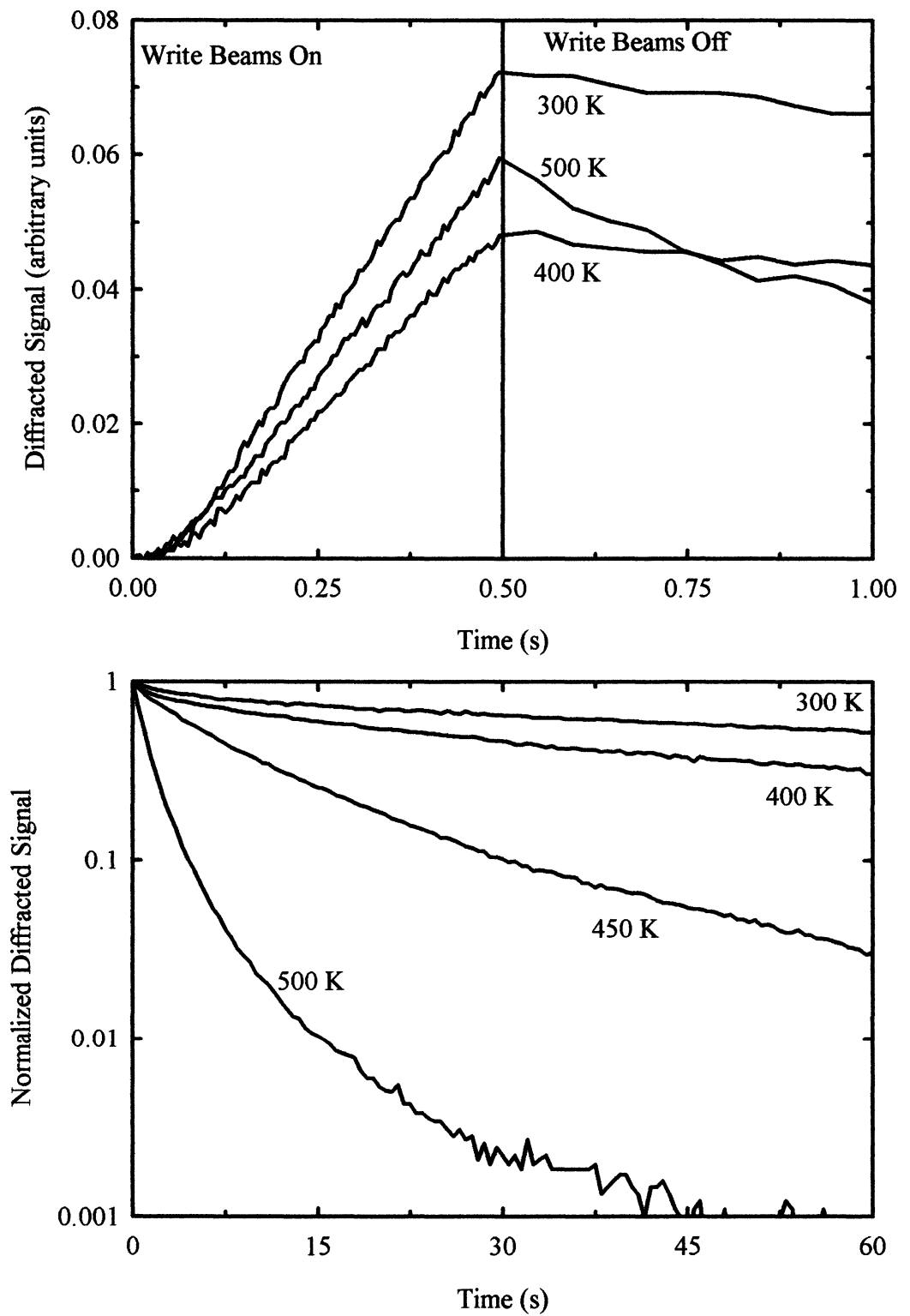


Figure 4.6 Typical photorefractive response of BGO:0.1%Cr and its normalized dark decays.

dark-decay is very slow. Compare the time scale for the normalized dark decays for BGO and BGO:0.1%Cr seen in Figures 4.5 and 4.6. At progressively higher temperatures, the dark decays progressively speed up. The normalized dark decays showed consistent results for all sets of experiments. A similar response was observed in BGO:0.5%Cr. Gratings were also written in the BGO:1%Cr sample but it has so much absorption the diffracted signal is very weak and was not pursued.

Figure 4.7 shows the typical response of a grating written in BGO:0.1%Cr at room temperature as it was heated to 500 K. The grating was written for 500 ms. The shutter in the path of the HeNe laser was closed except when taking a measurement to minimize optical erasure. The read shutter was opened for 50 ms. At first, there is hardly any decay at all; the decay seen is probably due to optical erasure. Once the temperature reaches approximately 400 K, the grating decays very fast. This temperature matches the decay of the photochromic effect in BGO:Cr seen in Chapter 3. A similar response was observed in BGO:0.5%Cr.

Figure 4.8 shows the diffracted signal of three gratings written in BGO:0.1%Cr at 300 K. The grating was written for 500 ms. The shutter in the path of the HeNe laser was closed except when taking a measurement to minimize optical erasure. The read shutter was opened for 50 ms. The gratings were read every 6, 12, and 60 minutes for 24 hours. As the gratings are read more frequently, the signal decays faster. This implies that optical erasure plays a role in the decay of the photorefractive signal. A similar response was observed in BGO:0.5%Cr.

BGO:Cr has a much slower write response and slower decay than that seen in undoped BGO at room temperature. The room temperature photorefractive response of

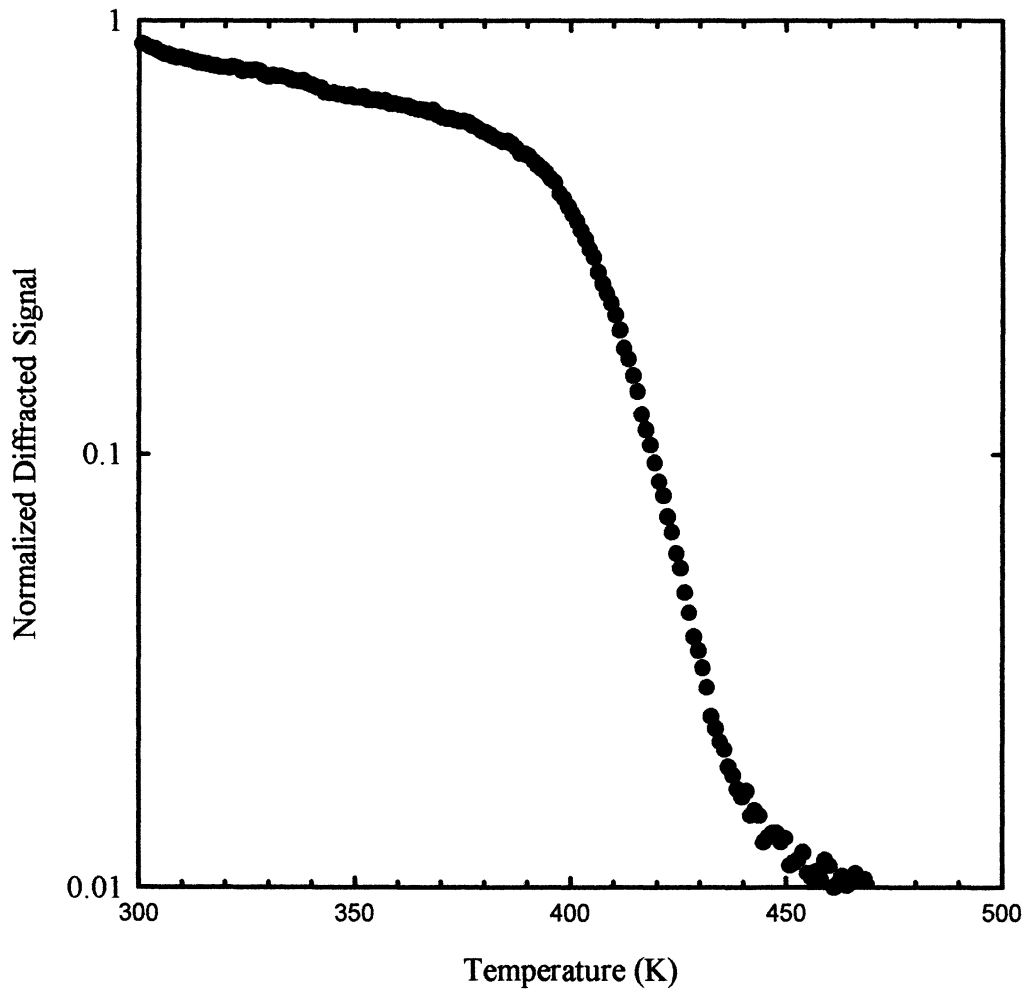


Figure 4.7 The temperature dependence of a grating written in BGO:0.1%Cr at room temperature.

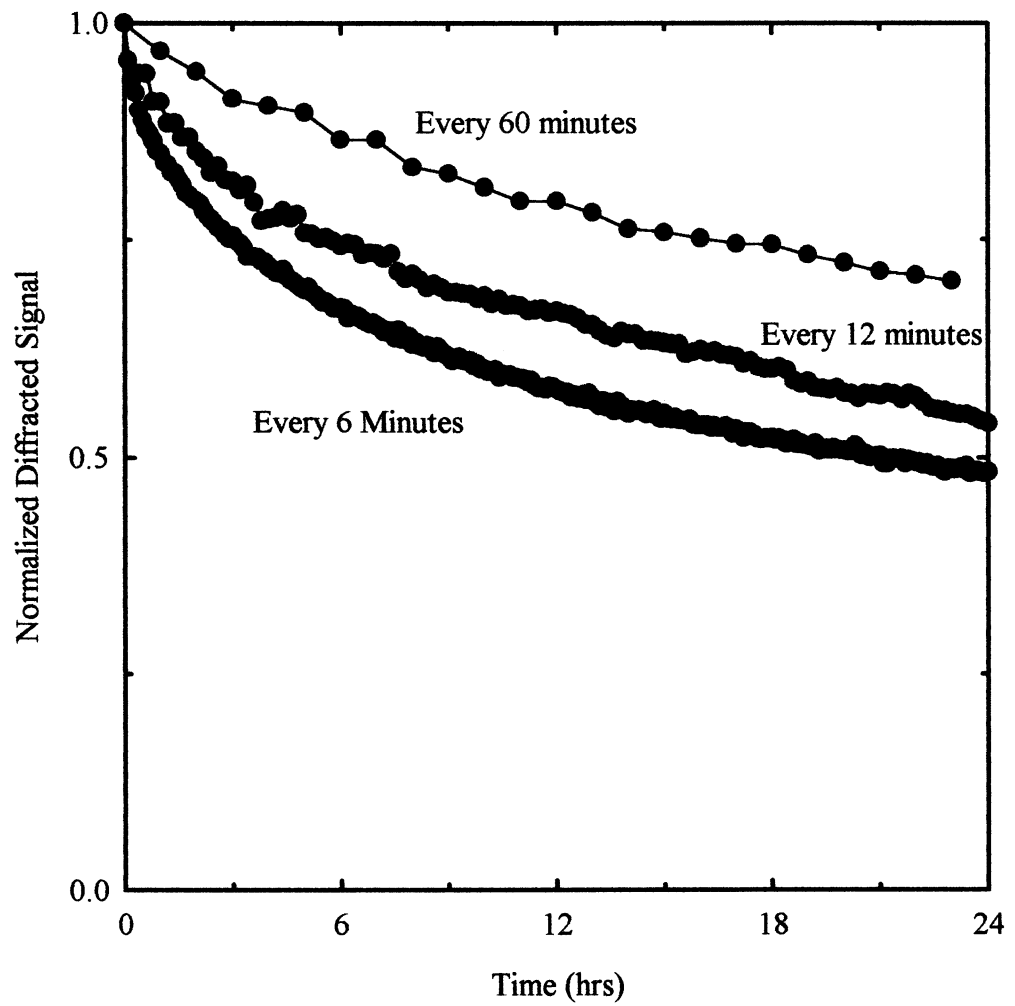


Figure 4.8 Gratings were written in BGO:0.1%Cr at room temperature and monitored for 24 hours.

BGO:Cr is very similar to the low temperature photorefractive response of undoped BGO. This suggests that the addition of chromium reduces mobility in BGO and introduces traps that are stable at room temperature. Harmon measured the photoconductivity of BGO and BGO:Cr and found that the addition of chromium reduces the photoconductivity by several orders of magnitude.¹⁶⁶ Mokrushina et al. found that the presence of chromium leads to a reduction of photoconductivity due to a sharp decrease of the small diffusion lengths.⁸² Since the photoconductivity is directly proportional to mobility, it seems very likely that the presence of chromium in BGO reduces the mobility.

As seen in Chapter 3, exposure to 442 nm light caused an increase in the absorption coefficient. The explanation given was that light was exciting electrons from the anti-site bismuth or other defects to Cr^{5+} creating more Cr^{4+} . This indicates that the dominant trap for the persistent gratings in BGO:Cr is Cr^{5+} . This is an electron trap. This trap is stable at room temperature and leads to persistent gratings at room temperature. Optical erasure and thermal erasure both play a role in the decay of the gratings. There is probably absorption gratings present along with the index grating due to chromium's strong absorption.

4.3.2 Manganese

The typical photorefractive response of BGO:0.5%Mn is shown in Figure 4.9. The write power was 10 mW before the beam splitter, the gratings were written for 500 ms, and the read beam was on continuously. At 300 K, the diffracted signal slowly builds up. This is much slower than that seen in undoped BGO, and is very similar to that seen in BGO:Cr. As the sample was heated to 500 K, the diffracted signal continues to

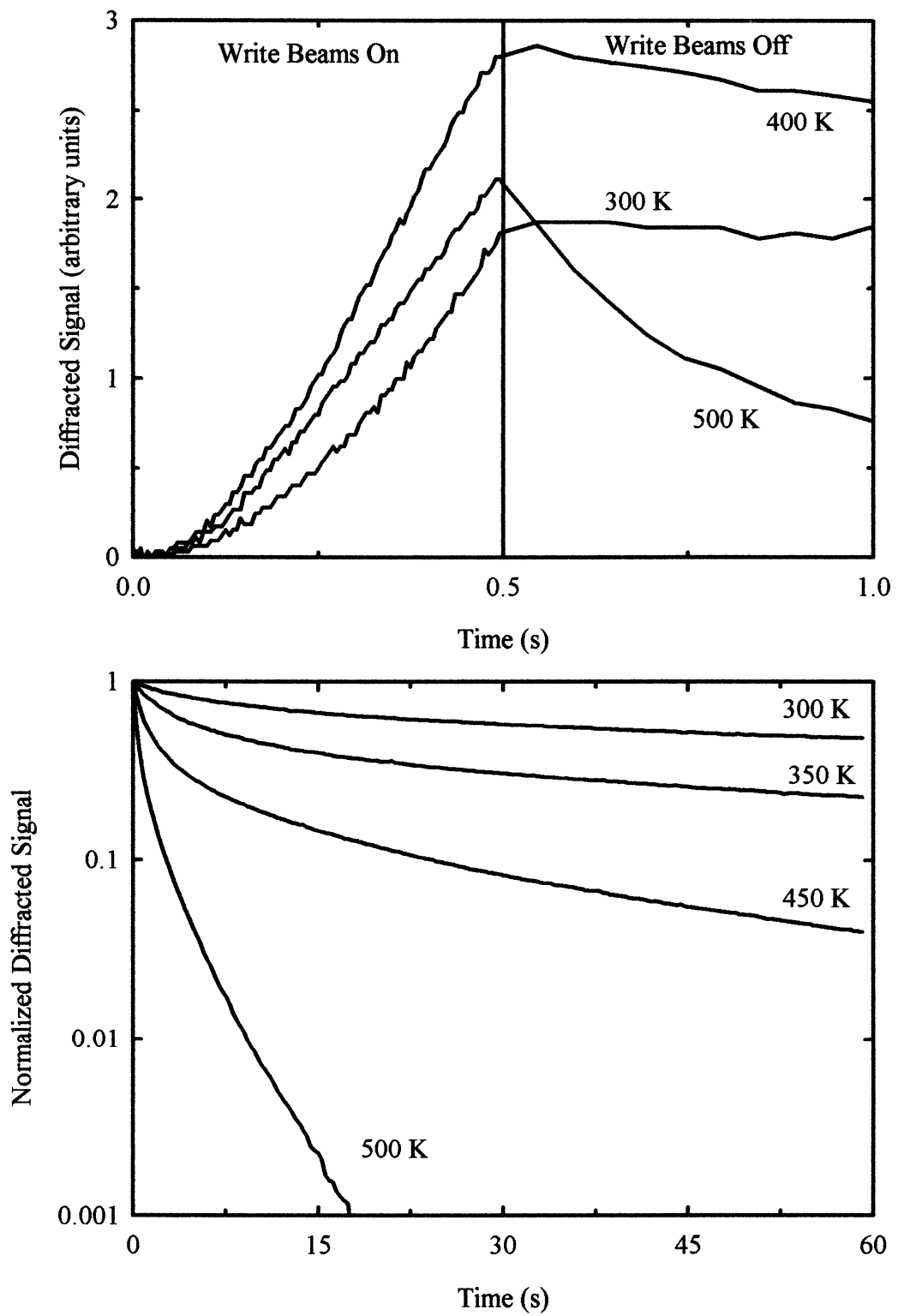


Figure 4.9 Typical photorefractive response of BGO:0.5%Mn and its normalized dark decays.

slowly build up. In some sets of experiments, the grating was strongest at 300 K; in other sets of experiments, the grating was strongest at a higher temperature. This is probably due to the history of the sample. In other words, the initial conditions were not exactly the same. At 300 K, once the write beams are turned off, the dark-decay is very slow. Compare the time scale for the normalized dark-decays for undoped BGO and BGO:0.5%Mn seen in Figures 4.5 and 4.9. At progressively higher temperatures, the dark-decays progressively speed up. The normalized dark-decays showed consistent results for all sets of experiments. A similar response was observed in BGO:1%Mn. This also matches the photorefractive response of BGO:Cr.

Figure 4.10 shows the typical response of a grating written in BGO:0.5%Mn at room temperature as it was heated to 500 K. The write power was 10 mW before the beam splitter, and the grating was written for 500 ms. The shutter in the path of the HeNe laser was closed except when taking a measurement to minimize optical erasure. The read shutter was opened for 50 ms. At first, there is hardly any decay at all; the decay seen is probably due to optical erasure. Once the temperature reaches approximately 425 K, the grating decays very fast. This temperature matches the decay of the photochromic effect in BGO:Mn seen in Chapter 3. A similar response was observed in BGO:1%Mn. This also matches the temperature dependence seen in BGO:Cr.

Figure 4.11 shows the diffracted signal of two gratings written in BGO:0.5%Mn at 300 K. The write power was 10 mW before the beam splitter, and the grating was written for 500 ms. The shutter in the path of the HeNe laser was closed except when taking a measurement to minimize optical erasure. The read shutter was opened for 50 ms. The gratings were read every 30 and 60 minutes for 24 hours. In both experiments, the signal

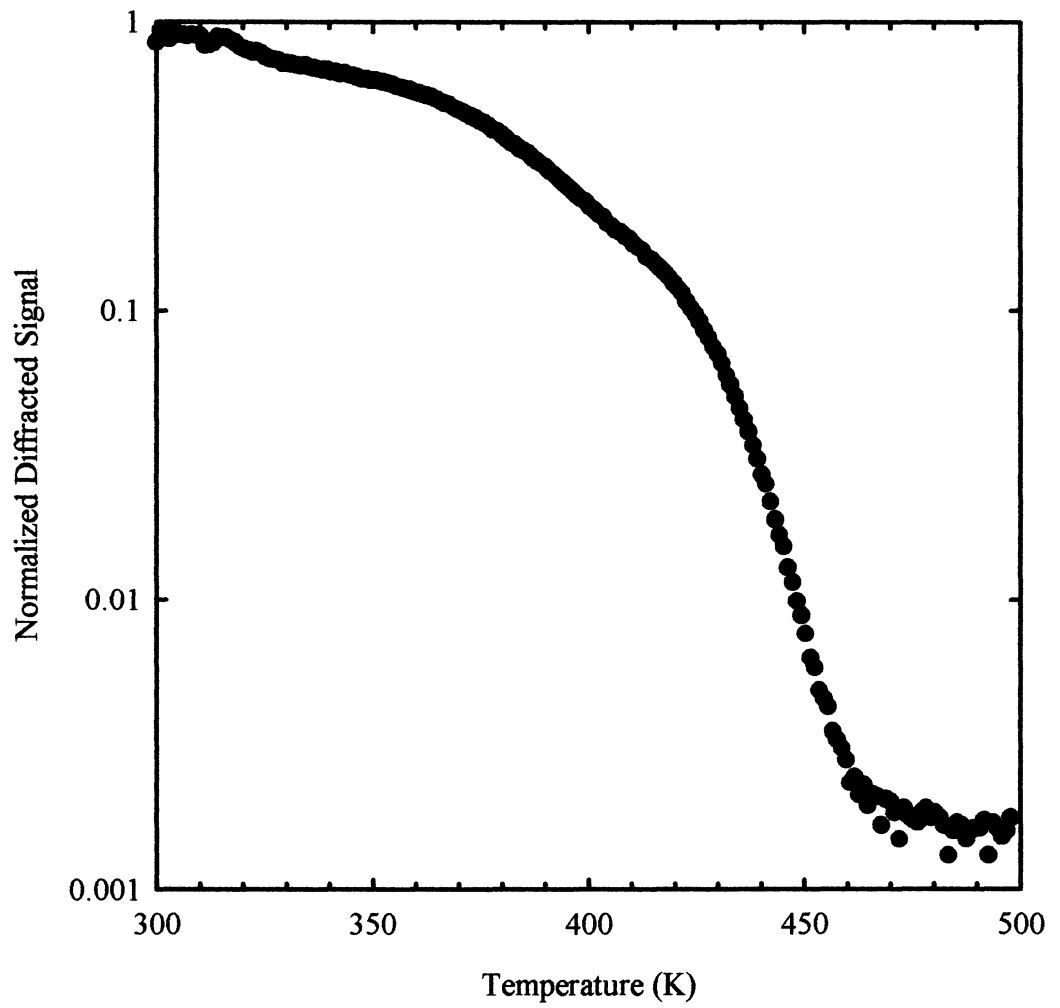


Figure 4.10 The temperature dependence of a grating written in BGO:0.5%Mn at room temperature.

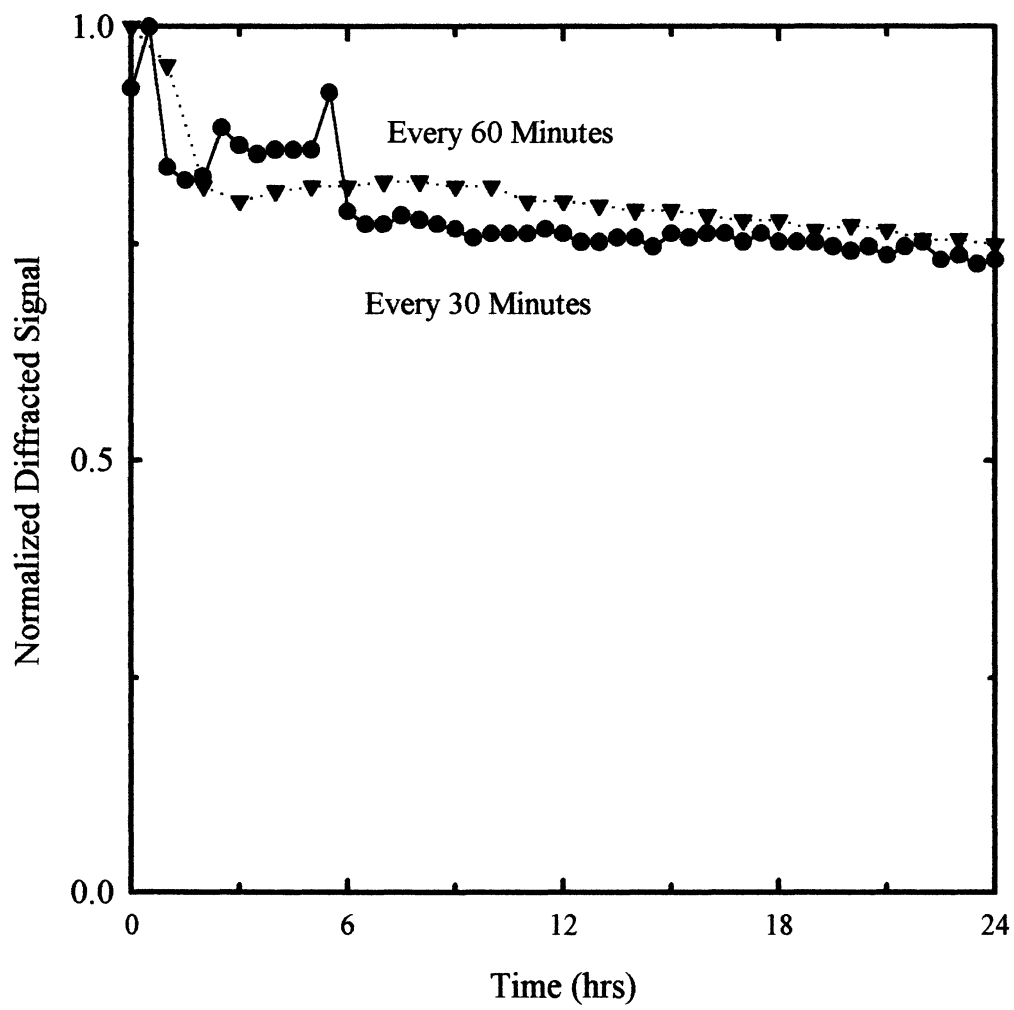


Figure 4.11 Gratings were written in BGO:0.5%Mn at room temperature and monitored for 24 hours.

fluctuates somewhat, but the general trend shows the more frequent the reading, the faster the decay. This implies that optical erasure plays a role in the decay of the photorefractive signal. A similar response was observed in BGO:1%Mn. This is very similar to what was seen in BGO:Cr, but the gratings in BGO:Mn are stronger after the 24 hour period than the gratings in BGO:Cr.

BGO:Mn has a much slower write response and slower decay than what is seen in undoped BGO at room temperature. The room temperature photorefractive response of BGO:Mn is very similar to the low temperature photorefractive response of undoped BGO and the room temperature photorefractive response of BGO:Cr. This suggests that the addition of manganese reduces mobility in BGO and introduces traps that are stable at room temperature.

As seen in Chapter 3, exposure to 442 nm light caused an increase in the absorption coefficient. The explanation given was that light was exciting electrons from the anti-site bismuth or other defects to Mn^{3+} creating more Mn^{2+} . This indicates that the dominant trap for the persistent gratings in BGO:Mn is Mn^{3+} . This would be an electron trap. This trap is stable at room temperature and leads to persistent gratings at room temperature. Optical erasure and thermal erasure both play a role in the decay of the gratings. There is probably absorption gratings present along with the index grating due to BGO:Mn's room temperature photochromic effect.

4.4 Summary And Conclusions

The addition of chromium and manganese in BGO decrease the mobility and introduce deep traps. The reduction of mobility slows down the photorefractive process,

and the deep traps lead to stable holographic gratings at room temperature. The index gratings are both optically and thermally activated. Gratings written at room temperature are stable up to near 420 K. Gratings written at room temperature and held at this temperature last longer than 24 hours when kept in the dark. BGO:Mn seems to be a better choice for storage applications due to the simple fact that it has weaker absorption in the visible and IR than BGO:Cr and appears to have less optical erasure than BGO:Cr.

CHAPTER 5

PHOTOREFRACTIVE SIMULATION MODEL

5.1 Introduction

The purpose of this chapter is to present a simple simulation model that describes the kinetics of grating formation and decay in photorefractive materials. The differential equations that describe the photorefractive effect were solved using a finite difference technique in a spreadsheet such as Excel or Quattro Pro.

Kukhtarev et al.¹⁶⁷⁻¹⁶⁹ provided the largest step forward in the theory since the discovery of the photorefractive effect. The history of the theory describing the photorefractive effect can be found in Solyman et al.¹³ Kukhtarev's band transport model consisted of standard semiconductor rate equations for the generation of charge and the subsequent motion due to diffusion and drift and Poisson's Equation (also referred to as Gauss's Law in the literature). Feinberg et al.¹⁷⁰ presented a hopping model to describe the photorefractive effect a couple of years after Kukhtarev's model was published. The hopping model was shown to be a special case of the band transport model when the

diffusion length is small by Hall et al.¹⁷¹ and Jaura et al.¹⁷² Numerous papers have been published on numerical simulations of the photorefractive effect.^{137,148,173-182}

5.2 The Theory

The model shown in Figure 5.1 was used. For simplicity, only electrons were considered, although holes may be the dominant carrier in some materials, or electrons and holes may both be present in similar concentrations in other materials. Under the proper illumination, electrons can be excited from the neutral donor into the conduction band. Once in the conduction band, the electrons can recombine with the ionized donor, or drift and diffuse until the electrons are trapped or recombined. This model only assumes one type of trap. Real materials may have several types of traps. The space charge field, created by the charge separation, modulates the index of refraction through the linear electro-optic or Pockels effect. The strength of the space charge field determines the magnitude of the change in the index of refraction. Kogelnic¹⁸⁴ showed that the diffraction efficiency of a holographic index grating is:

$$\eta = \sin^2 \left(\frac{\pi \Delta n d}{\lambda \cos(\theta)} \right), \quad 5.1$$

where d is the sample thickness, λ is the wavelength of the light at the Bragg angle, θ is the Bragg angle, and Δn is the change in the index of refraction. The change in the index of refraction is:

$$\Delta n = \frac{1}{2} n^3 r E, \quad 5.2$$

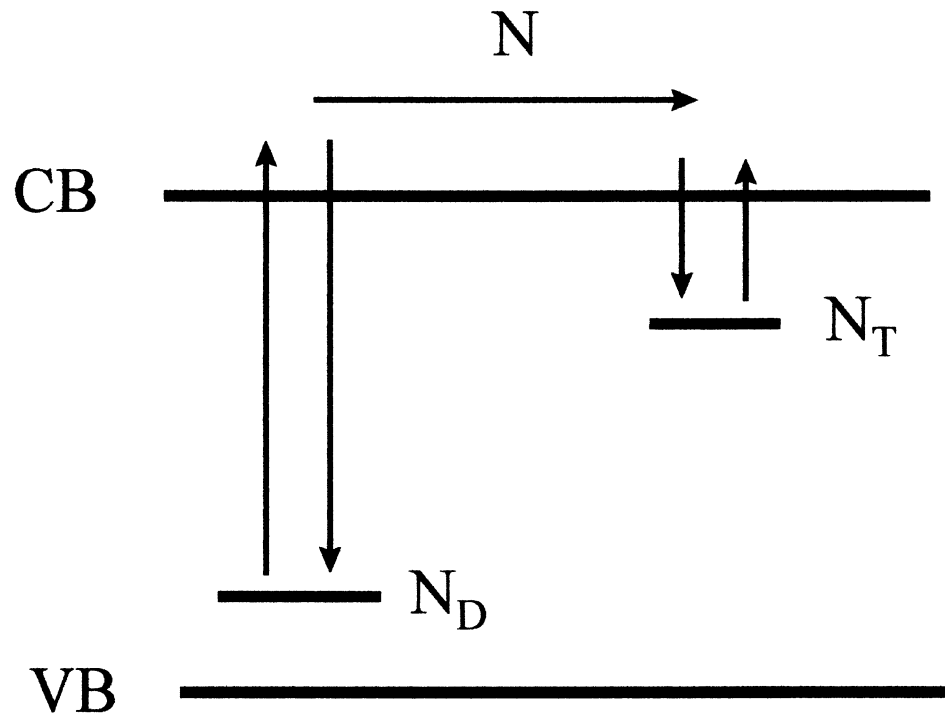


Figure 5.1 Model used for simulations of the photorefractive effect in BGO. CB is the conduction band, VB is the valence band, N is the concentration of electrons in the conduction band, N_D is the concentration of donors, and N_T is the concentration of traps.

where n is the index of refraction, r is the electro-optic coefficient and E is the space charge field. For small index changes, which is true for the sillenites, the sine function can be ignored which implies that the diffraction efficiency is proportional to the square of the electric field. Therefore, to model the kinetics of grating formation and decay, it is only necessary to calculate the space charge field. However, the space charge field depends on the concentration of ionized donors, concentration of electrons in the conduction band, and the concentration of trapped electrons.

The rate equation for the generation of electrons or ionized donors is:

$$\frac{\partial N_D^i}{\partial t} = (\beta + sI)(N_D - N_D^i) - \gamma NN_D^i, \quad 5.3$$

where N_D^i is the ionized donor density, β is the thermal ionization rate, s is the donor light excitation cross section, I is the light intensity, N_D is the unionized donor density, γ is the donor recombination coefficient, and N is the electron density in the conduction band.

The rate equation for electrons in the conduction band is:

$$\frac{\partial N}{\partial t} = \frac{\partial N_D^i}{\partial t} - \frac{\partial N_T^i}{\partial t} + \frac{1}{q} \frac{\partial}{\partial x} (qD \frac{\partial N}{\partial x} + q\mu NE), \quad 5.4$$

where N_T^i is the ionized trap concentration, q is the magnitude of the charge of an electron, D is the diffusion constant, μ is the mobility, and E is the space charge field. Equation 5.4 does not include a term for photovoltaic drift since it is not important in the sillenites. However, photovoltaic drift is important in some photorefractive materials

such as LiNbO₃ and LiTaO₃ so $\chi_{ph}IN_D$ must be added to the current density. χ_{ph} is the photovoltaic coefficient, I is the light intensity, and N_D is the donor density.

The rate equation for electron trapping is:

$$\frac{\partial N_T^i}{\partial t} = -(\beta_T + s_T I)N_T^i + \gamma_T N(N_T - N_T^i), \quad 5.5$$

where β_T is the thermal ionization rate for traps, s_T is the light excitation cross section for traps, N_T is the density of traps, and γ_T is the recombination coefficient for traps.

The space charge field, E , is written as

$$E = \frac{1}{\epsilon K} q(N_D^i - N - N_T^i), \quad 5.6$$

where q is the magnitude of the charge on an electron, ϵ is the permittivity of the material, and K is the magnitude of the grating wavevector. All of the preceding rate equations and the electric field are coupled and nonlinear. Closed form solutions are not available so the equations must be solved numerically.

Simplifying assumptions were made to facilitate the numerical solutions. First, it was assumed that $N_D \gg N_D^i$, which means the donor density is much greater than the ionized donor density. Similarly, it was assumed that $N_T \gg N_T^i$, which means the trap density is much greater than the ionized trap density. Also, the donor thermal ionization rate was set to zero since the donor sits deep in the band gap. With these assumptions, the equations become:

$$\frac{\partial N_D^i}{\partial t} = sIN_D - \gamma NN_D^i, \quad 5.7a$$

$$\frac{\partial N}{\partial t} = \frac{\partial N_D^i}{\partial t} - \frac{\partial N_T^i}{\partial t} + \frac{1}{q} \frac{\partial}{\partial x} (qD \frac{\partial N}{\partial x} + q\mu NE), \quad 5.7b$$

$$\frac{\partial N_T^i}{\partial t} = -(\beta_T + s_T I)N_T^i + \gamma_T NN_T^i, \quad 5.7c$$

and

$$E = \frac{1}{\epsilon K} q(N_D^i - N - N_T^i). \quad 5.7d$$

The preceding equations are somewhat simpler but the quantities that determine the electric field vary upon position and time. In order to eliminate the spatial dependence, the quantities are expressed as a Fourier Series and truncated to the first two terms yielding:

$$N_D^i = N_{D_0}^i + N_{D_1}^i \cos(Kx), \quad 5.8a$$

$$N = N_0 + N_1 \cos(Kx), \quad 5.8b$$

$$N_T^i = N_{T_0}^i + N_{T_1}^i \cos(Kx), \quad 5.8c$$

and

$$E = E_1 \sin(Kx), \quad 5.8d$$

where K is the magnitude of the grating wavevector. These solutions were assumed because the ionized donor, ionized trap, and conduction band densities should follow the

light intensity pattern, $I = I_0 (1 + \cos(Kx))$. The space charge field is 90° out of phase with the light intensity pattern and has no term independent of position since there is no applied field. Substituting the assumed solutions, Equation 5.8, and the light intensity pattern into the differential equations, Equation 5.7, using the Trigonometric identity, $\cos(2\alpha) = \cos^2(\alpha) - \sin^2(\alpha) = 2\cos^2(\alpha) - 1$, collecting like terms, and ignoring higher order terms, the resulting differential equations are:

$$\frac{\partial N_{D0}^i}{\partial t} = sI_0 N_D - \gamma N_0 N_{D0}^i - \frac{1}{2} \gamma N_1 N_{D1}^i \quad 5.9a$$

$$\frac{\partial N_{D1}^i}{\partial t} = sI_0 N_D - \gamma N_0 N_{D1}^i - \gamma N_1 N_{D0}^i \quad 5.9b$$

$$\frac{\partial N_0}{\partial t} = \frac{\partial N_{D0}^i}{\partial t} - \frac{\partial N_{T0}^i}{\partial t} \quad 5.9c$$

$$\frac{\partial N_1}{\partial t} = \frac{\partial N_{D1}^i}{\partial t} - \frac{\partial N_{T1}^i}{\partial t} - K^2 D N_1 + \mu K N_0 E_1 \quad 5.9d$$

$$\frac{\partial N_{T0}^i}{\partial t} = -\beta_T N_{T0}^i - s_T I_0 N_{T0}^i - \frac{1}{2} s_T I_0 N_{T1}^i + \gamma_T N_T N_0 \quad 5.9e$$

$$\frac{\partial N_{T1}^i}{\partial t} = -\beta_T N_{T1}^i - s_T I_0 N_{T1}^i - s_T I_0 N_{T0}^i + \gamma_T N_T N_1 \quad 5.9f$$

$$E_1 = \frac{1}{\epsilon K} q(N_{D1}^i - N_1 - N_{T1}^i) \quad 5.9g$$

Additional simplifications made the actual calculations much easier. First, Equation 5.9g was inserted into 5.9d. Also, in each of the terms in the differential equations, all constants were grouped together. For example, instead of finding separate constants for s , I_0 , and N_D , one constant was found for sI_0N_D . Finally, when calculating E^2 for the diffraction efficiency, the constants in Equation 5.9g were ignored.

All of the preceding derivations were for the write process. For the dark decay, a few things need to be changed. First there is no generation term. This eliminates the first term in Equations 5.9a and 5.9b. Also, the grating is monitored with uniform light. This eliminates the third term in Equations 5.9e and 5.9f and I_0 is now the intensity of the read beam.

5.3 Simulations

Figure 5.2 shows a write power dependence and dark decay simulation for undoped BGO. This was generated by using different values for the generation rate. A larger generation rate implies a higher write power. The graph generally agrees with experimental results. At high powers a leading edge peak is present which quickly decays to a steady state value. At lower powers the leading edge peak is not present but the grating slowly builds up to the same steady state value.

The temperature dependence of undoped BGO was also simulated. This is shown in Figure 5.3 for the write process and for the dark decay. As the temperature is lowered the mobility decreases and there is less thermally activated detrapping. This accounts for

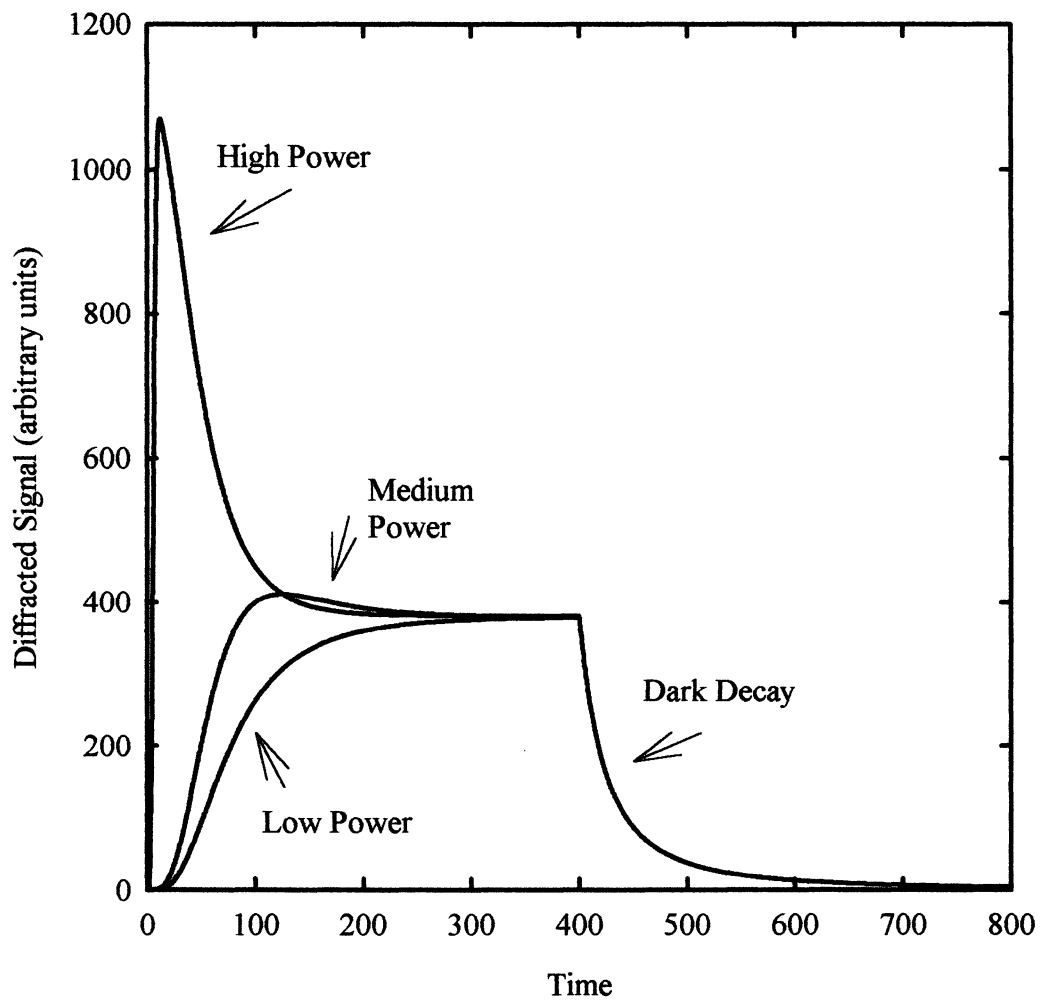


Figure 5.2 Simulation of the write power dependence on grating formation and the dark decay for undoped BGO at room temperature.

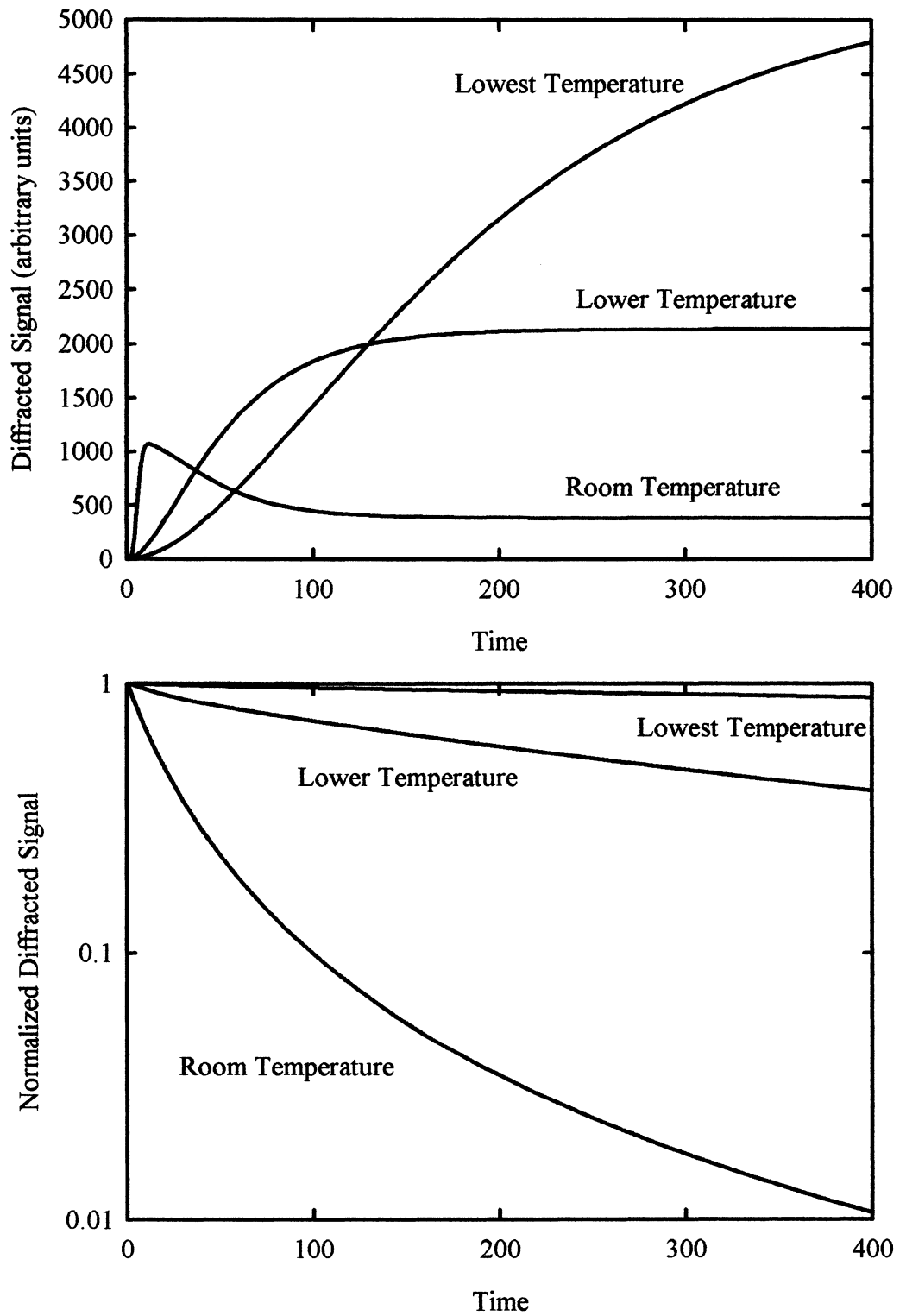


Figure 5.3 Simulation of the temperature dependence on grating formation and the dark decay for undoped BGO.

the larger signal at low temperature and the slower build-up. The dark decay is also much slower. Again, this agrees with experimental results.

The grating formation and decay was also simulated for BGO:Cr and BGO:Mn. This is shown in Figure 5.4. The mobility was lowered from the room temperature value used for undoped BGO and there was no thermally activated detrapping. As the temperature is increased, thermally activated detrapping causes the grating to decay faster. Figure 5.4 agrees with experimental results.

5.4 Summary And Conclusions

A simple model simulating the kinetics of grating formation and decay has been presented. The power dependence and temperature dependence of grating formation was simulated for undoped BGO. The dark decay was also simulated at room temperature and two lower temperatures for undoped BGO. Grating formation was also simulated for BGO:Cr and BGO:Mn at room temperature. The dark decay was also simulated at room temperature and two higher temperatures for BGO:Cr and BGO:Mn. This model gave results which were observed experimentally.

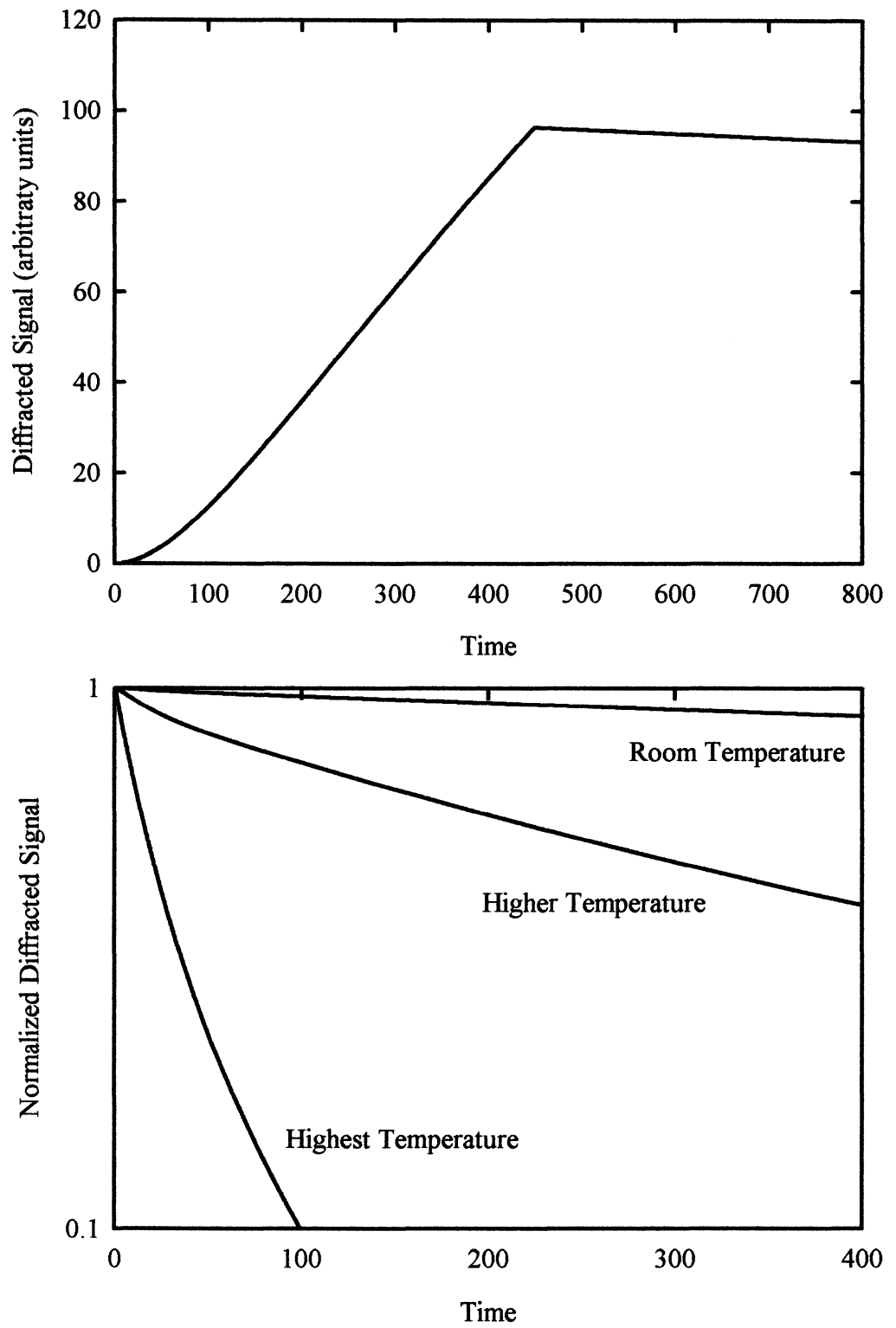


Figure 5.4 Simulation of the grating formation and the temperature dependence of the dark decay in BGO:Cr and BGO:Mn.

CHAPTER 6

CONCLUSIONS

6.1 Summary

This dissertation has presented the results of an investigation of doping the photorefractive material, BGO, with chromium and manganese. The addition of chromium introduces absorption not seen in BGO. Exposure with VIS-UV light causes an increase in the absorption coefficient. This additional absorption is stable up to around 425 K. The addition of manganese causes very weak absorption which goes away when illuminated with visible light and increases the absorption shoulder. This additional absorption is stable up to around 425 K.

The addition of chromium and manganese also reduced the electron mobility and allowed persistent gratings to be written at room temperature. As the samples are heated, the gratings decay around 425 K, which matches the decay of the photochromic effect. BGO:Mn seems to be a better overall choice for holographic applications because it has less absorption than BGO:Cr.

The kinetics of grating formation and decay was also simulated using a simple band transport model. This model gave results which agree with experimental results at different write powers and different temperatures.

6.2 Future Work

There are several things one could work on to advance the knowledge of BGO:Cr and BGO:Mn. It was found that UV and VIS light introduced photochromic absorption bands in these materials. Knowing that optical erasure plays a role in the decay of holographic index gratings, it might be possible to bleach the photoinduced absorption by illuminating with light of another wavelength.

The actual diffraction efficiency of the holographic index gratings in BGO:Cr and BGO:Mn should be measured. One should use samples of the same thickness and of the same orientation. The largest diffracted signal will come from samples with the (110) orientation.

High temperature (between 300 K and 500 K) thermally stimulated conductivity measurements would determine the actual depth of the traps the addition of chromium and manganese introduce. Photoconductivity measurements should also be performed on BGO:Mn.

BIBLIOGRAPHY

1. P. Gunter, *Physics Reports*, **93**, 199 (1982).
2. H. J. Eichler, P. Gunter, and D. W. Pohl, *Laser-Induced Dynamic Gratings*, Springer-Verlag, Berlin, 1986.
3. P. Gunter, and J. P. Huignard, Eds., *Photorefractive Materials and Their Applications I*, Springer-Verlag, Berlin, 1988.
4. P. Gunter, and J. P. Huignard, Eds., *Photorefractive Materials and Their Applications II*, Springer-Verlag, Berlin, 1989.
5. A. Yariv, *Quantum Electronics*, 3rd Ed., John Wiley & Sons, New York, 1989.
6. A. Yariv, *Optical Electronics*, 4th Ed., Saunders College Publishing, Philadelphia, 1991.
7. M. P. Petrov, S. I. Stepanov, and A. V. Khomenko, *Photorefractive Crystals in Coherent Optical Systems*, Springer-Verlag, Berlin, 1991.
8. B. E. A. Saleh, and M. C. Teich, *Fundamentals of Photonics*, John Wiley & Sons, New York, 1991.
9. R. W. Boyd, *Nonlinear Optics*, Academic Press, San Diego, 1992.
10. P. Yeh, *Introduction to Photorefractive Nonlinear Optics*, John Wiley & Sons, New York, 1993.
11. F. Agullo-Lopez, J. M. Cabrera, and F. Agullo-Rueda, *Electrooptics: Phenomena, Materials, and Applications*, Academic Press, London, 1994.
12. M. Gower, and D. Proch, *Optical Phase Conjugation*, Springer-Verlag, Berlin, 1994.

13. L. Solymar, D. J. Webb, and A. Grunnet-Jepsen, *The Physics and Applications of Photorefractive Materials*, Clarendum Press, Oxford, 1996.
14. L. Arizmendi, J. M. Cabrera, and F. Agullo-Lopez, *International Journal of Optoelectronics*, **7**, 149, (1992).
15. A. Ashkin, G. D. Boyd, J. M. Dziedzic, R. G. Smith, A. A. Ballman, J. J. Levinstein, and K. Nassau, *Appl. Phys. Lett.*, **9**, 72, (1966).
16. A. Yariv, and P. Yeh, *Optical Waves in Crystals*, John Wiley & Sons, New York, 1984.
17. L. G. Sillen, *Arkiv For Kemi, Mineralogi Och Geologi*, Band 12A , No. 18, 1, (1937).
18. J. L. Bernstein, *Journal of Crystal Growth*, **1**, 45, (1967).
19. S. C. Abrahams, P. B. Jamieson, and J. L. Bernstein, *The Journal of Chemical Physics*, **47**, 4034, (1967).
20. S. L. Hou, R. B. Lauer, and R. E. Aldrich, *J. of Appl. Phys.*, **44**, 2652, (1973).
21. M. T. Harris, J. J. Larkin, and J. J. Martin, *Appl. Phys. Lett.*, **60**, 2162, (1992).
22. J. J. Larkin, M. T. Harris, and J. J. Martin, *SPIE*, **2481**, 216, (1995).
23. R. Oberschmid, *phys. stat. sol. (a)*, **89**, 263, (1985).
24. D. C. Craig, and N. C. Stephenson, *Journal of Solid State Chemistry*, **15**, 1, (1975).
25. H.-J. Reyher, U. Hellwig, and O. Thiemann, *Physical Review B*, **47**, 5638, (1993).
26. B. Briat, H. J. Reyher, A. Hamri, N. G. Romanov, J. C. Launay, and F. Ramaz, *J. Phys: Condens. Matter*, **7**, 6951, (1995).
27. O. F. Schirmer, *J. Physique*, **41**, 479, (1980).
28. B. C. Grabmaier, and R. Oberschmid, *phys. stat. sol. (a)*, **96**, 199, (1986).
29. W. Rehwald, K. Frick, G. K. Lang, and E. Meier, *J. of Appl. Phys.*, **47**, 1292, (1976).
30. J. J. Martin, I. Foldvari, and C. A. Hunt, *J. of Appl. Phys.*, **70**, 7554, (1991).

31. D. W. Hart, C. A. Hunt, D. D. Hunt, and J. J. Martin, *J. of Appl. Phys.*, **73**, 1443, (1993).
32. D. W. Hart, C. A. Hunt, and J. J. Martin, *J. of Appl. Phys.*, **73**, 3974, (1993).
33. J. S. McCullough, A. Harmon, J. J. Martin, M. T. Harris, and J. J. Larkin, *J. of Appl. Phys.*, **78**, 2010, (1995).
34. W. Wardzynski, M. Baran, and H. Szymczak, *Physica*, **111B**, 47, (1981).
35. H. J. von Bardeleben, *J. Phys. D: Appl. Phys.*, **16**, 29, (1983).
36. M. G. Jani and L. E. Halliburton, *J. Appl. Phys.*, **64**, 2022, (1988).
37. J. A. Baquedano, F. J. Lopez, and J. M. Cabrera, *Solid State Communications*, **72**, 233, (1989).
38. W. Wardzynski, H. Szymczak, K. Pataj, T. Lukasiewicz, and J. Zmija, *J. Phys. Chem. Solids*, **43**, 767, (1982).
39. R. E. Aldrich, S. L. Hou, and M. L. Harvill, *J. Appl. Phys.*, **42**, 493, (1971).
40. R. B. Lauer, *J. Appl. Phys.*, **42**, 2147, (1971).
41. B. Kh. Kostyuk, A. Yu. Kudzin, and G. Kh. Sokolyanskii, *Sov. Phys. Solid State*, **22**, 1429, (1980).
42. C. W. M. Timmermans, and G. Blasse, *Journal of Solid State Chemistry*, **52**, 222, (1984).
43. R. Oberschmid, *phys. stat. sol. (a)*, **89**, 657, (1985).
44. L. B. Kuleva, E. I. Leonov, and V. M. Orlov, *Sov. Phys. Solid State*, **29**, 1240, (1987).
45. L. B. Kuleva, E. I. Leonov, and V. M. Orlov, *Sov. Phys. Solid State*, **30**, 536, (1988).
46. N. Benjelloun, M. Tapiero, J. P. Zielinger, J. C. Launay, and F. Marsaud, *J. Appl. Phys.*, **64**, 4013, (1988).
47. S. Denagbe, M. Martinaud, M. Schvoerer, F. Marsaud, J. C. Launay, and P. Hagenmuller, *J. Phys. Chem. Solids*, **51**, 171, (1990).
48. T. Takamori, and D. Just, *J. Appl. Phys.*, **67**, 848, (1990).

49. T. Takamori, and D. Just, *J. Appl. Phys.*, **68**, 5700, (1990).
50. T. Takamori, and D. Just, *J. Appl. Phys.*, **69**, 3958, (1991).
51. D. Just, and T. Takamori, *Materials Science and Engineering*, **B9**, 469, (1991).
52. I. Foldvari, L. E. Halliburton, and G. J. Edwards, *Solid State Communications*, **77**, 181, (1991).
53. A. Ennouri, M. Tapiero, J. P. Vola, J. P. Zielinger, J. Y. Moisan, and J. C. Launay, *J. Appl. Phys.*, **74**, 2180, (1993).
54. D. W. Hart, M. Hamilton, C. A. Hunt, J. J. Martin, M. Harris, and J. J. Larkin, *Journal of Luminescence*, **60 & 61**, 578, (1994).
55. D. Petre, I. Pintilie, T. Botila, and M. L. Ciurea, *J. Appl. Phys.*, **76**, 2216, (1994).
56. S. L. Sochava, K. Buse, and E. Kratzig, *Physical Review B*, **51**, 4684, (1995).
57. W. B. Leigh, J. J. Larkin, M. T. Harris, and R. N. Brown, *J. Appl. Phys.*, **76**, 660, (1994).
58. T. J. Tayag, T. E. Batchman, and J. J. Sluss, Jr., *J. Appl. Phys.*, **76**, 967, (1994).
59. A. Cremades, M. T. Santos, A. Remon, J. A. Garcia, E. Dieguez, and J. Piqueras, *J. Appl. Phys.*, **79**, 7186, (1996).
60. D. E. Davies, and M. T. Harris, *J. Mater. Res.*, **12**, 308, (1997).
61. D. Bloom, and S. W. S. McKeever, *J. Appl. Phys.*, **77**, 6511, (1995).
62. D. Bloom, and S. W. S. McKeever, *J. Appl. Phys.*, **77**, 6521, (1995).
63. D. Bloom, and S. W. S. McKeever, *Materials Science Forum*, **239-241**, 325, (1997).
64. D. Bloom, and S. W. S. McKeever, *J. Appl. Phys.*, **82**, 249, (1997).
65. A. A. Ballman, *Journal of Crystal Growth*, **1**, 37, (1967).
66. J. C. Brice, M. J. Hight, O. F. Hill, and P. A. C. Whiffin, *Philips tech. Rev.*, **37**, 250, (1977).
67. T. M. Bruton, *Journal Of Solid State Chemistry*, **9**, 173, (1974).

68. T. M. Bruton, J. C. Brice, O. F. Hill, and P. A. C. Whiffin, *Journal of Crystal Growth*, **23**, 21, (1974).
69. J. C. Brice, T. M. Bruton, O. F. Hill, and P. A. C. Whiffin, *Journal of Crystal Growth*, **24/25**, 429, (1974).
70. J. C. Brice, *Journal of Crystal Growth*, **42**, 427, (1977).
71. A. R. Tanguay, Jr., S. Mroczkowski, and R. C. Barker, *Journal of Crystal Growth*, **42**, 431, (1977).
72. W. Piekarczyk, M. Swirkowicz, and S. Gazda, *Mat. Res. Bull.*, **13**, 889, (1978).
73. Y. Okano, H. Wada, T. Fukuda, and S. Miyazawa, *Japanese Journal of Applied Physics*, **30**, L 1307, (1991).
74. T. S. Yeh, L. J. Hu, S. L. Tu, S. J. Yang, S. E. Hsu, and K. Hsu, *J. Appl. Phys.*, **73**, 7872, (1993).
75. S. Balakumar, R. Ilangoan, and C. Subramanian, *Materials Research Bulletin*, **30**, 499, (1995).
76. W. Wardzynski, T. Lukasiewicz, and J. Zmija, *Optics Communications*, **30**, 203, (1979).
77. W. Wardzynski, and H. Szymczak, *J. Phys. Chem. Solids*, **45**, 887, (1984).
78. T. V. Panchenko, A. Yu. Kudzin, and V. Kh. Kostyuk, *Inorganic Materials*, **19**, 1031, (1983).
79. B. Briat, V. Topa, C. L. Boudy, and J. C. Launay, *Journal of Luminescence*, **53**, 524, (1992).
80. V. Sainov, M. Gospodinov, S. Sainov, and V. Marinova, *Optics Communications*, **101**, 5, (1993).
81. T. S. Yeh, W. J. Lin, I. N. Lin, L. J. Hu, S. P. Lin, S. L. Tu, C. H. Lin, and S. E. Hsu, *Appl. Phys. Lett.*, **65**, 1213, (1994).
82. E. V. Mokrushina, A. A. Nechitailov, and V. V. Prokofiev, *Optics Communications*, **123**, 592, (1996).
83. A. V. Egorysheva, V. I. Burkov, Yu. F. Kargin, and V. V. Volkov, *Inorganic Materials*, **33**, 483, (1997).

84. C. Coya, J. L. G. Fierro, and C. Zaldo, *J. Phys. Chem. Solids*, **58**, 1461, (1997).
85. M. V. Shilova, L. V. Chertkova, V. M. Orlov, and E. E. Kolosoz, *Inorganic Materials*, **20**, 464, (1984).
86. A. Witek, *Physica*, **128B**, 39, (1985).
87. M. V. Shilova, V. M. Orlov, E. I. Leonov, E. E. Kolosov, and I. A. Karpovich, *Inorganic Materials*, **22**, 87, (1986).
88. A. B. Dubovskii, A. A. Marin, G. A. Sidorenko, and A. A. Fotchenkov, *Inorganic Materials*, **22**, 1640, (1986).
89. T. V. Panchenko, and N. A. Truseyeva, *Ferroelectrics*, **115**, 73, (1991).
90. M. Gospodinov, V. Marinova, V. Sainov, and P. Sveshtarov, *Mat. Res. Bull.*, **28**, 445, (1993).
91. M. Harris, J. Larkin, J. E. Cormier, A. F. Armington, *Journal of Crystal Growth*, **137**, 128, (1994).
92. D. Petrova, M. Gospodinov, and P. Sveshtarov, *Mat. Res. Bull.*, **30**, 1201, (1995).
93. T. V. Panchenko, and N. A. Truseyeva, *SPIE*, **2706**, 83, (1996).
94. T. V. Panchenko, *Physics of the Solid State*, **40**, 415, (1998).
95. T. V. Panchenko, and L. M. Karpova, *Physics of the Solid State*, **40**, 432, (1998).
96. T. M. Wilson, Oklahoma State University, Private Communication, (1999).
97. E. Moya, L. Contreras, and C. Zaldo, *J. Opt. Soc. Am. B*, **5**, 1737, (1988).
98. F. J. Lopez, E. Moya, and C. Zaldo, *Solid State Communication*, **76**, 1169, (1990).
99. H. R. Verdun, L. M. Thomas, D. M. Andrauskas, T. McCollum, and A. Pinto, *Appl. Phys. Lett.*, **53**, 2593, (1988).
100. W. Jia, H. Liu, S. Jaffe, and W. M. Yen, *Physical Review B*, **43**, 5234, (1991).
101. L. D. Merkle, T. H. Allik, B. H. T. Chai, *Optical Materials*, **1**, 91, (1992).
102. A. G. Okhrimchuk, A. V. Shestakov, *Optical Materials*, **3**, 1, (1994).

103. N. V. Kuleshov, V. P. Mikhailov, V. G. Scherbitsky, B. I. Minkov, T. J. Glynn, and R. Sherlock, *Optical Materials*, **4**, 507, (1995).
104. S. G. Demos, V. Petricevic, and R. R. Alfano, *Physical Review B*, **52**, 1544, (1995).
105. D. M. Calistru, W. B. Wang, V. Petricevic, and R. R. Alfano, *Physical Review B*, **51**, 14980, (1995).
106. S. Kuck, K. Petermann, U. Pohlmann, and G. Huber, *Physical Review B*, **51**, 17323, (1995).
107. S. Kuck, K. Petermann, U. Pohlmann, and G. Huber, *Journal of Luminescence*, **68**, 1, (1996).
108. M. F. Hazenkamp, H. U. Gudel, M. Atanasov, U. Kesper, and D. Reinen, *Physical Review B*, **53**, 2367, (1996).
109. R. Moncorge, H. Manaa, F. Deghoul, Y. Guyot, Y. Kalisky, S. A. Pollack, E. V. Zharikov, and M. Kokta, *Optics Communications*, **132**, 279, (1996).
110. K. V. Yumashev, N. V. Kuleshov, P. V. Prokoshin, A. M. Malyarevich, and V. P. Mikhailov, *Appl. Phys. Lett.*, **70**, 2523, (1997).
111. N. V. Kuleshov, V. G. Shcherbitsky, V. P. Mikhailov, S. Hartung, T. Danger, S. Kuck, K. Petermann, and G. Huber, *Journal of Luminescence*, **75**, 319, (1997).
112. R. Moncorge, H. Manaa, and G. Boulon, *Optical Materials*, **4**, 139, (1994).
113. M. A. Scott, T. P. J. Han, H. G. Gallagher, and B. Henderson, *Journal of Luminescence*, **72-74**, 260, (1997).
114. V. P. Mikhailov, N. V. Kuleshov, N. I. Zhavoronkov, P. V. Prokoshin, K. V. Yumashev, and V. A. Sandulenko, *Optical Materials*, **2**, 267, (1993).
115. J. A. Capobianco, G. Cormier, C. A. Morrison, and R. Moncorge, *Optical Materials*, **1**, 209, (1992).
116. J. A. Capobianco, G. Cormier, R. Moncorge, H. Manaa, and M. Bettinelli, *Appl. Phys. Lett.*, **60**, 163, (1992).
117. L. D. Merkle, A. Pinto, H. R. Verdun, and B. McIntosh, *Appl. Phys. Lett.*, **61**, 2386, (1992).
118. M. Herren, T. Riedener, H. U. Gudel, C. Albrecht, U. Kaschuba, and D. Reinen, *Journal of Luminescence*, **53**, 452, (1992).

119. J. A. Capobianco, G. Cormier, M. Bettinelli, R. Moncorge, and H. Manaa, *Journal Of Luminescence*, **54**, 1, (1992).
120. L. D. Merkle, B. H. T. Chai, and Y. Guyot, *Mat. Res. Soc. Symp. Proc.*, **329**, 239, (1994).
121. M. Atanasov, H. Adamsky, and D. Reinen, *Chemical Physics*, **202**, 155, (1996).
122. L. C. Ferracin, M. R. Davolos, and L. A. O. Nunes, *Journal of Luminescence*, **72-74**, 185, (1997).
123. M. Herren, H. U. Gudel, C. Albrecht, and D. Reinen, *Chemical Physics Letters*, **183**, 98, (1991).
124. J. D. Kingsley, J. S. Prener, and B. Segall, *Physical Review*, **137**, A 189, (1965).
125. J. Milstein, and S. L. Holt, *Inorganic Chemistry*, **8**, 1021, (1969).
126. J. B. Milstein, J. Ackerman, S. L. Holt, and B. R. McGarvey, *Inorganic Chemistry*, **11**, 1178, (1972).
127. R. Borromei, L. Oleari, and P. Day, *J. Chem. Soc., Faraday Trans. 2*, **73**, 135, (1977).
128. R. Borromei, L. Oleari, and P. Day, *J. Chem. Soc., Faraday Trans. 2*, **77**, 1563, (1981).
129. H. Lachwa, and D. Reinen, *Inorganic Chemistry*, **28**, 1044, (1989).
130. W. Wardzynski, H. Szymczak, M. T. Borowiec, K. Pataj, T. Lukasiewicz, and J. Zmija, *J. Phys. Chem. Solids*, **46**, 1117, (1985).
131. T. N. Nguyen, and M. T. Borowiec, *J. Phys. Chem. Solids*, **49**, 1379, (1988).
132. Sh. M. Efendiev, V. E. Bagiev, A. Kh. Zeinally, M. Grandolfo, and P. Vecchia, *Ferroelectrics*, **43**, 217, (1982).
133. L. Kovacs, E. Moya, K. Polgar, F. J. Lopez, and C. Zaldo, *Appl. Phys. A*, **52**, 307, (1991).
134. J. P. Huignard, and F. Micheron, *Applied Physics Letters*, **29**, 591, (1976).
135. P. N. Gunter, *Optics Communications*, **41**, 83, (1982).
136. R. A. Mullen, and R. W. Hellwarth, *J. Appl. Phys.*, **58**, 40, (1985).

137. Ph. Refregier, L. Solymar, H. Rajbenbach, and J. P. Huignard, *J. Appl. Phys.*, **58**, 45, (1985).
138. G. Lesaux, G. Roosen, and A. Brun, *Optics Communications*, **56**, 374, (1986).
139. A. E. Attard, and T. X. Brown, *Applied Optics*, **25**, 3253, (1986).
140. G. Pauliat, J. M. Cohen-Jonathan, M. Allain, J. C. Launay, and G. Roosen, *Optics Communications*, **59**, 266, (1986).
141. J. Ferrier, J. Gazengel, X. Nguyen Phu, and G. Rivoire, *Optics Communications*, **58**, 343, (1986).
142. J. P. Herriau, and J. P. Huignard, *Appl. Phys. Lett.*, **49**, 1140, (1986).
143. J. C. Jonathan, R. W. Hellwarth, and G. Roosen, *IEEE Journal of Quantum Electronics*, **QE-22**, 1936, (1986).
144. G. Pauliat, M. Allain, J. Launay, and G. Roosen, *Optics Communications*, **61**, 321, (1987).
145. F. P. Strohkendl, and R. W. Hellwarth, *J. Appl. Phys.*, **62**, 2450, (1987).
146. A. E. Attard, *Applied Optics*, **27**, 232, (1988).
147. L. Arizmendi, *J. Appl. Phys.*, **65**, 423, (1989).
148. F. P. Strohkendl, *J. Appl. Phys.*, **65**, 3773, (1989).
149. P. A. M. dos Santos, P. M. Garcia, and J. Frejlich, *J. Appl. Phys.*, **66**, 247, (1989).
150. A. Delboulbe, C. Fromont, J. P. Herriau, S. Mallick, and J. P. Huignard, *Appl. Phys. Lett.*, **55**, 713, (1989).
151. J. A. Baquedano, L. Contreras, E. Dieguez, and J. M. Cabrera, *J. Appl. Phys.*, **66**, 5146, (1989).
152. A. E. Attard, *J. Appl. Phys.*, **66**, 3211, (1989).
153. F. P. Strohkendl, P. Tayebati, and R. W. Hellwarth, *J. Appl. Phys.*, **66**, 6024, (1989).
154. P. Tayebati, *J. Appl. Phys.*, **70**, 4082, (1991).

155. J. E. Millerd, E. M. Garmire, M. B. Klein, B. A. Wechsler, F. P. Strohkendl, and G. A. Brost, *J. Opt. Soc. Am. B*, **9**, 1449, (1992).
156. C. Soutar, W. A. Gillespie, and C. M. Cartwright, *Optics Communications*, **90**, 329, (1992).
157. J. B. Norman, J. H. Hong, and T. Y. Chang, *J. Appl. Phys.*, **75**, 4873, (1994).
158. J. Khoury, M. Cronin-Golomb, and C. Woods, *J. Appl. Phys.*, **77**, 7, (1995).
159. J. G. Murillo, L. F. Magana, M. Carrascosa, and F. Agullo-Lopez, *J. Appl. Phys.*, **78**, 5686, (1995).
160. M. P. Petrov, V. M. Petrov, Y. S. Raptis, L. P. Xu, and E. Anastassakis, *J. Appl. Phys.*, **79**, 2846, (1996).
161. L. Arizmendi, and R. C. Powell, *J. Appl. Phys.*, **62**, 896, (1987).
162. I. Foldvari, J. J. Martin, C. A. Hunt, R. C. Powell, R. J. Reeves, and S. A. Holmstrom, *Optical Materials*, **2**, 25, (1993).
163. I. Foldvari, J. J. Martin, C. A. Hunt, R. C. Powell, R. J. Reeves, and A. Peter, *J. Appl. Phys.*, **74**, 783, (1993).
164. D. Bloom and S. W. S. McKeever, *J. of Appl. Phys.*, **84**, 1830, (1998).
165. J. J. Martin, Oklahoma State University, Private Communication, (1999).
166. A. Harmon, Oklahoma State University, Private Communication, (1996).
167. N. V. Kukhtarev, *Sov. Tech. Phys. Lett.*, **2**, 438, (1976).
168. N. V. Kukhtarev, V. B. Markov, S. G. Odulov, M. S. Soskin, and V. L. Vinetskii, *Ferroelectrics*, **22**, 949, (1979).
169. N. V. Kukhtarev, V. B. Markov, S. G. Odulov, M. S. Soskin, and V. L. Vinetskii, *Ferroelectrics*, **22**, 961, (1979).
170. J. Feinberg, D. Heiman, A. R. Tanguay, Jr., and R. W. Hellwarth, *J. Appl. Phys.*, **51**, 1297, (1980).
171. T. J. Hall, R. Jaura, L. M. Connors, and P. D. Foote, *Prog. Quant. Electr.*, **10**, 77, (1985).
172. R. Jaura, T. J. Hall, and P. D. Foote, *Optical Engineering*, **25**, 1068, (1986).

173. G. C. Valley, *Applied Optics*, **22**, 3160, (1983).
174. G. A. Brost, R. A. Motes, and J. R. Rotge, *J. Opt. Soc. Am. B*, **5**, 1879, (1988).
175. P. Tayebati, and D. Mahgerefteh, *J. Opt. Soc. Am. B*, **8**, 1053, (1991).
176. G. A. Brost, *J. Opt. Soc. Am. B*, **9**, 1454, (1992).
177. G. A. Brost, *Optics Communications*, **96**, 113, (1993).
178. E. Serrano, V. Lopez, M. Carrascosa, and F. Agullo-Lopez, *IEEE Journal of Quantum Electronics*, **30**, 875, (1994).
179. E. Serrano, V. Lopez, M. Carrascosa, and F. Agullo-Lopez, *J. Opt. Soc. Am. B*, **11**, 670, (1994).
180. G. A. Brost, K. M. Magde, J. J. Larkin, and M. T. Harris, *J. Opt. Soc. Am. B*, **11**, 1764, (1994).
181. E. Serrano, M. Carrascosa, and F. Agullo-Lopez, *Optics Letters*, **20**, 1910, (1995).
182. L. Solymar, M. Aguilar, and F. Agullo-Lopez, *J. Appl. Phys.*, **80**, 1268, (1996).
183. E. Serrano, M. Carrascosa, and F. Agullo-Lopez, *J. Opt. Soc. Am. B*, **13**, 2587, (1996).
184. H. Kogelnik, *The Bell System Technical Journal*, **48**, 2909, (1969).

APPENDICES

Appendix A

Program For Writing A Grating And Monitoring The Grating At Different Temperatures

```
10 PRINT " TAKES FOTOREF DATA FROM SCOPE & DMM "  
11 PRINT " CONTROLS THE SHUTTER VIA THE SERIAL PORT "  
20 OPTION BASE 1 !ARRAYS START AT INDEX 1  
30 DIM Preamble(10),Sig1(1000),Sig(1000),Dvmsig1(200),Dvmsig(200)  
40 DIM Tdvm(200),Iscope(200),Tscope(200),Ts(100)  
50 INTEGER Waveform(1000)  
60 PRINT "THE # OF POINTS READ IS 1000"  
70 INPUT "ENTER THE DRIVE & DIRECTORY AS:DR:\DIR\",Dr$  
80 !CONFIGURE THE INTERFACE  
90 ASSIGN @Isc TO 7  
100 ASSIGN @Scope TO 707 !SCOPE ADDRESS  
120 ASSIGN @Refrig TO 703 !VHF RY BOX FOR REFRIG ON/OFF  
130 ASSIGN @Tri TO 704 !TRI CYRO-TEMP CONTROLLER  
140 ASSIGN @Fast TO 707;FORMAT OFF !TURN CONTROLLER FORMATING  
OFF  
150 CLEAR @Isc  
160 !SET THE SERIAL PORT TO 300 BAUD  
170 CONTROL 9,3;300  
171 !SET THE SERIAL PORT TO 8 DATA BITS, NO STOP BITS, NO PARITY  
172 CONTROL 9,4;3  
173 !NOTE THE "B" COMMAND FIRES THE SHUTTER  
174 S$="B"  
180 !CONFIGURE THE DVM TO TAKE 200 READINGS
```

```

190 REMOTE 726
200 OUTPUT 726;"S0X" !SET FOR 2.59ms INTEGRATION TIME (4.5 DIGITS)
210 OUTPUT 726;"F0R2X" !SET DVM FOR DCV ON3V RANGE
220 INPUT "ENTER THE TIME IN ms BETWEEN THE 200 DVM
READINGS",Tdvm$
230 Dmm$="T2Q"&Tdvm$&"I200X"
240 OUTPUT 726;Dmm$
250 ON KEY 1 LABEL "SCOPE" GOSUB Takedata
260 ON KEY 2 LABEL "PLOTSCOPE" GOSUB Plotscope
270 ON KEY 3 LABEL "PLOTDVM" GOSUB Plotdvm
280 ON KEY 4 LABEL "LOG-GRAF" GOSUB Loggraf
290 ON KEY 5 LABEL "STORE" GOSUB Storedata
300 ON KEY 7 LABEL "CHNG-DVM" GOSUB Changedvm
310 ON KEY 8 LABEL "DUMP" GOSUB Dumpgraf
320 ON KEY 12 LABEL "TSETUP" GOSUB Tsetup
330 ON KEY 9 LABEL "ANNEAL" GOSUB Anneal
340 !KEY LABELS ON
350 GOTO 350
360 Takedata: !COLLECTS THE DATA
370 !GOSUB Refrig
380 !GET AVG BACKGROUND FOR THE DVM
390 OUTPUT 726;"T2Q20I100X"
400 TRIGGER 726
410 Dvmavg=0
420 OUTPUT 726;"B1G3X"
430 FOR I=1 TO 100
440 ENTER 726;V,J
450 Dvmavg=V+Dvmavg
460 NEXT I
470 Dvmavg=Dvmavg/100
480 !RESET DVM
490 OUTPUT 726;Dmm$
500 OUTPUT @Scope;":WAVEFORM:SOURCE CHAN1" !SET CHANNEL1
FOR DATA
510 OUTPUT @Scope;":ACQUIRE:TYPE NORMAL" !NORMAL DATA
ACQUISITION
520 OUTPUT @Scope;":ACQUIRE:COMPLETE 100" !COMPLETION
CRITERION
530 OUTPUT @Scope;":WAVEFORM:POINTS 1000" !SET # OF POINTS TO
1000
540 OUTPUT @Scope;":WAVEFORM:FORMAT WORD"
550 OUTPUT @Scope;":DIGITIZE CHAN1" !MACRO TO ACQUIRE DATA
& STOP
560 OUTPUT @Scope;":WAVEFORM:DATA?" !ASK SCOPE FOR THE
DATA

```



```

570 WAIT 1 !WAIT FOR THE SCOPE THEN WRITE GRATING
580 TRIGGER 726
590 !FIRE THE SHUTTER
600 OUTPUT 9;S$
620 ENTER @Scope USING "#,2A,8D";Header$,Bytes !STRIP OFF HEADER
630 PRINT "READING ";Bytes;" BYTES FROM THE SCOPE"
640 ENTER @Fast;Waveform(*)
650 ENTER @Scope USING "-K,B";End$
660 OUTPUT @Scope;":WAVEFORM:PREAMBLE?" !ASK FOR THE PREAMBLE
670 ENTER @Scope;Preamble(*)
680 !PRINT THE PREAMBLE
690 IMAGE "PREAMBLE(",2D,") = ",SD.DDE
700 FOR I=1 TO 10
710 PRINT USING 690;I,Preamble(I)
720 NEXT I
730 !GET THE DATA FROM THE DVM BY ASKING FOR SINGLE DATA STORE
READINGS
740 OUTPUT 726;"B1G3X"
750 FOR I=1 TO 200
760 ENTER 726;Dvmsig1(I)
770 NEXT I
780 PRINT "THE DATA ARE IN THE COMPUTER, PLEASE WAIT I'M BUSY"
790 !CONVERT WAVEFORM TO THE SIGNAL IN VOLTS AS DISPLAYED
WITH 0 IN THE CENTER
800 FOR I=1 TO 1000
810 Sig1(I)=Preamble(8)*(Waveform(I)-Preamble(10))
820 NEXT I
830 !CALCULATE THE BASELINE BY AVGING THE 1st 100 POINTS--B4
THE TRIGGER
840 Avg=0
850 FOR I=1 TO 100
860 Avg=Avg+Sig1(I)
870 NEXT I
880 Avg=Avg/100
890 INPUT "ENTER THE CURRENT AMP GAIN IN VOLTS/AMP",Gain
910 !NOW CALCULATE THE SCALED FWM SIGNAL
920 FOR I=1 TO 1000
930 Sig(I)=(Sig1(I)-Avg)/Gain !Amps
931 Sig(I)=Sig(I)*1.E+6 !microAmps
940 NEXT I
950 !REDUCE SCOPE DATA TO 188 POINTS AND SMOOTH THE DATA
960 !FIRST 100 AT INTERVALS DELTAT, NEXT AT INTERVALS OF
10*DELTAT
970 Delt=Preamble(5) !IN SECONDS
980 FOR I=1 TO 100

```

```

990  Tscope(I)=Delt*(I-1)!IN SECONDS
1000  Iscope(I)=Sig(I+100) !IGNORE THE FIRST 100 POINTS (B4 THE TRIGGER)
1010  NEXT I
1020  !THERE ARE 800 (100<J<1000) SIG(*) POINTS REMAINING
1030  I=I-1
1040  FOR J=100 TO 900 STEP 10
1050  I=I+1 !STEP INDEX I
1060  Tscope(I)=Delt*(J-1) !IN SECONDS
1070  Iscope(I)=Sig(J+100)
1080  NEXT J
1090  Nscope=I !NUMBER OF SCOPE POINTS
1100  !NOW CALCULATE THE DVM READINGS
1110  FOR I=1 TO 200
1120  Dvmsig(I)=(Dvmsig1(I)-Dvmavg)/Gain !Amps
1121  Dvmsig(I)=Dvmsig(I)*1.E+6 !microAmps
1130  Tdvm(I)=(I-1)*VAL(Tdvm$)/1000 !IN SECONDS
1140  NEXT I
1150  PRINT "DONE--READY TO PLOT AND STORE"
1160  RETURN
1170 Plotscope: !DRAW THE AXES FOR THE GRAPH
1180  CLEAR SCREEN
1190  GCLEAR
1200  IMAGE "FULE SCALE TIME = ",D.DDE," SEC"
1210  PRINT USING 1200;Preamble(3)*Preamble(5)
1220  INPUT "ENTER TMAX IN SECONDS AND TTICK IN SECONDS",Tmax,Ttick
1230  IMAGE "THE MAX SIGNAL = ",DDDD.DDDD
1240  PRINT USING 1230;MAX(Sig(*))
1250  INPUT "ENTER YMAX AND YTICK",Ymax,Ytick
1260  CLEAR SCREEN
1270  DEG
1280  GRAPHICS ON
1290  VIEWPORT 0,50*RATIO,30,100
1300  WINDOW -.2*Tmax,1.1*Tmax,-.3*Ymax,1.1*Ymax
1310  CLIP 0,Tmax,0,Ymax
1320  AXES Ttick,Ytick,0,0
1330  AXES Ttick,Ytick,Tmax,Ymax
1340  CLIP OFF
1350  !LABEL AXES
1360  LORG 6
1370  CSIZE 3,.5
1380  Y=-.01*Ymax
1390  FOR T=0 TO Tmax STEP Ttick
1400  MOVE T,Y
1410  LABEL T
1420  NEXT T

```

```

1430 MOVE Tmax/2,-.12*Ymax
1440 LABEL "TIME (s)"
1450 LORG 8
1460 T=-.01*Tmax
1470 FOR Y=0 TO Ymax STEP Ytick
1480 MOVE T,Y
1490 LABEL Y
1500 NEXT Y
1510 LDIR 90
1520 MOVE -.15*Tmax,Ymax/2
1530 LORG 5
1540 LABEL "SIGNAL (microAmps)"
1550 LDIR 0
1560 LORG 2
1570 CLIP 0,Tmax,0,Ymax !NOW PLOT THE SCOPE DATA
1580 MOVE 0,0
1590 FOR I=1 TO Nscope
1600 DRAW Tscope(I),Iscope(I)
1610 NEXT I
1620 MOVE .2*Tmax,.8*Ymax
1630 LABEL Dr$&F$
1640 RETURN
1650 Storedata: !STORE DATA ON DISC
1660 !STORE SCOPE DATA WITH EXTENSION .SCP
1670 INPUT "ENTER THE FILE NAME--F$ ",F$
1680 CREATE Dr$&F$&".SCP",2*N+1
1690 ASSIGN @File TO Dr$&F$&".SCP";FORMAT ON
1700 DIM A$[50]
1710 IMAGE 15A
1720 OUTPUT @File USING 1710;"SCOPEDATA"
1730 IMAGE D.4D,"",SD.DDE
1740 FOR I=1 TO Nscope
1750 OUTPUT @File USING 1730;Tscope(I),Iscope(I)
1760 NEXT I
1770 !STORE THE DVM DATA WITH EXTENSION .DVM
1780 ASSIGN @File TO *
1790 CREATE Dr$&F$&".DVM",2*N+1
1800 ASSIGN @File TO Dr$&F$&".DVM";FORMAT ON
1810 OUTPUT @File USING 1710;"DVMDATA"
1820 IMAGE 3D.2D,"",SD.DDE
1830 FOR I=1 TO 200
1840 OUTPUT @File USING 1820;Tdvm(I),Dvmsig(I)
1850 NEXT I
1860 ASSIGN @File TO *
1861 IMAGE "THE DATA HAVE BEEN STORED AS ", 20A

```

```

1862 PRINT USING 1861;Dr$&F$
1870 RETURN
1880 Dumpgraf: !
1890 !CONFIGURE DUMP TO "HP-PCL"
1900 DUMP DEVICE IS 10,EXPANDED
1910 DUMP GRAPHICS #10
1920 PRINTER IS 10
1930 PRINT CHR$(12)
1940 PRINTER IS 1
1950 RETURN
1960 Changedvm: !ALLOWS YOU TO CHANGE THE INTERVAL BETWEEN DVM
READINGS
1970 INPUT "ENTER THE NEW TIME INTERVAL IN ms",Tdmv$
1980 Dmm$="T2Q"&Tdmv$&"I100X"
1990 OUTPUT 726;Dmm$
2000 RETURN
2010 Plotdvm: !PLOT THE DVM DATA
2020 INPUT "ENTER TMAX IN SECONDS AND TTICK IN SECONDS",Tmax,Ttick
2030 INPUT "ENTER YMAX AND YTICK",Ymax,Ytick
2040 VIEWPORT 50*RATIO,100*RATIO,30,100
2050 WINDOW -.2*Tmax,1.1*Tmax,-.3*Ymax,1.1*Ymax
2060 CLIP 0,Tmax,0,Ymax
2070 AXES Ttick,Ytick,0,0
2080 AXES Ttick,Ytick,Tmax,Ymax
2090 CLIP OFF
2100      !LABEL AXES
2110 LORG 6
2120 CSIZE 4,5
2130 Y=-.01*Ymax
2140 FOR T=0 TO Tmax STEP Ttick
2150   MOVE T,Y
2160   LABEL T
2170 NEXT T
2180 MOVE Tmax/2,-.12*Ymax
2190 LABEL "TIME (s)"
2200 LORG 8
2210 T=-.01*Tmax
2220 FOR Y=0 TO Ymax STEP Ytick
2230   MOVE T,Y
2240   LABEL Y
2250 NEXT Y
2260 LDIR 90
2270 MOVE -.15*Tmax,Ymax/2
2280 LORG 5
2290 LABEL "SIGNAL (microAmps)"

```

```

2300 LDIR 0
2310 LORG 2
2320 !NOW PLOT THE SCOPE DATA
2330 MOVE 0,0
2340 FOR I=1 TO Nscope
2350 DRAW Tscope(I),Iscope(I)
2360 NEXT I
2370 MOVE .1*Tmax,1.05*Ymax
2380 LABEL F$
2390 MOVE Tdvm(2),Dvmsig(2)
2400 FOR I=2 TO 200
2410 DRAW Tdvm(I),Dvmsig(I)
2420 NEXT I
2430 RETURN
2440 Loggraf: !DRAWS LOG VS TIME FOR FWMDATA
2450 DEG
2460 INPUT "ENTER TMAX AND TTICK IN SECONDS",Tmax,Ttick
2470 INPUT "ENTER MAX POWER OF TEN FOR THE LOG SIGNAL
SCALE",Ymax
2480 VIEWPORT 50*RATIO,100*RATIO,20,100
2490 WINDOW -.2*Tmax,1.1*Tmax,Ymax-4.7,Ymax+.2
2500 CLIP 0,Tmax,Ymax-4,Ymax
2510 AXES Ttick,1,0,Ymax-4
2520 AXES Ttick,1,Tmax,Ymax
2530 CLIP OFF
2540 !LABEL TIME AXIS
2550 CSIZE 3,.5
2560 LORG 6
2570 Y=Ymax-4.05
2580 FOR T=0 TO Tmax STEP Ttick
2590 MOVE T,Y
2600 LABEL T
2610 NEXT T
2620 Y=Ymax-4.3
2630 MOVE Tmax/2,Y
2640 LABEL "TIME (s)"
2650 !LABEL SIGNAL AXIS
2660 T=-.11*Tmax
2670 LORG 1
2680 FOR Y=Ymax-4 TO Ymax
2690 MOVE T,Y
2700 LABEL Y
2710 NEXT Y
2720 LORG 8
2730 FOR Y=Ymax-4 TO Ymax

```

```

2740 MOVE T,Y
2750 LABEL "10"
2760 NEXT Y
2770 LDIR 90
2780 MOVE -.2*Tmax,Ymax-2.
2790 LORG 4
2800 LABEL "SIGNAL (microAmps)"
2810 LDIR 0
2820 LORG 2
2830 !PLOT THE SCOPE DATA
2840 MOVE Tscope(5),Iscope(5) !IGNORE THE FIRST 4 POINTS
2850 FOR I=5 TO Nscope
2860 DRAW Tscope(5),LGT(ABS(Iscope(5)))
2870 NEXT I
2880 !PLOT THE DVM DATA
2890 MOVE Tdvm(3),Dvmsig(3)
2900 FOR I=3 TO 200
2910 DRAW Tdvm(I),LGT(ABS(Dvmsig(I)))
2920 NEXT I
2930 RETURN
2940 Tsetup: !SETS UP THE THE TRI CONTROLLER
2950 IMAGE "P",3D.D
2960 !SENSOR #1
2970 OUTPUT @Tri;"S1"
2980 !SET GAIN TO 40
2990 OUTPUT @Tri;"G40"
3000 WAIT 1
3010 !SET INTEGRAL TO 20
3020 OUTPUT @Tri;"I20"
3030 WAIT 1
3040 !SET DERIVATIVE TO 0.2
3050 OUTPUT @Tri;"D.2"
3060 WAIT 1
3070 !SET INITIAL SETPOINT TO 4K
3080 OUTPUT @Tri USING 2950;4
3090 !START CONTROL LOOP
3100 OUTPUT @Tri;"R"
3110 !SET REFRIG COLDHEAD TO RUN
3120 OUTPUT @Refrig USING "K";"A1"
3130 RETURN
3140 Anneal: !USES TRI CONTROLLER TO SET ANNEAL T AND TURNS OFF
COLD HEAD"
3150 INPUT "ENTER DESIRED ANNEAL TEMP",Tanl
3160 IMAGE "P",DDD.DD
3170 IMAGE "TEMPERATURE = ",3D.DD,"K"

```

```
3180     OUTPUT @Tri USING 3160;Tanl
3190     WAIT 1
3200     !STOP REFRIG COLD HEAD
3210     OUTPUT @Refrig USING "K";"A2"
3220     OUTPUT @Tri;"O1"
3230     ENTER @Tri;Temp
3240     DISP USING 3170;Temp
3250     IF Temp<Tanl THEN 3220
3260     !RETURN SETPOINT TO 4K AND START COLDHEAD
3270     OUTPUT @Tri USING 3160;4
3280     OUTPUT @Refrig USING "K";"A1"
3290     FOR I=1 TO 100
3300     OUTPUT @Tri;"O1"
3310     ENTER @Tri;Ts(I)
3320     PRINT USING 3170;Ts(I)
3330     WAIT 3
3340     NEXT I
3350     IMAGE "ANNEAL TEMP = ",3D.D," K"
3360     PRINT USING 3350;MAX(Ts(*))
3370     RETURN
3380     END
```

Appendix B

Program For Writing A Grating And Monitoring The Grating As The Sample Is Heated.

```
10 PRINT " MEASURES PERSISTENT GRATING VS T "  
20 PRINT " USES KEITHLEY DMM: ADDR 726 "  
21 PRINT " USES 3478A DMM: ADDR 717 and HP PS PROGRAMMER: ADDR  
703 "  
30 OPTION BASE 1  
40 DIM Tc(200),Dvmsig1(200),Dvmsig(200),Tm(200)  
50 INPUT "ENTER DRIVE AND DIRECTORY AS (FOR EX) A:\DR",Dr$  
60 PRINT "DR$ = ",Dr$  
70 INPUT "IS THIS OK? Y OR N",Ok$  
71 IF Ok$="N" OR Ok$="n" THEN 50  
80 !FILES WITH FORMAT ON  
90 IMAGE "2",DDD  
91 !SET UP THE COM1 SERIAL PORT FOR THE WRITE SHUTTER  
92 CONTROL 9,3;300  
93 CONTROL 9,4;3  
100 !DATA FOR TYPE-K (CH-AL) TC POLYNOMIAL EXPANSION  
110 READ P(*)  
120 DATA -0.051,24850.3,-382662,99661057,-10820624000,603928550000,-  
1.9109E13,3.4782347E14,-3.991028E15,1.3828514E16  
130 OUTPUT 703 USING 90;0  
140  
|*****  
150 ON KEY 1 LABEL "AXES" GOSUB Graph  
160 ON KEY 2 LABEL "PARAMS" GOSUB Params  
170 ON KEY 3 LABEL "TAKE DATA" GOSUB Take_data  
190 ON KEY 4 LABEL "T-MONITOR" GOSUB T_monitor
```



```

191 ON KEY 5 LABEL "STOREDATA" GOSUB Storedata
193 ON KEY 8 LABEL "DUMPGRAF" GOSUB Dumpgraf
220 !KEY LABELS ON
230 GOTO 230
240 T_monitor:
!*****
250 !USES HP 3478A DMM ADDR 717
260 IMAGE "TEMPERATURE = ",4D.D,"C FOR READING #",3D
261 INPUT "ENTER THE NUMBER OF READINGS",Nreadings
270 FOR I=1 TO Nreadings
290 ENTER 717;V
300 T=0
310
T=P(1)+V*(P(2)+V*(P(3)+V*(P(4)+V*(P(5)+V*(P(6)+V*(P(7)+V*(P(8)+V*(P(9)+V*
P(10))))))))))
350 DISP USING 260;T,I
360 WAIT 5
370 NEXT I
380 RETURN
390 Graph:
!*****
400 !SETUP THE AXES
410 DEG
420 CSIZE 5,.5
430 GINIT
440 CLEAR SCREEN
450 Vp=35
460 INPUT "ENTER THE MAX TEMP FOR PLOTTING IN 100'Cs",Tmax
470 INPUT "ENTER THE MAX POWER OF TEN FOR LOG SIGNAL
SCALE",Ymax
510 PEN 1
520 VIEWPORT 10,100*RATIO,Vp,100
530 WINDOW -.2*Tmax,1.1*Tmax,Ymax-4.7,Ymax+.5
540 CLIP 0,Tmax,Ymax-4,Ymax
550 AXES 10,1,0,Ymax-4
560 AXES 10,1,Tmax,Ymax
570 CLIP OFF
580 !LABEL T AXIS
590 IMAGE D,"OO"
600 LORG 6
601 CSIZE 4,.5
610 Y=Ymax-4.05
620 MOVE 0,Y
630 !LABEL "O"
640 FOR X=0 TO Tmax STEP 50

```

```

650  MOVE X,Y
660  LABEL X
710  NEXT X
720  CSIZE 5,.6
730  MOVE Tmax/2,Ymax-4.3
740  LABEL "TEMPERATURE (°C)"
750  CSIZE 4,.5
760  !LABEL Y AXIS
770  LORG 8
780  X=-.05*Tmax
790  FOR Y=Ymax-4 TO Ymax
800  MOVE X,Y
810  LABEL "10"
860  NEXT Y
870  LORG 1
880  IMAGE D
890  FOR Y=Ymax-4 TO Ymax
900  MOVE X,Y
910  LABEL Y
920  NEXT Y
950  LDIR 90
960  CSIZE 5,.5
970  LORG 4
980  MOVE -.1*Tmax,Ymax-2
990  LABEL "SIGNAL"
1000 LDIR 0
1010 LORG 2
1020 CSIZE 4,.5
1030 RETURN
1040 Params:
!*****
1050 !ENTER THE PARAMETERS FOR THE DATA RUN"
1060 IMAGE "(1) FILE NAME F$=",8A
1061 IMAGE "(2) CURRENT AMP GAIN =",D.DE
1110 IMAGE "(3) STOPPING TEMPERATURE = ",4D,"C"
1120 M=0
1130 CLEAR SCREEN
1140 INPUT "ENTER THE FILE NAME--8 CHARACTERS MAX ",F$
1150 IF M>0 THEN 1330
1151 INPUT "ENTER THE CURRENT AMP GAIN",Gain
1270 INPUT "ENTER THE STOPPING TEMPERATURE",Tstop
1290 IF M>0 THEN 1330
1300 CLEAR SCREEN
1310 M=M+1
1320 PRINT "THE RUN PARAMETERS ARE:"

```

```

1330 PRINT USING 1060;F$
1331 PRINT USING 1061;Gain
1380 PRINT USING 1110;Tstop
1390 INPUT "ARE ALL OF THESE OK? Y OR N",Ok$
1400 IF Ok$="Y" THEN 1500
1410 INPUT "ENTER THE (I) OF THE PARAMETER YOU WISH TO CHANGE",Ip
1430 IF Ip>3 OR Ip<1 THEN 1410
1440 IF Ip=1 THEN 1140
1441 IF Ip=2 THEN 1151
1450 IF Ip=3 THEN 1270
1500 !THE ABOVE ASSUME THAT WE ARE USING THE ORTEC 0-3KV SUPPLY
1510 !PRINT OUT THE PARAMETERS
1520 PRINTER IS 10
1530 PRINT USING 1060;F$
1540 PRINT USING 1061;Gain
1550 PRINT USING 1110;Tstop
1580 PRINTER IS 1
1590 DISP "NOW USE KEY F1 TO DRAW THE AXES; THEN F3 TO TAKE THE
DATA"
1600 RETURN
1610 Take_data:
!*****
1620 !RAMPS THE SETPOINT AND TAKES THE DATA
1621 Gain=10000./Gain
1622 !SET UP THE KEITHLEY 199
1623 OUTPUT 726;"S0X" !SET FOR 2.59ms INTEGRATION TIME, 4.5 DIGITS
1624 OUTPUT 726;"F0R2X" !SET FOR 3 V DC
1625 OUTPUT 726;"T3X" !SET FOR ONE SHOT ON TRIGGER
1630 J=1
1640 MOVE 10,Ymax+.05
1650 LABEL Dr$&F$
1660 CSIZE 2,.5
1670 LORG 5
1671 !COLLECT THE AVG BACKGROUND SIGNAL
1672 Dmvavg=0
1673 FOR I=1 TO 10
1674 TRIGGER 726
1675 ENTER 726;V
1676 Dvmavg=Dvmavg+V
1677 NEXT I
1678 Dvmavg=Dvmavg/10
1679 DISP "DVMAVG=",Dvmavg
1680 PAUSE
1682 !WRITE THE GRATING
1683 OUTPUT 9;"B"

```

```

1684 !TAKES A READING EVERY 1 DEG
1690 Tstart=TIMEDATE MOD 86400
1700 IMAGE "TIME IN SECONDS SINCE THE START =",8D
1710 J=1
1730 !MEASURE AND PLOT THE DATA
1731 !MEASURE T
1732 ENTER 725;V
1733
T=P(1)+V*(P(2)+V*(P(3)+V*(P(4)+V*(P(5)+V*(P(6)+V*(P(7)+V*(P(8)+V*(P(9)+V*
P(10))))))))))
1735 Tc(J)=T
1736 !FIRE THE READ SHUTTER
1737 OUTPUT 11;"B"
1738 WAIT .01
1739 TRIGGER 726
1740 ENTER 726;Dvmsig1(J)
1741 Dvmsig(J)=Gain*(Dvmsig1(J)-Dvmavg)
1742 Tm(J)=TIMEDATE MOD 86400-Tstart
1743 MOVE Tc(J),LGT(ABS(Dvmsig(J)))
1744 LABEL "+"
1745 FOR J=2 TO 200
1747 !MEASURE T
1760 ENTER 725;V
1770 T=0
1780
T=P(1)+V*(P(2)+V*(P(3)+V*(P(4)+V*(P(5)+V*(P(6)+V*(P(7)+V*(P(8)+V*(P(9)+V*
P(10))))))))))
1810 T=T
1820 Ttest=T
1830 IF Ttest>Tc(J-1)+1 THEN 1920
1840 IF Ttest>Tstop THEN 2121
1850 DISP USING 1700;TIMEDATE MOD 86400-Tstart
1860 !RAMP THE HEATER VOLTAGE PROPORTIONAL TO (T-30) IN DEG C
1870 V0=10 !INITIAL PS VOLTAGE OUTPUT
1880 V=.25*(V0+30*(Ttest-10)/(Tstop-10))
1881 V=INT(100*V)
1890 IMAGE "2",DDD
1900 OUTPUT 703 USING 1890;V
1910 GOTO 1760
1920 !MEASURE AND PLOT THE DATA
1921 !MEASURE T
1922 ENTER 717;V
1923
T=P(1)+V*(P(2)+V*(P(3)+V*(P(4)+V*(P(5)+V*(P(6)+V*(P(7)+V*(P(8)+V*(P(9)+V*
P(10))))))))))

```

```

1925 Tc(J)=T
1926 !FIRE THE READ SHUTTER
1927 OUTPUT 11;"B"
1928 WAIT .01
1929 TRIGGER 726
1930 ENTER 726;Dvmsig1(J)
1931 Dvmsig(J)=Gain*(Dvmsig1(J)-Dvmavg)
1932 Tm(J)=TIMEDATE MOD 86400-Tstart
1933 MOVE Tc(J),LGT(ABS(Dvmsig(J)))
1934 LABEL "+"
2110 IF Tc(J)>Tstop THEN 2121
2120 NEXT J
2121 !SET HEATER POWER TO ZERO
2122 V=0
2123 OUTPUT 703 USING 1890;V
2130 RETURN
2140 Storedata: !*****
2150 !SET HTR PWR TO 0
2151 V=0
2160 OUTPUT 703 USING 1890;V
2180 CREATE Dr$&F$&".TXT",3*N+1
2190 ASSIGN @File TO Dr$&F$&".TXT";FORMAT ON
2200 OUTPUT @File;Gain
2201 IMAGE SD.DDE,"",3D.D,"",4D.D
2210 FOR I=1 TO J
2220 OUTPUT @File USING 2201;Dvmsig(I),Tc(I),Tm(I)
2230 NEXT I
2240 ASSIGN @File TO *
2280 RETURN
!*****
3170 Dumpgraf: !
3180 CONFIGURE DUMP TO "HP-PCL"
3190 DUMP GRAPHICS #10
3200 PRINTER IS 10
3210 PRINT CHR$(12)
3220 PRINTER IS 1
3230 RETURN
3240 END

```

Appendix C

Program For Writing A Grating And Monitoring The Grating Over Long Time Periods

```
10 PRINT " MEASURES VERY SLOWLY DECAYING GRATINGS "  
20 PRINT " GATES THE READ BEAM USING THE NEW SHUTTER AT ISC 11  
(COM2) "  
30 PRINT " WRITES THE GRATING USING THE OLD SHUTTER AT ISC 9  
(COM1) "  
40 PRINT " SHUTTERS ARE CONTROLLED VIA THE SERIAL PORTS "  
50 OPTION BASE 1 !ARRAYS START AT INDEX 1  
60 DIM T(500),Dvmsig1(500),Dvmsig(500)  
70 PRINT "READS 500 POINTS"  
80 PRINT "CYCLE THE POWER ON THE KEITHLEY 199 DVM TO CLEAR  
PREVIOUS SETTINGS"  
90 !SET COM1 TO 300 BAUD FOR THE OLD SHUTTER  
100 CONTROL 9,3;300  
110 !SET COM1 TO 8 DATA BITS, NO STOP BITS, NO PARITY  
120 CONTROL 9,4;3  
130 !NOTE "B" FIRES THE SHUTTER  
140 ON KEY 1 LABEL "GRAPH" GOSUB Graph  
150 ON KEY 2 LABEL "DATA" GOSUB Takedata  
160 ON KEY 3 LABEL "STORE" GOSUB Storedata  
170 ON KEY 8 LABEL "DUMPGRAF" GOSUB Dumpgraf  
180 KEY LABELS ON  
190 GOTO 190  
200 Graph: !  
210 CLEAR SCREEN  
230 DEG  
240 GRAPHICS ON  
250 VIEWPORT 0,100*RATIO,30,100
```

```

260 INPUT "ENTER Tmax AND Ttick IN HOURS",Tmax,Ttick
270 INPUT "ENTER MAX POWER TO TEN FOR THE LOG SIGNAL
SCALE",Ymax
280 WINDOW -.2*Tmax,1.1*Tmax,Ymax-4.7,Ymax+.5
290 CLIP O,Tmax,Ymax-4,Ymax
300 AXES Ttick,1,0,Ymax-4
310 AXES Ttick,1,Tmax,Ymax
320 CLIP OFF
330 !LABEL TIME AXES
340 CSIZE 4,.5
350 LORG 6
360 Y=Ymax-4.05
370 FOR Tx=0 TO Tmax STEP Ttick
380 MOVE Tx,Y
390 LABEL Tx
400 NEXT Tx
410 Y=Ymax-4.3
420 MOVE Tmax/2,Y
430 LABEL "TIME(Hrs)"
440 !LABEL SIGNAL AXES
450 LORG 1
460 Tx=-.11*Tmax
470 FOR Y=Ymax-4 TO Ymax
480 MOVE Tx,Y
490 LABEL Y
500 NEXT Y
510 LORG 8
520 FOR Y=Ymax-4 TO Ymax
530 MOVE Tx,Y
540 LABEL "10"
550 NEXT Y
560 LDIR 90
570 MOVE -.2*Tmax,Ymax-2
580 LORG 4
590 LABEL "SIGNAL"
600 LDIR 0
610 LORG 2
620 RETURN
630 Takedata: !
640 !TAKES THE DATA
650 !SETUP THE DVM
660 OUTPUT 726;"S0X" !SET FOR 2.59ms INTEGRATION TIME 4.5 DIGITS
670 OUTPUT 726;"F0R2X" !SET FOR 3V DC
671 INPUT "ENTER THE CURRENT AMP GAIN IN VOLTS/AMP",Gain
672 Gain=1.E+4/Gain

```

```

675 INPUT "ENTER THE WRITE-TIME IN SECONDS",Twrite
676 INPUT "ENTER THE TIME BETWEEN DATA POINTS, Tdelay",Tdelay
678 INPUT "ENTER THE NUMBER OF POINTS <500",Npoints
680 !RECORD THE AVG
690 OUTPUT 726;"T3X" !ONE SHOT ON TRIGGER
691 Dvmavg=0
700 FOR I=1 TO 10
710 TRIGGER 726
720 ENTER 726;V
730 Dvmavg=Dvmavg+V
740 NEXT I
750 Dvmavg=Dvmavg/10
751 DISP "DVMAVG=",Dvmavg
752 PAUSE
760 !WRITE THE GRATING AND TAKE THE DATA
780 OUTPUT 9;"B"
781 WAIT Twrite
785 T0=TIMEDATE !START TIME IN SECONDS
790 !START THE READ SHUTTER
810 FOR I=1 TO Npoints
811 !FIRE THE READSHUTTER
812 OUTPUT 11;"B"
813 WAIT .01
814 TRIGGER 726
820 ENTER 726;Dvmsig1(I)
830 Dvmsig(I)=Gain*(Dvmsig1(I)-Dvmavg)
840 T(I)=TIMEDATE-T0
841 T(I)=T(I)/3600 !TIME IN HOURS
850 MOVE T(I),LGT(ABS(Dvmsig(I)))
860 LABEL "+"
861 ON KEY 4 LABEL "EXIT" GOTO 880
863 WAIT Tdelay
870 NEXT I
880 DISP "DONE"
881 RETURN
890 Storedata: ! STORE THE DATA
900 INPUT "ENTER DRIVE AND DIRECTORY AS DR:\DRIVE\","Dr$
910 IMAGE SDD.2D," ",SD.DDE
920 INPUT "ENTER THE FILE NAME--F$","F$
930 CREATE Dr$&F$&".TXT",2*N+1
940 ASSIGN @File TO Dr$&F$&".TXT";FORMAT ON
950 OUTPUT @File;Twrite
960 FOR I=1 TO Npoints
970 OUTPUT @File USING 910;T(I),Dvmsig(I)
980 NEXT I

```



```
985      ASSIGN @File TO *
990      MOVE Tmax/2, Ymax-.1
1000     LORG 4
1010     LABEL Dr$&F$&".TXT"
1020     RETURN
1030 Dumpgraf: !
1040     CONFIGURE DUMP TO "HP-PCL"
1050     DUMP DEVICE IS 10,EXPANDED
1060     DUMP GRAPHICS #10
1070     PRINTER IS 10
1080     PRINT CHR$(12)
1081     PRINTER IS 1
1090     RETURN
1100     END
```

VITA

Jeffrey Scott McCullough

Candidate for the Degree of

Doctor of Philosophy

Thesis: THE PHOTOCHROMIC AND PHOTOREFRACTIVE RESPONSE OF
CZOCHELSKI GROWN $\text{Bi}_{12}\text{GeO}_{20}$ DOPED WITH CHROMIUM AND
MANGANESE

Major Field: Physics

Biographical:

Personal Data: Born in Dallas, Texas, on February 7, 1970, the son of Bill and Helen McCullough. Married in Reno, Nevada, on December 29, 1995, to Desiree' Ann Butler.

Education: Graduated from Tishomingo High School, Tishomingo, Oklahoma in May 1988, Valedictorian. Received Bachelor of Science degree in Physics and Mathematics from Southeastern Oklahoma State University, Durant, Oklahoma in May 1992, Magna Cum Laude. Completed the requirements for the Doctor of Philosophy degree with a major in Physics at Oklahoma State University in July 1999.

Professional Experience: Graduate Teaching Assistant, Oklahoma State University, Fall 1992 to Spring 1997; Graduate Research Assistant, Oklahoma State University, Summer 1993 to Present.

Professional Memberships: Optical Society of America, American Physical Society